Micro Mechanical Modelling of Natural Fibres for Composite Materials

Nilsson, Torulf

2006

Document Version:
Publisher's PDF, also known as Version of record

LUND UNIVERSITY

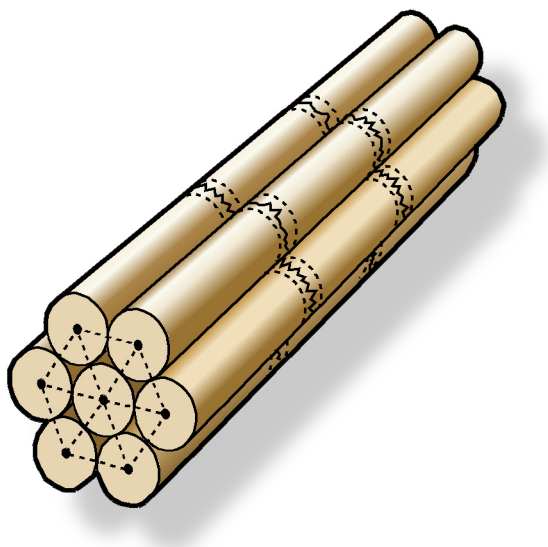

MICROMECHANICAL MODELLING OF NATURAL FIBRES FOR COMPOSITE MATERIALS

TORULF NILSSON

Structural Mechanics

Licentiate Dissertation

Department of Construction Sciences
Structural Mechanics

ISRN LUTVDG/TVSM--06/3067--SE (1-127)
ISSN 0281-6679

MICROMECHANICAL MODELLING OF NATURAL FIBRES FOR COMPOSITE MATERIALS

TORULF NILSSON

Printed by KFS I Lund AB, Lund, Sweden, May 2006.

For information, address:
Division of Structural Mechanics, LTH, Lund University, Box 118, SE-221 00 Lund, Sweden.
Homepage: http://www.byggmek.lth.se

Preface

The work presented in this licentiate dissertation was carried out during the period 2002-2006 at the Division of Structural Mechanics, Lund University, Sweden. The financial support from FORMAS is gratefully acknowledged.

I wish to thank my supervisor Prof. Per Johan Gustafsson for his invaluable guidance throughout the work. Without his enthusiastic encouragement and support this work would most probably not have been completed. I would also like to thank my research colleague and friend, PhD-student Christer Wretfors at SLU, Alnarp, Sweden for many interesting and giving discussions. I also wish to express my gratitude to his supervisor docent Bengt Svennerstedt for his visionary ideas.

A special thanks goes to my colleagues at the Division of Structural Mechanics, no one mentioned no one forgotten, for valuable help of various kind and for making the daily work a pleasure.

Finally I wish to thank family and friends for their support and encouragement, especially Maria for her love and patience during the tough periods of the work.

Lund, April 2006

Torulf Nilsson

Contents

Summary of Papers 1-3

Introduction

Paper 1 T. Nilsson (2005), *Flax and hemp fibres and their composites – A literature study of structure and mechanical properties*, Report TVSM-7139, Division of Structural Mechanics, Lund University

Paper 2 T. Nilsson and P. J. Gustafsson (2005), *Influence of dislocations and plasticity on the tensile behaviour of flax and hemp fibres*, submitted for publication in Composites Part A: Applied Science and Manufacturing

Paper 3 T. Nilsson and P. J. Gustafsson (2006), *Micromechanical modelling and testing of strength of natural fibres*, to be submitted for publication

Appendix Analytical calculation of stiffness of fibres with dislocations

Summary of papers 1-3

Paper 1 This literature study was compiled to gain knowledge of flax and hemp fibres and their composites. When the work of this dissertation started, the knowledge of these fibres and their composites was negligible at the division of Structural Mechanics. In order to have a base for the research, this review was written. The paper covers the structure and mechanical properties of flax and hemp fibres. Further are models for prediction of composite properties treated. Important models of stiffness, strength and hygroexpansion are reviewed.

Paper 2 In this paper, elementary natural fibres are examined by means of finite element analyses. Plasticity and large deformation strain measures are used to model the non-linear tensile behaviour of elementary fibres. The non-linear effect is a consequence of structural misalignments, so called dislocations. The dislocations can also explain that elementary fibres of increasing diameter have a decreasing stiffness.

Paper 3 This paper presents a micromechanical model of a technical fibre and a finite element implementation of the model. The model explains and predicts the strength and non-linear stress versus strain performance of a technical fibre. The model takes in to account the shear interface between the elementary fibres. Defects in the elementary fibres are modelled using Weibull theory. The model is compared with test results of flax and hemp fibres. The shear interface of the test result is changed by testing both glued and non-glued fibres. The importance of the shear interface strength and fracture energy is shown both by the computational and the experimental results.

Introduction

Background

Flax and hemp are annual plants that give fibres with good mechanical properties. Both flax and hemp can successfully be grown in the Nordic countries and they may in the future give the raw material for an extensive domestic production of several structural materials. The usage of flax and hemp fibres for composite materials is today predominantly for interior components in cars. The German automotive industry has increased the usage of natural fibres from 4000 tonnes in 1996 to 15500 tonnes in 1999. It has been projected that the usage by the European automotive industry may increase to more than 100000 tonnes by 2010. The main type of fibre used for these applications is flax, but hemp is rapidly increasing. The reason to their usage is both commercial and technical (Evans et.al. [1]).

According to Kessler [2], the reasons to the usage of natural fibres are a combination of favourable pricing and good mechanical properties. The main reason to the use of long fibres is their capability to make up composites with complex forms. Short fibres, for instance wood fibres, are too short to make composites of these forms. According to Evans et al [1], the natural fibres are used for applications such as door liners, boot liners, seat backs etc. Hence, they are today not used as high performance composites with extensive load carrying capability.

Figure 1. *Mercedes E-class showing interior parts of natural fibres [1].*

In order to use the natural fibres for more elaborate engineering applications it is necessary to be able to manufacture composites of a high and predictive quality. This is the main objective in the present work. This dissertation is a part of the project 'Plant fibres as raw material for accurately characterized structural materials", which is a research collaboration between the Swedish Agricultural University at Alnarp (SLU) and the Division of Structural Mechanics, Lund University. The agricultural part of the project aims at developing methods for quality quantification of the fibres (Wretfors [3]) and the aim of the present work is to establish tools for prediction of the mechanical properties of their composites. Important mechanical properties for

design of contemporary products are stiffness, strength, moisture sensitivity, creep and fracture toughness.

A forthcoming method for investigation of advanced composite behaviour is homogenisation using finite element analyses. The advantage of this method is that a small piece of the material with complex geometry and material properties of the constituents can be analysed very accurately. The average result can then be used for continuum modelling. Examples of successful studies of this kind are Persson [4], who modelled the microstructure of wood and Heyden [5] who studied the properties of fibre fluff by means of network mechanics in conjunction with finite element analyses.

Present work

The objective of this licentiate dissertation study has been to develop methods to predict and explain mechanical properties of composites containing flax and hemp fibres. Since the knowledge of these fibres and their composites were poor in the beginning of the project, a thorough review was written. This review covers the structure and mechanical properties of flax and hemp fibres. Further are models for prediction of composite properties treated. Important models of stiffness, strength and hygroexpansion are reviewed. The review is presented as Paper 1.

During the work with the review several areas of interest to investigate further was found. Two of them were assumed more important for the development of models for prediction of the mechanical properties of the composite. The first phenomenon studied is that elementary fibres have a non-linear tensile performance and a decreasing stiffness with increasing diameter. (An elementary fibre is defined as one single cell of the plant fibres. The size of an elementary fibre is approximately a diameter of 20 μm and a length up to 50 mm.) Both these phenomenon are believed to be caused by structural misalignments of the cellulose chains, so called dislocations. In Paper 2, finite element analyses are performed on elementary fibres with dislocations taken in to account. The dislocations were modelled as kinked trusses embedded in hemicellulose. The hemicellulose was modelled with 3D-continuum elements. The non-linear tensile performance of the fibre could be described by giving the hemicellulose a plastic material model in conjunction with large deformation strain measures. It was found that the dislocations gave local rotations of the elementary fibres that resulted in the non-linear tensile performance.

When bundles of fibres, referred to as technical fibres, are tensile tested the tensile performance is almost completely linear elastic. This is believed to be caused by that the pectin interface between the fibres prevents local rotations. The same mechanism is believed to be valid also in a composite where the adhesive prevents these rotations. The decreasing stiffness with increasing diameter was a consequence of the geometry of the dislocations. The dislocation was kinked in the tangential direction. Together with the helical structure of the cellulose, the effect of this assumption was that the angle of the dislocation increases for an increasing diameter of the fibre, which in turn gave a decrease of the tensile stiffness of the fibre. An analytical expression for the variation of stiffness is presented in the Appendix. For comparison, the result is

shown together with the computational result from the finite element analyses in Figure 2.

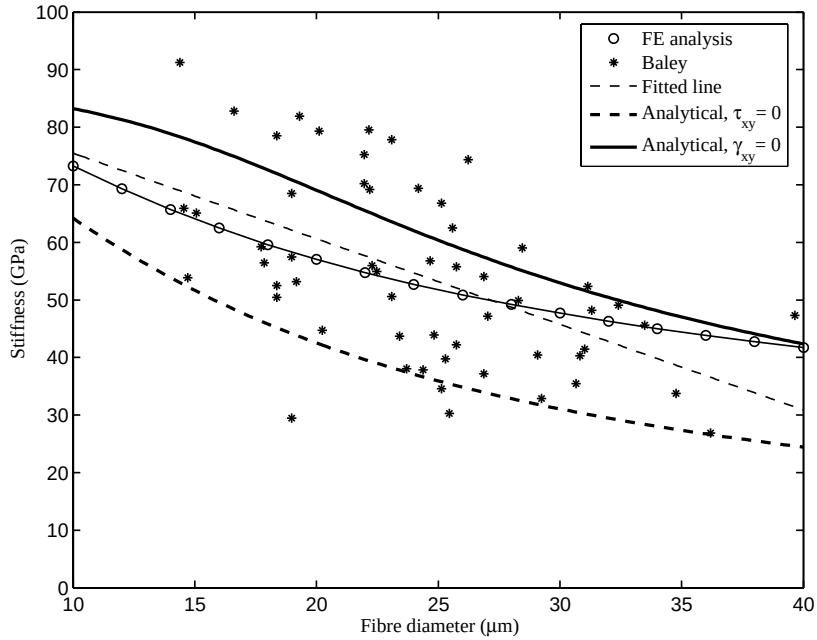

Figure 2 *Stiffness of elementary fibre versus fibre diameter.*

Secondly, Paper 1 revealed that models for accurate prediction of the stiffness of composites are readily available, whereas models of strength are less accurate and not suitable for natural fibres with such a vast variation in strength. This gave the impetus to try to predict the strength of their composites. A first attempt is described in Paper 3. In this study is the strength of technical fibres examined both experimentally and by means of finite element analyses. The finite element model takes defects in to account and each defect is assigned strength according to Weibull theory. The shear interface, transferring stress from one fibre to the adjacent, is described by means of non-linear fracture mechanics. The solution method gives a possibility to follow non-stable stress-displacement curves. By adjusting parameters it was possible to fit the computational result to the experimental. Further, a substantial parameter study was performed in order to show the influence of the different parameters.

Future work

In Paper 3 it was experienced that it is possible to predict and explain the strength of elementary fibres cooperating with an adhesive. The technical fibre can be said to be a composite itself although it only contains up to approximately 25 elementary fibres. A composite used for engineering applications however contains thousands of fibres. The natural next step is therefore to increase the number of elementary fibres in order to simulate a unidirectional composite. An initial attempt of doing so gave the result according to Figure 3 and 4. The model and its parameters are described in Paper 3.

The analyses are performed for τ_f = 15 MPa, m = 2, σ_0 = 9000 MPa, D = 8.1 defects/mm, l_m = 10 μm and l_e = 0.2 mm and the length of the composite was 3 mm.

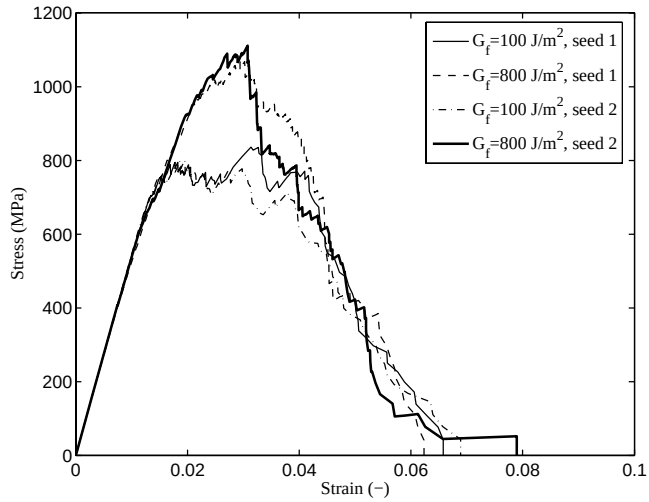

Figure 3 *Tensile curves of composite model with 100 elementary fibres.*

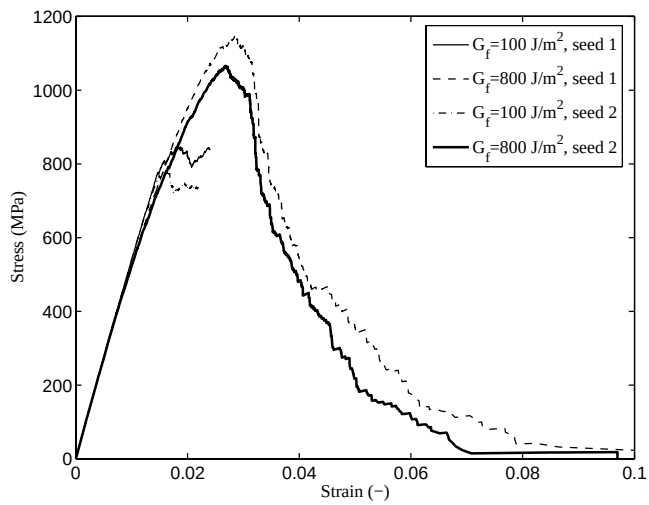

Figure 4 *Tensile curves of composite model with 400 elementary fibres.*

The number of parallel elementary fibres is 100 and 400, respectively, and the defects are located at random. Two seeds were used for the random generation of the microstructure and the micro strength properties of the composite. The fracture energy parameter G_f represents the shear deformation toughness of the interface layer between elementary fibres. The result of the analysis of the composite containing 400 parallel fibres with G_f = 100 J/m^2 is not completed. These analyses were performed during 168 hours at an AMD Opteron 148 (2.2 GHz) cluster, which gives an

an indication of the required computer time. The computer time of the analyses with 100 parallel elementary fibres was 2-4 hours and the analyses with 400 parallel fibres and G_f = 800 J/m^2 was approximately 150 hours. The stress measure is calculated as the global force divided by the cross sectional area of the fibres. The nominal cross sectional area of the composite also takes into account the space between the fibres and the lumen. The stress reported in Figure 3 and 4 are therefore higher than in the composite.

So far only the tensile properties in the direction of the fibres of the composite have been investigated. For engineering applications it is however important to be able to predict properties in other load directions. For a complete determination of the composite, the tensile properties transverse the fibres, the compressive properties both in the direction and transverse the fibres needs to be investigated. Furthermore, the shear properties have to be considered.

When models for all load directions of the unidirectional composite have been established, continuum models can be developed. Micro mechanical analyses of the kind shown in Paper 3 are extremely computer time consuming and therefore possible to apply to a small volume of material. Applied analysis in relation to design of industrial products calls for finite element analysis by means of continuum material modelling at the assumption of homogeneity of the material. Thus, further and future work on homogenisation continuum material modelling and applied finite element analysis is proposed.

In the experimental tensile tests, it was found that the scatter of both stiffness and strength is vast and it can be questioned whether the strength and stiffness properties is relevant for estimation of the properties of a fibre in the composite. It is therefore proposed that a standard composite is developed for evaluation of the stiffness and the strength of natural fibres. This composite should be unidirectional and the resin and manufacturing method should be standardised. Testing of such a composite is much easier to perform and the scatter will most likely decrease since a large number of fibres are loaded simultaneously.

References

1. W. J. Evans, D. H. Isaac, B. C. Suddell, A. Crosky, *Natural fibres and their composites: A global perspective*, Proceedings of the 23rd Risö International symposium on materials science, Risö national laboratory, Denmark 2002
2. Personal communication with Professor Rudolf Kessler, Institut für Angewandte Forschung, Fachhochschule Reutlingen, Germany, 2003
3. C. Wretfors, *Cultivation, processing and quality analysis of fibres from flax and industrial hemp – an overview with emphasis on fibre quality*
4. K. Persson, *Micromechanical modelling of wood and fibre properties*, Doctoral thesis, Structural mechanics Lund institute of technology, 2000
5. S. Heyden, *Network modelling for the evaluation of mechanical properties of cellulose fibre fluff*, Doctoral thesis, Structural mechanics Lund institute of technology, 2000

Paper 1

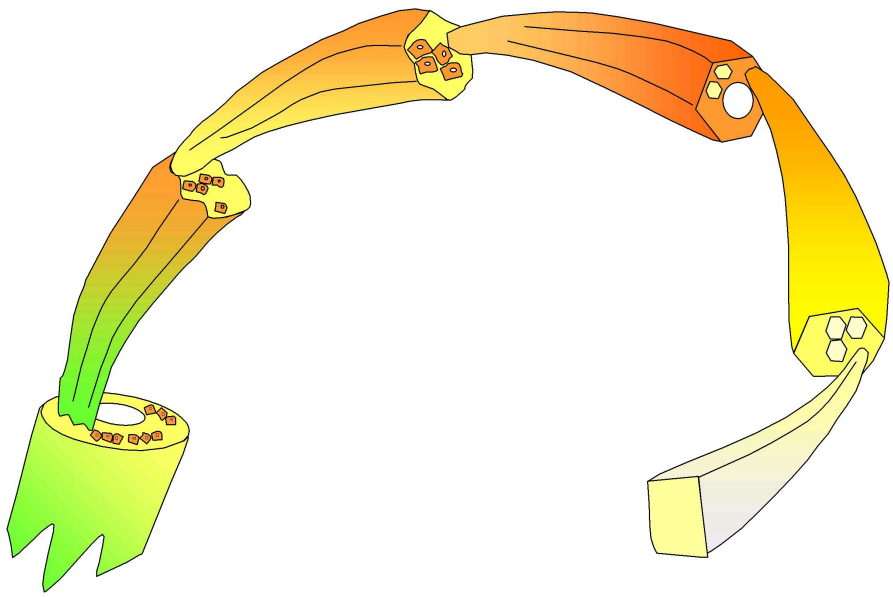

FLAX AND HEMP FIBRES AND THEIR COMPOSITES –A Literature Study of Structure and Mechanical Properties

TORULF NILSSON

1. INTRODUCTION **3**

1.1. General introduction **3**

1.2. Possible products **3**

1.3. Required mechanical properties for different products **5**

1.4. Manufacturing methods **7**

2. THE PLANT FIBRES **9**

2.1. Structure **9**
2.1.1. The elementary fibre 10
2.1.2. The technical fibre 12

2.2. Stiffness and strength **14**
2.2.1. Tensile stress vs. strain behaviour 14
2.2.2. Stiffness 16
2.2.3. Tensile strength 17
2.2.4. Compressive strength 19

2.3. Moisture and effects of moisture **21**
2.3.1. Transport and absorption 21
2.3.2. Effects on mechanical properties 24
2.3.3. Effects on durability 28
2.3.4. Hygroexpansion 28

2.4. Miscellaneous mechanical properties **32**
2.4.1. Creep 32
2.4.2. Fatigue 32
2.4.3. Impact strength 33

3. PHYSICAL PROPERTIES OF MATRIX MATERIALS **35**

4. MECHANICAL PROPERTIES AND MODELLING **37**

4.1. General **37**

4.2. Stiffness of the composite **38**
4.2.1. The Voigt and Reuss approximation 38
4.2.2. The Halpin-Tsai equations 39
4.2.3. Arbitrarily oriented fibres 39
4.2.4. Fibres with large variation of stiffness 40
4.2.5. Other models of stiffness 40
4.2.6. Experimental values 40

4.3. Failure of the composite **42**
4.3.1. Axial tensile strength of composites with continuous fibres 42

4.3.2. Axial tensile strength of composites with non-continuous fibres 43
4.3.3. Consideration to varying fibre strength 44
4.3.4. Axial compressive strength 46
4.3.5. Continuum failure theories 48
4.3.6. Damage 53

4.4. Modelling of hygroscopic and thermal expansion 54

4.5. Homogenisation 56

4.6. Miscellaneous mechanical composite properties 57
4.6.1. Creep 57
4.6.2. Fatigue 57
4.6.3. Impact strength (toughness) 57

5. DISCUSSION AND CONCLUSIONS 59

5.1. Additional aspects 59

5.2. Concluding remarks 59

6. REFERENCES 61

7. ACKNOWLEDGMENTS 65

8. APPENDIX 67

The cover picture shows the multi-scale structure of the materials in flax and hemp. The figure was kindly provided by Harriëtte L. Bos, Technische Universiteit Eindhoven, the Netherlands.

1. Introduction

1.1. General introduction

Flax and hemp are annual plants that give fibres with good mechanical properties. Both flax and hemp can successfully be grown in the Nordic countries and they may in the future give the raw material for an extensive domestic production of several structural materials with well-defined engineering properties, competing with established materials like wood and wood based materials, mineral fibre materials, glass-fibre reinforced plastics, aluminium and steel.

Flax and hemp fibres have historically been important handicraft materials. However, to reach consideration in the process of choice of material in contemporary engineering design of industrial products there are other and much higher demands in terms of uniform material quality and knowledge about engineering properties and structural performance.

This report deals with current knowledge of the mechanical properties and structure of flax and hemp fibres and flax and hemp fibre based composites.

1.2. Possible products

Possible products for contemporary engineering designs are found in many branches of the industry. At present it appears that the automotive industry is leading in development and modern industrial use of composite materials based on fibres from flax and hemp. It seems that the choice of materials in this case is due to the combination of good mechanical properties and a favourable prizing [1]. The automotive industry may be leading the development because of the financial resources for research and product development in this branch of the industry. Several examples of current and imaginable products within various branches of the industry are listed below. Although several examples are listed, it is only a few of all possibilities. Examples of more possible products are presented in [2]. The best possibilities for use of large quantities of flax and hemp fibre materials might be in the construction and packaging industry branches. For other branches the use of the fibre materials might be of greater interest for the material and processing industries than for the producers of fibre raw material.

Table 1.1 *Possible products in different branches of the industry.*

Branch	*Products*
Automotive industry	Inner fenders
	Interior parts
	Bumpers
Construction industry	Reinforcing of concrete
	Reinforcing of timber and glulam
	Insulation
	Laminate floors
	Window frames
	Hard Boards (HB)
	Medium Density Fibreboards (MDF)
	Particle board
	Studs
Packaging industry	"Tetra paks"
	Cardboard
	High strength paper
Electronics industry	Outer casings (e.g. VCR, Mobile phones)
Furniture industry	Chairs
	Tables
	Shelves etc.
Other industries	Blades for wind turbines
	Pleasure boats

1.3. Required mechanical properties for different products

When designing a product several classes of properties of the material to be chosen have to be considered. Table 1.2 shows the classification of properties according to [3]. As can be seen the properties to consider are not only mechanical. The table can be extended by both classes and properties, for instance by the class environmental properties with properties like recyclability and CO_2 neutrality.

Table 1.2 *Classes of properties for designing a product* [3].

Properties	*Class of property*
Price and availability	Economic properties
Density	
Modulus and damping	
Yield strength, tensile strength, hardness	Bulk mechanical properties
Fracture toughness	
Fatigue strength, thermal fatigue resistance	
Creep strength	
Thermal properties	
Optical properties	Bulk non-mechanical properties
Magnetic properties	
Electrical properties	
Oxidation and corrosion	Surface properties
Friction, abrasion and wear	
Ease of manufacture	Production properties
Fabrication, joining, finishing	
Appearance, texture, feel	Aesthetic properties

The most important mechanical properties for some of the products listed in Table 1.1 are indicated in Table 1.3. For the selection of products, properties that are estimated to be of importance for each product are marked with an X.

Table 1.3 *Necessary mechanical properties for some of the products above.*

	Property							
	1	**2**	**3**	**4**	**5**	**6**	**7**	**8**
Product								
Inner fender			X		X		X	
Interior parts (automotive)	X	X			X			
Bumpers	X	X	X		X		X	X
Reinforcing of concrete	X	X	X	X			X	
Window frames			X	X				
Cardboard		X	X	X	X		X	
Blades for wind turbines	X	X	X	X	X	X	X	
Outdoor furniture	X	X	X	X			X	
Indoor furniture	X	X		X				

1 = Stiffness and damping, 2 = Strength, 3 = Moisture effects, 4 = Creep, 5 = Density, 6 = Fatigue, 7 = Durability, 8 = Impact strength (fracture toughness, ductility)

The following mechanical properties are estimated to be of interest in engineering design and analysis of natural fibre based materials and products:

- Stiffness
- Damping
- Strength
- Hygroexpansion (Moisture induced expansion)
- Moisture transport ("Water diffusion")
- Durability
- Creep
- Density
- Fatigue
- Impact strength, fracture toughness and ductility

Each of these properties can in general be quantified by one or more parameters together with a material model. Thus, for instance, if the stiffness properties may be characterised as orthotropic linear static, then the in-plane stiffness properties are defined by five parameters: the material orientation angle and four independent parameters in the stiffness matrix.

1.4. Manufacturing methods

Several methods for manufacturing of composites in general are available. Several of them are presumably not appropriate for use in bio fibre based composites. The methods used for manufacturing of bio fibre based composites found in the literature are briefly described below. The development of manufacturing methods is rapid, especially in the automotive branch of the industry.

Manual lay-up

The simplest technique to manufacture a composite is called lay-up moulding, wet lay-up or laminating. This method is performed by applying (by hand) layer upon layer of fibres (or mats of fibres) with resin in between on a shaped surface. This is repeated until the desired thickness is obtained after which pressure is applied, normally by hand rolling.

Vacuum bagging (bag moulding)

A little bit more elaborate than the manual lay-up method, is to impregnate a mat with a resin, (referred to as a prepreg), which is placed on the shaped surface with a bag on top. The pressure is applied either by evacuating the air inside, creating a vacuum, or by pressurising the bag on the outside with compressed air.
Both manual lay-up and vacuum bagging are then cured at room temperature or at an elevated temperature. These two methods work best for thermoset resins [4].

Sheet moulding compound (SMC)

SMC is a thin mat of short/continuous fibres impregnated by a thermoset resin. The mats are placed in a hot-pressing machine, where heat and pressure is applied which activates the curing process [5].

Bulk moulding compound (BMC)

BMC is a pre-mix of short/continuous fibres and normally a thermoset resin. The mixture is cured under pressure and heat [6].

Natural fibre mat thermoplastic (NMT)

NMT is a development of GMT, which is a Glass fibre Mat with non-oriented short fibres impregnated by a Thermoplastic. The fibres in the NMT are natural fibres such as flax and hemp, thereby the replacement of the G in GMT to an N!
The manufacturing starts out by placing the NMT in an oven. When the matrix starts to melt the NMT is pressed to the desired shape in a hydraulic press. The matrix cools in the press and the matrix solidifies [5].

Preform sheet resin (PSR)

PSR is similar to the SMC method. A preform of fibres is placed in a mould with a sheet of resin on top. Then the mould is closed and curing occurs in vacuum [5].

Pultrusion

Pultrusion is a continuous manufacturing process for manufacturing long straight profiles with a constant cross sectional area. The process is basically performed by squeezing the mixture of resin and fibres through a heated die, similar to extrusion of aluminium profiles [5].

The manufacturing methods appropriate for a thermoset or a thermoplastic resin is summarised in Table 1.4

Table 1.4 *Manufacturing methods for different types of raw material.*

Fibre raw material	*Thermoset*	*Thermoplastic*
Mat	Maual lay-up Vacuum bagging Sheet moulding compound	Natural fibre mat thermoplastic
Bulk	Bulk moulding compound Pultrusion	Bulk moulding compound Pultrusion
Preform	Preform sheet resin	

2. The plant fibres

The plant fibres discussed in this text are flax (Linum Usitatissimum) and hemp (Cannabis Sativa L). It should be emphasised that the hemp plants used for fibres are so called industrial hemp with a very small content of THC, the active substance in hemp used for drugs. Regulations in the EU have set the limit of THC in industrial hemp to less than 0.2 % by weight.

2.1. Structure

The structure of the fibres described in this report is limited to the structure of the elementary fibre and the technical fibre. The structural differences of flax and hemp are small. Their stems have a similar structure where the bast fibres are situated near the bark as shown in Figure 2.1. The bast fibre is the supporting plant tissue containing lengthy fibres of usually dead cells with strong and thick cell walls. The bast fibre bundles runs along the stem from root to top of the plant.

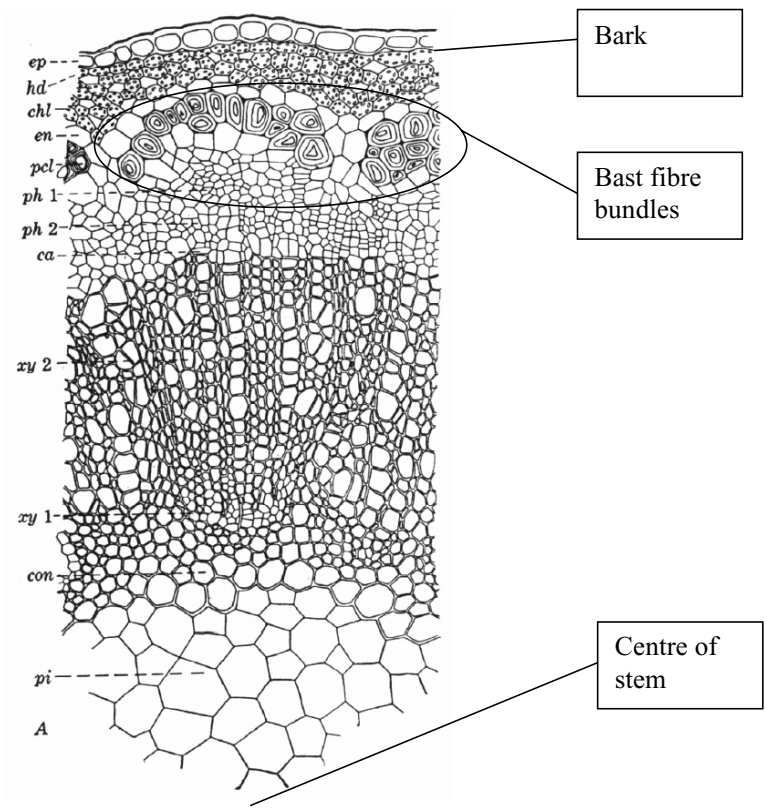

Figure 2.1 *Cross section of a flax stem* [7].

The technical fibre is simply a smaller part of a bast fibre bundle. The elementary fibre (sometimes referred to as ultimate or single fibre) is one cell of the bast fibres. The principle of the different levels of fibres in the plant is described in Figure 2.2.

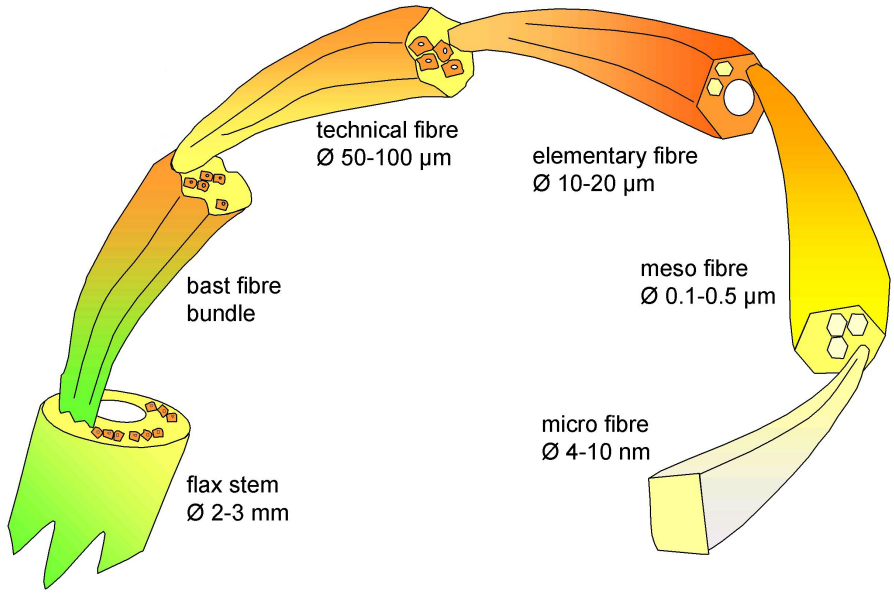

Figure 2.2 *Fibre classification in a flax stem* [8].

2.1.1. The elementary fibre

The elementary fibre in plant science refers by definition to a single cell in the plant. The structure of the elementary fibres of flax and hemp are similar. A simple way to distinguish fibres from flax and hemp without chemical or microscopic examination is to wet the fibres. Since the helical disposed cellulose goes in different directions, flax has a so called S-shaped helix and hemp a Z-helix, the flax fibre will rotate clockwise and hemp counter clockwise [9]. It seems that the science community has so far not agreed on the true structure of the elementary fibres in flax and hemp. Models of the elementary fibres however exist [7,10]. Figure 2.3 shows models of the structure of a single cell, i.e. the elementary fibre and Figure 2.4 shows pictures of flax and hemp fibres respectively.

The length/diameter ratio of the elementary fibres varies somewhat between hemp and flax. Typical values of length and "diameter" of the elementary fibre for hemp and flax are shown in Table 2.1. The quotation marks on the word "diameter" are due to the fact that the cross section is rather polyhedrical than circular.

Table 2.1 *Reported values of length and diameter of hemp and flax* [7,11], *spruce is listed for comparison.*

Plant	*Length of an elementary fibre (mm)*	*"Diameter" of an elementary fibre (µm)*
Flax	3-50	10-25
Hemp	5-100	18-26
Spruce	1-4	20-40

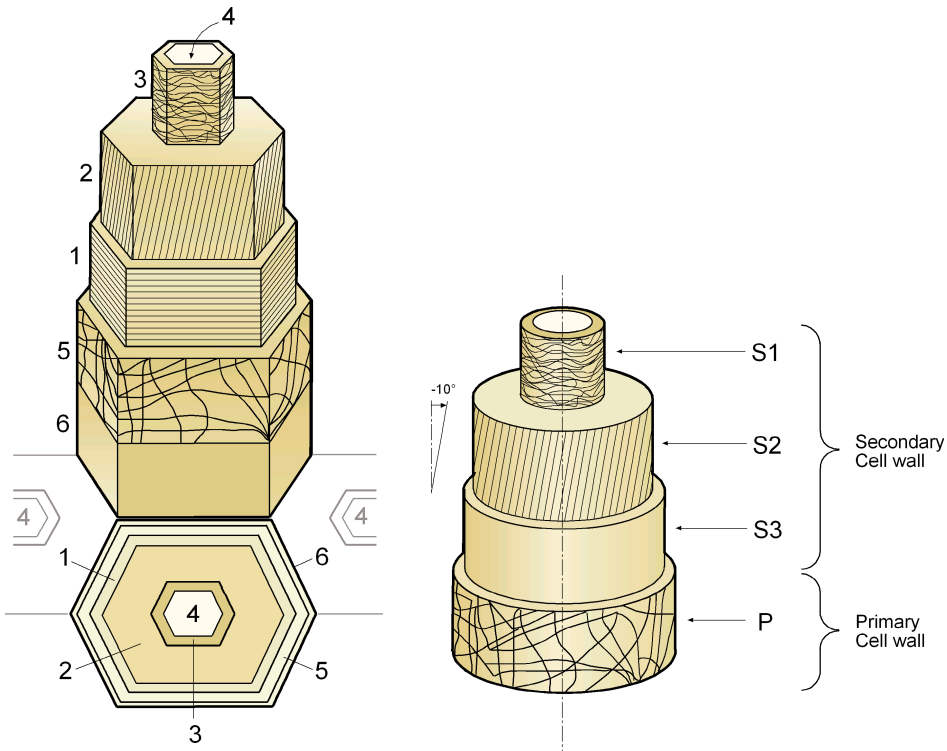

Figure 2.3 *Two different models of the structure of an elementary fibre. (1-3) - Secondary cell wall, (4) - Lumen, (5) – Primary cell wall and (6) – Middle lamella* [7, 10].

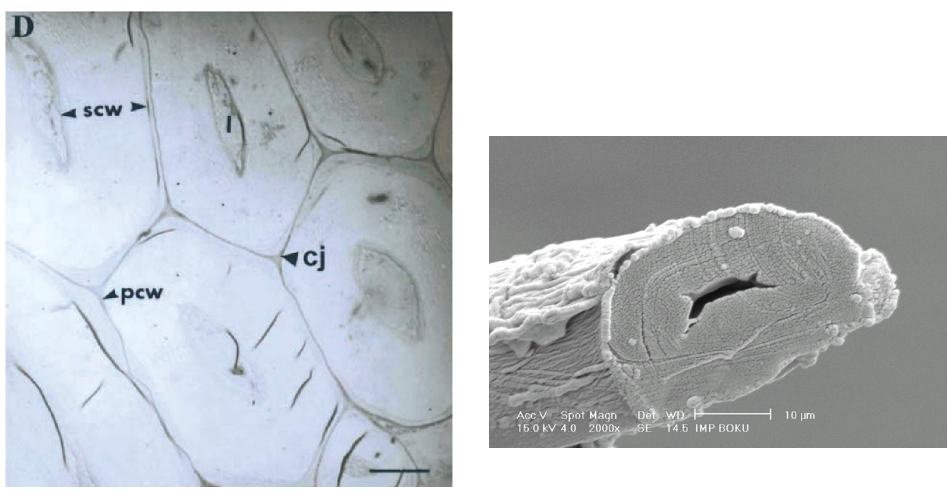

Figure 2.4 *Left figure [12] shows cross sections of flax elementary fibres and right figure [13] shows hemp.*

The science community seems to have agreed on that the cell wall consists of a primary cell wall, a secondary cell wall and a lumen, which is an open channel in the centre of the cell. Somewhat uncertain is that the secondary cell wall consists of the three sub layers S_1, S_2 and S_3.

The middle lamella is not really considered to be a part of the cell, but rather a matrix bonding the cells together. In [14], the following thickness relations of the cell wall was used for stiffness prediction of a flax fibre: P = 8%, S_1 = 8%, S_2 = 76% and S_3 = 8%. According to [8], the thickness of the primary cell wall is only about 0.2 µm. The lumen can be as small as 1.5 % of the cross section [8].

The primary cell wall (P) consists of lignin, pectin and randomly oriented cellulose [8,11,15].

The secondary cell wall (S_1- S_3) is the major part of the fibre diameter, where the S_2 layer clearly dominates. It consists of highly crystalline cellulose microfibrils bounded together by lignin and hemicellulose. The microfibrils are oriented spirally around the fibre axis. The microfibrils in the S_2 layer have an angle of 5-10^o with respect to the fibre axis, which explains the stiffness and strength of the fibre in the axial direction [8,9,11,16]. This is because cellulose is stiff and strong in axial loading. The total chemical composition of the cell of flax and hemp is shown in Table 2.2.

Table 2.2 *Chemical composition of flax and hemp elementary fibres.* [9,15].

Substance	*Content (flax) (wt.%)*	*Content (hemp) (wt.%)*
Cellulose	64.1	68.1
Hemi cellulose	12.0	15.1
Pectin	1.8	-
Lignin	2.0	10.6
Water soluble substances	3.9	-
Wax	1.5	-
Water	10.0	-

It should be noted that the sum of the values in the columns does not equal 100%. No explanation has been given in the references, but it is likely that there are other substances present. The chemical composition should be viewed as typical values. For instance, figures of the amount of cellulose in flax found in literature ranges between 64.1 and 78.5 % and the content of lignin between 2 and 8.5 % [9,15]. The amount of lignin is known to increase at the end of the growth period, so the amount of lignin depends on when the fibres are harvested.

2.1.2. The technical fibre

According to [8] the technical bast fibre (or bundles of elementary fibres) consists of elementary fibres overlapped over a considerable length and glued together by the middle lamella, which consists mainly of pectin and hemi cellulose. The principle of bundles of fibres is shown in Figure 2.5. The flax plant is approximately 1 meter tall,

which yields a technical fibre of the same length. Hemp grown in Sweden is approximately 3 meter, which presumably means that the technical hemp fibre reaches a length of 3 meters.

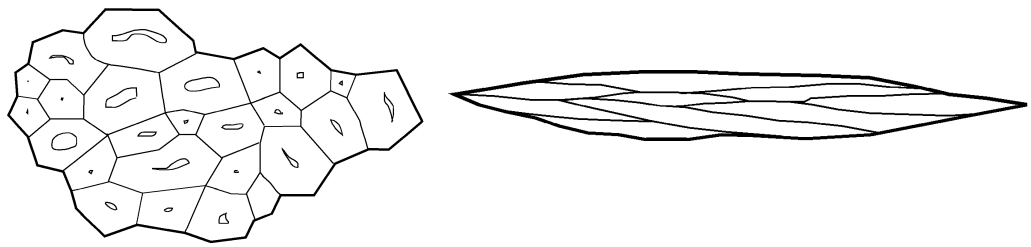

Figure 2.5 *Principle of bundles. Left figure shows the cross section and the right shows the bundle from the side. Note that the side view is not to scale.*

2.2. Stiffness and strength

2.2.1. Tensile stress vs. strain behaviour

A typical load-extension curve of an elementary flax fibre is shown in Figure 2.6. It is obvious that the relation is not linear for a continuously increasing load [10].

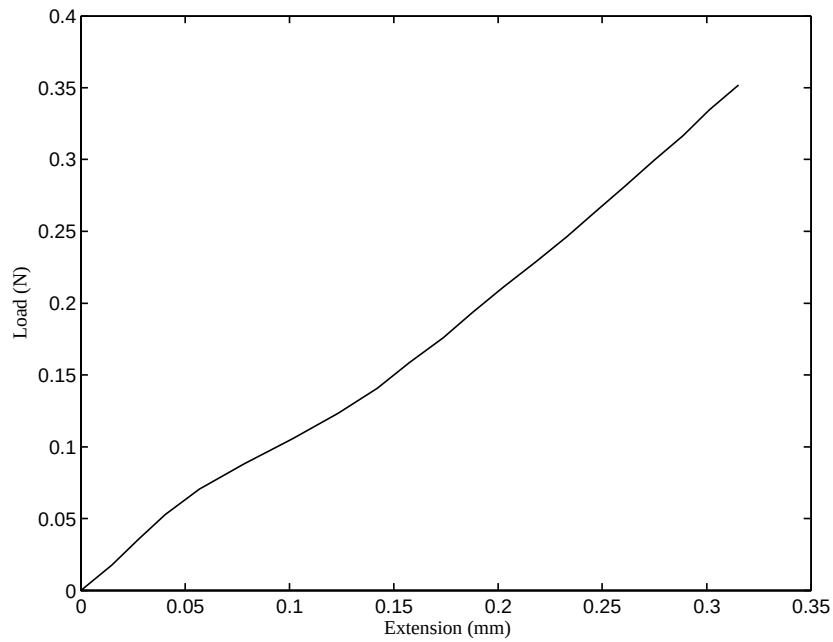

Figure 2.6 *Typical load-displacement of an elementary flax fibre, clamping length 10 mm* [10].

If the fibre is subjected to a successive loading-unloading the load-extension curve behaves as shown in Figure 2.7 [10]. This indicates that the fibre behaves elasto-plastically at least at the first loading cycle. The reason can, according to [10], be explained on the structural level of the cell.
It is well known that during a deformation the microfibrils are oriented towards the fibre axis. This behaviour is believed to be caused by one or more of the three following deformation mechanisms [10]:

1. The length of the fibrils and the non-crystalline regions in between are increased.
2. The fibre extends like a spiral spring together with a contraction of the fibrils, of the interface in between and voids.
3. The interface between the fibrils is deformed plastically? and the fibrils are straightened.

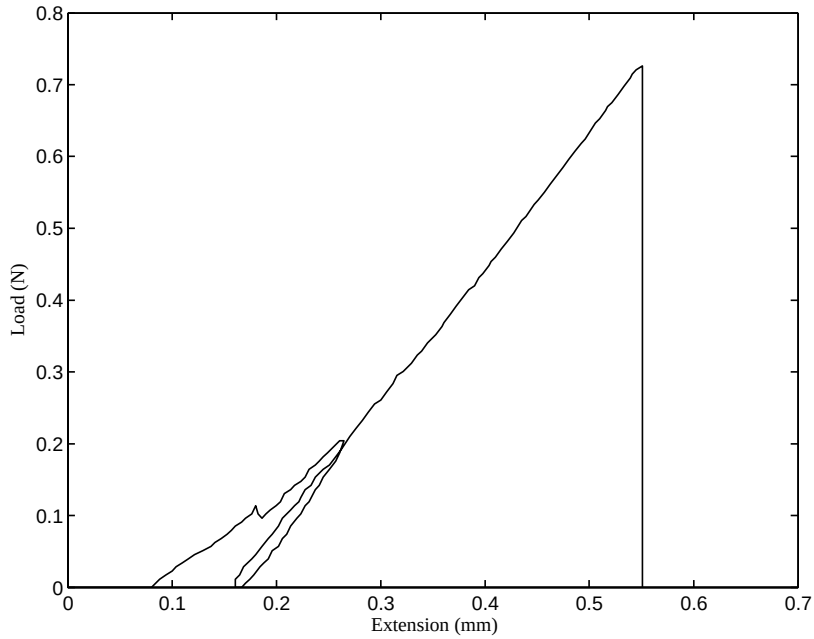

Figure 2.7 *Elasto-plastic behaviour of an elementary fibre* [10].

The behaviour of a technical fibre is somewhat different from the elementary fibre. As can be seen in Figure 2.8 the constitutive relation between stress and strain is almost linear. This has however to be taken with precaution. What happens if the test is carried out in a successively increasing loading-unloading?

It is however likely that the pectin interface between the elementary fibres prevents rotation and the microfibrils to be straightened out during deformation, which could explain the linear behaviour.

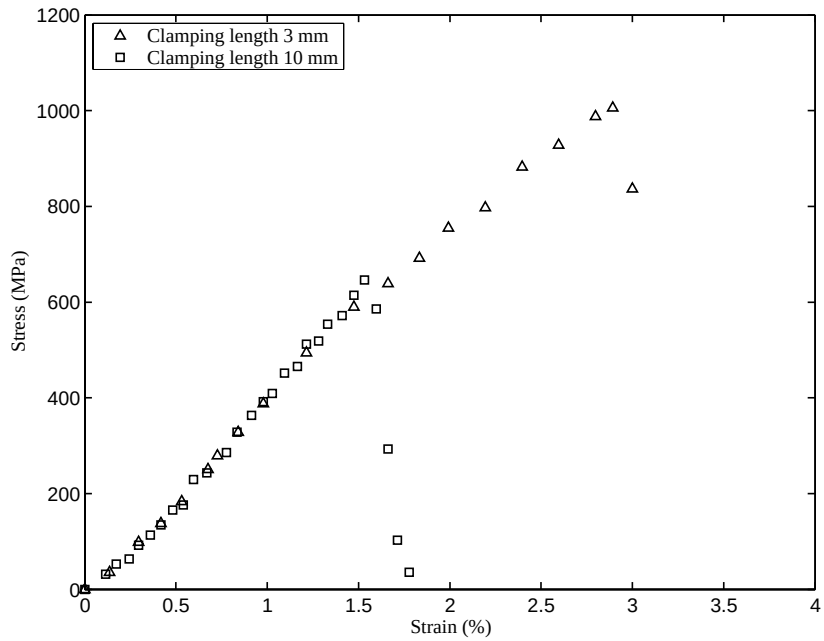

Figure 2.8 *Stress-strain curve of a technical flax fibre* [8].

2.2.2. Stiffness

The compilation in Table 2.3 shows that various authors have reported different values of the average E-modulus in the direction of the fibre of flax and hemp. The variation of stiffness is also vast, Madsen et. al. [13] have reported an average E-modulus of single hemp fibres of 25.4 GPa and a coefficient of variation of 53.3 %. The variation can have many explanations. One important factor, which also justifies a part of this research project, is the growing conditions such as area of growth, climate and when harvested. The growing conditions affect the content of the substances (e.g. cellulose) and the structure of the fibres [15]. As described above the stiffness is highly dependent on the secondary cell wall layer, which contains a large amount of cellulose. Another important factor is how the fibre is separated from the plant, i.e. the defibration process. Several methods exist; mechanical, physical and chemical. Depending on the method the structure or the chemical composition of the fibre can be affected.

Further, the method of determining the cross sectional area of the fibre seems to vary between different authors. If the area is defined differently the evaluation of the stiffness of the material will, of course, be affected. Additionally, if the elementary fibre behaves as shown in Figure 2.6, which slope of the curve should be used for evaluation of the E-modulus?

Finally, the moisture content in the fibre has a great influence on the stiffness. This important factor is discussed in more detail in section 2.3.

Table 2.3 *Typical average values of stiffness from different references.*

Ref	*E-modulus Flax (GPa)*	*E-modulus Hemp (GPa)*
[15]	27.6	-
[17]	60	32
[18]	43.5	19.1
[19]	80	-

Note: It is not evident whether the results refer to elementary or bundles of fibres.

No values of transversal stiffness have been found in the literature. Several attempts to model the stiffness of an elementary fibre in the direction of the fibre have been presented in the literature. The methods are discussed in [8,14,15]. As in the case of stiffness in the direction of the fibre, it should be possible to determine the stiffness in the transversal direction from the elastic properties of cellulose, hemicellulose and lignin. The elastic properties of the constituents are shown in section 2.3 due to their high dependence on moisture content.

2.2.3. Tensile strength

As in the case of stiffness, the reported values of tensile strength are different in different references, see Table 2.4. The different authors also report a large scatter of strength in their tests, for instance, [13] reports an average strength of elementary hemp fibres of 1249 MPa with a coefficient of variation of 32.4 %. It is widely accepted that defects determine the strength of most materials, which probably is the case also for natural fibres. This is supported by [8], who made tensile tests on flax fibres decorticated by two different methods. The standard decorticated fibres gave a strength of 1522±400 MPa and the more gentle by hand decorticated fibres yielded a strength of 1834±900 MPa. This indicates that defects are induced during the decortication process. Somewhat contradictory is that the scatter increases when the average strength increases. It seems like defects already exists in the plant, which again can be related to the growing conditions.

A typical defect in an elementary fibre is shown in Figure 2.9. The defects are presumably kink bands [10] sometimes referred to as "nodes" or "dislocations".
The strength distribution can be described by a Weibull plot, where the Weibull modulus is a measure of the scatter. For a high modulus the scatter is small and vice versa.

Table 2.4 *Typical values of tensile strength from different references.*

Ref	*Strength of Flax (MPa)*	*Strength of Hemp (MPa)*
[15]	345-1035	690
[17]	1000	700
[18]	270	270
[19]	800	-

Note: It is not evident whether the results refer to elementary or bundles of fibres.

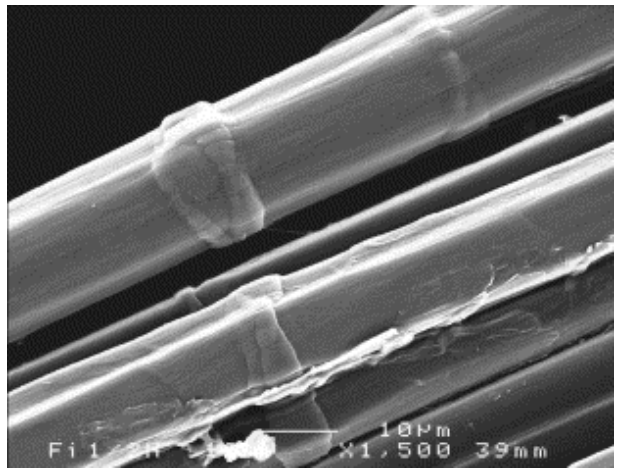

Figure 2.9 *Examples of defects in flax fibres* [10].

An interesting phenomenon is that when bundles of fibres are tensile tested, the scatter of strength decreases compared to elementary fibres. Partly this may be because the average strength of a bundle is only half of the strength of an elementary fibre. The reason for the decrease of scatter is probably that the pectin interface between the elementary fibres transfers the forces from a damaged fibre to the adjacent fibre, which might be undamaged. This kind of phenomenon might be possible to use when designing a composite. In that case the interface between the fibres is the man made matrix, which is easier to control than the natural existing pectin.

Another important phenomenon is that the strength of a technical, and presumably an elementary fibre, increases as the clamping length is decreased. Figure 2.10 shows a plot of the tensile strength of technical fibres versus the clamping length. This behaviour has two probable causes [8]. Firstly, the risk of presence of a critical damage on the fibre increases with increasing length. Secondly, since the technical fibre is composed of overlapping elementary fibres with a weak pectin layer in between, the failure at large clamping lengths is believed to occur by shearing of the pectin layer. This is also supported by [20] who have noticed a much lower tensile strength of well-retted technical fibres than for unretted fibres. (Retting removes the pectin interface between the elementary fibres.) At shorter clamping lengths, in the order of an elementary fibre, the stress redistributes to the fibres yielding a higher value of tensile strength. This behaviour leads to the following question: What happens when the fibres are embedded in a man-made matrix? What is the "clamping length"?

Strength differences due to moisture are discussed in section 2.3.

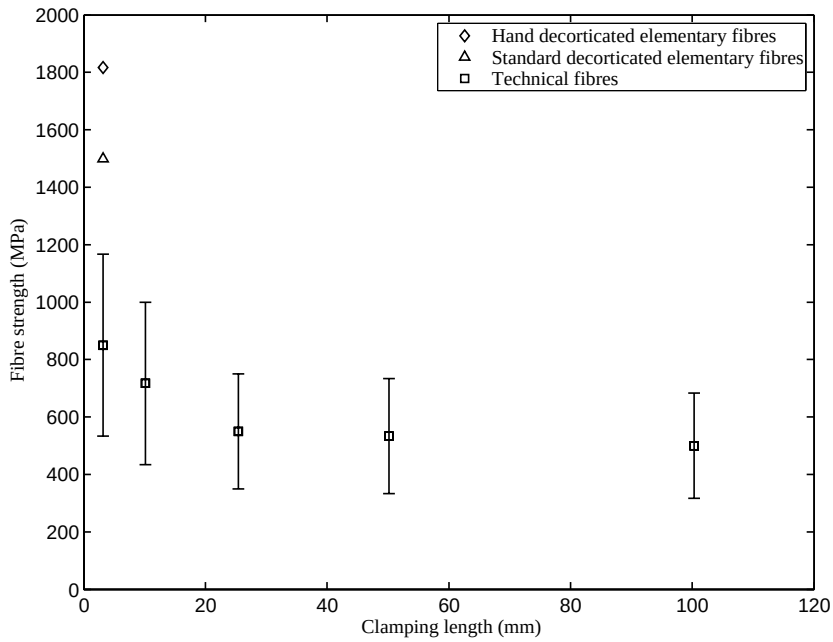

Figure 2.10 *Fibre strength versus the clamping length. Error bars indicate standard deviation* [8].

2.2.4. Compressive strength

The compressive stiffness modulus is usually assumed to be equal to the tensile modulus [8]. The compressive strength of an elementary flax fibre has been examined by [8], who used an elastica loop (Figure 2.11) originally developed by Sinclair (reference 17 in [8]). When the loop is tightened the relation c/a remains constant at a value of approximately 1.34 until a non-linear deformation occurs in top of the loop. At this instant the critical value c_{crit} is measured and the compressive strength can be calculated as:

$$\sigma_{fc} = \frac{1.34 E_{fc} d}{c_{crit}} \qquad 2.1$$

where E_{fc} is Young's modulus in compression, here assumed equal to Young's modulus in tension, and d is the fibre diameter.

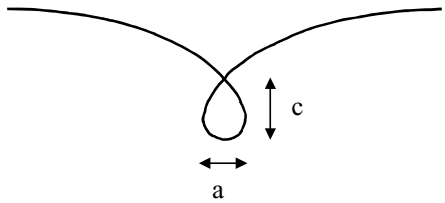

Figure 2.11 *Geometry of the elastica loop.*

The test showed that the elementary flax fibres failed at a compressive stress of 1200±370 MPa. The failure mechanism is however different from tensile fracture. The main reason is that during compression the cell wall buckles and creates kink bands. A buckled elementary fibre is shown in Figure 2.12. Similar tests can presumably be carried out for hemp fibres, but no reported test results have been found in the literature.

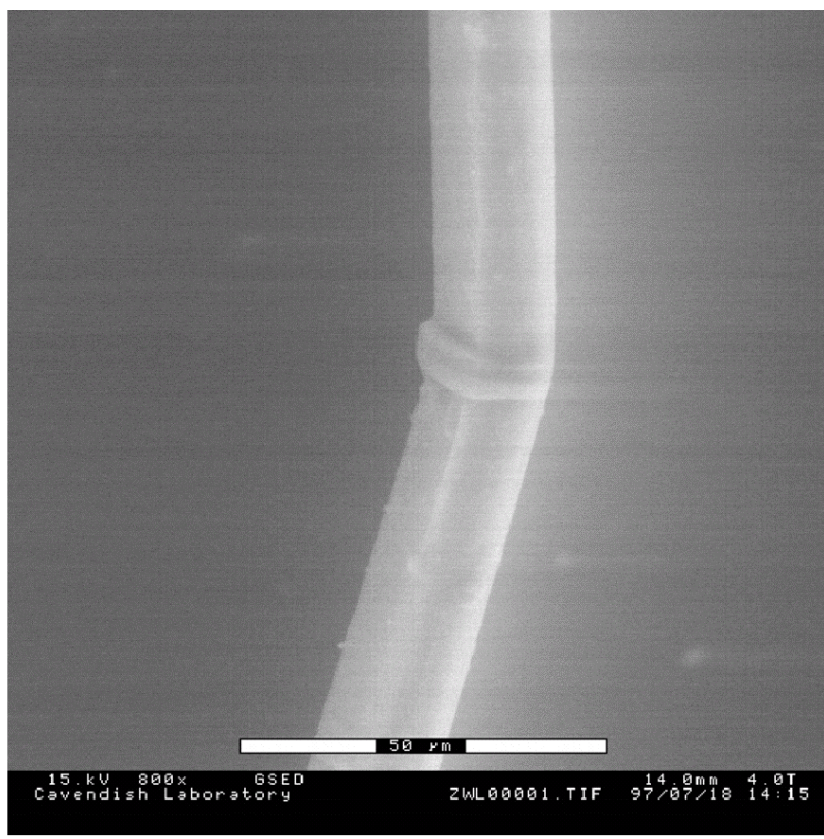

Figure 2.12 *Kink band formation in compressive test* [8].

2.3. Moisture and effects of moisture

2.3.1. Transport and absorption

Due to the nature of growing plants, materials like flax, hemp and wood are hygroscopic. A lot of research has been carried out on moisture effects and moisture transport in wood. Since wood and plant fibres contain the same basic constituents, a lot of the general results found for wood can be applied on flax and hemp. Figure 2.13 shows the equilibrium moisture content versus the relative humidity in humid air of the constituents in wood. The moisture content is measured as weight of water per weight of dry material.

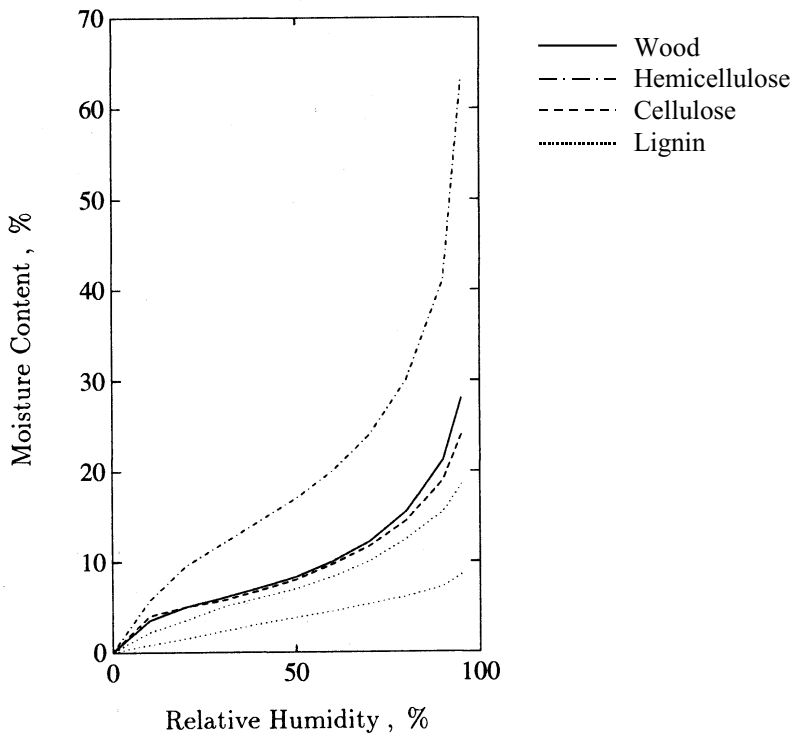

Figure 2.13 *Absorption isotherms of wood and its constituents. Two curves are shown for lignin prepared with different methods* [16].

Recently (2000) an absorption isotherm of flax fibres was reported in [21], the result is shown in Figure 2.14, and comprises the equilibrium moisture content at 20, 66, 93 and 100 % relative humidity. A smoother curve could have been obtained by measuring at closer intervals. In [22], absorption isotherms are reported both for flax straw and hemp stalks. Although the isotherms are reported for the stems, the result might be valid also for the fibres.

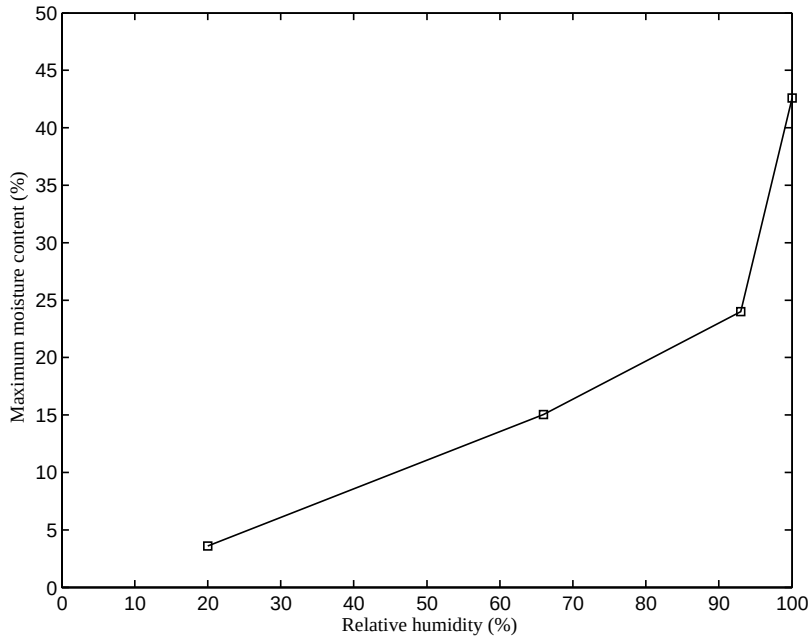

Figure 2.14 *Moisture absorption of flax fibres versus the relative humidity* [21].

Transport of moisture is often assumed to be a diffusion process where the driving force is the gradient of the moisture content. The basic equation describing diffusion is

$$F = -D_c \frac{\partial c}{\partial x} \qquad 2.2$$

where F is the flux measured in kg/m^{2}s, D_c is the diffusivity measured in m^2/s and $\partial c/\partial x$ is the gradient of the concentration (kg/m^3) with respect to the distance (m). This equation is commonly referred to as Fick's first law. By conservation of mass, i.e.

$$\frac{\partial F}{\partial x} = -\frac{\partial c}{\partial t} \qquad 2.3$$

Fick's second law of diffusion is obtained as;

$$\frac{\partial c}{\partial t} = D_c \frac{\partial^2 c}{\partial x^2} \qquad 2.4$$

To be able to describe the sorption of vapour into the fibre, the isotherm (as shown in Figure 2.14) has to be known:

$$c = f(\phi) \qquad 2.5$$

where ϕ is the relative humidity.

Values of the diffusivity, D_c, for a single elementary fibre of flax and hemp have not been found in the literature. Bundles of flax fibres, however, have been examined by [21], who measured the moisture content of initially dry fibres as a function of time in 66% relative humidity. The test was carried out on bundles bounded together to a radius of approximately 1.5 mm. The plot is shown in Figure 2.15. The diffusion coefficient in this case is determined to $D_c = 4.04 \cdot 10^{-6}$ cm^2/s. This is to be considered as a value valid for this special case. For a more general value of diffusivity the moisture transport in the pores within the fibres and the interface between the humid air and the fibre have to be accounted for. This is discussed in detail in [23].

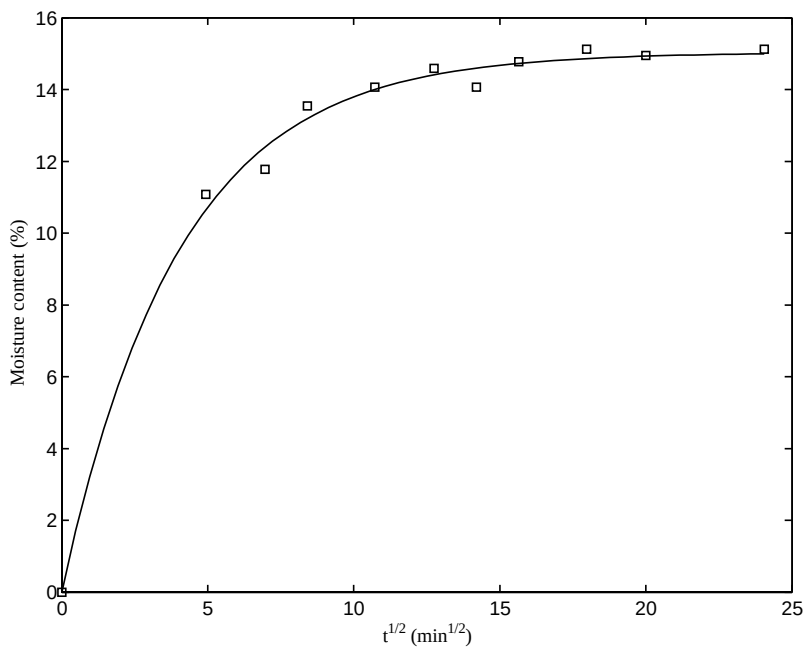

Figure 2.15 *Moisture content of flax at 66% of relative humidity* [21].

The mentioned equations are used to describe the moisture transport when the fibre is surrounded by humid air. If the fibre is surrounded by water, the equations are different. In [24] it is suggested how to describe the sorption process in such a case.

2.3.2. Effects on mechanical properties

The mechanical properties of the plant fibre are affected by the moisture content. Since no information of how the stiffness of flax and hemp are affected by the moisture content could be found in the literature, the chemical constituents are described in this section. A thorough review of how the mechanical properties of the plant constituents are influenced by moisture have been carried out by Persson [25]. The review is concerning wood fibres but the plant cells seem to contain the same substances, although with different proportions and geometry.

The stiffness of the microfibrils is believed to be independent of the moisture content. The microfibril is regarded to be a transversely isotropic material. This means that the stresses in the plane perpendicular to the axial direction are isotropic. The stiffness matrix of such a material can be written as [25]:

$$\boldsymbol{D}_{\mathrm{C}} = \begin{bmatrix} D_{11} & D_{12} & D_{12} & 0 & 0 & 0 \\ D_{12} & D_{22} & D_{23} & 0 & 0 & 0 \\ D_{12} & D_{23} & D_{22} & 0 & 0 & 0 \\ 0 & 0 & 0 & D_{44} & 0 & 0 \\ 0 & 0 & 0 & 0 & D_{44} & 0 \\ 0 & 0 & 0 & 0 & 0 & \frac{1}{2}(D_{22} - D_{23}) \end{bmatrix} \qquad 2.6$$

where the 1-direction is along the axis of the fibril and the 23-plane is isotropic. The index C indicates cellulose. Stiffness data for native cellulose is reported in [25] and shown in Table 2.5. By means of this data and ***C***-matrix shown in appendix, the components of the $\boldsymbol{D}_{\mathrm{C}}$ matrix for native cellulose can be calculated.

Table 2.5 *Stiffness coefficients of native cellulose* [25].

Coefficient	*Value*	*Method and Reference*
E_{11} (GPa)	135	Measured, ref 60 in [25]
	138	Measured, ref 47 in [25]
	140	Measured, ref 43 in [25]
	168	Molecular model, ref 68 in [25]
E_{22} (GPa)	17.7	Molecular models, ref 68 in [25]
	27	Molecular model, ref 41 in [25]
	18	Estimated, ref 12 in [25]
G_{12} (GPa)	4.4	Molecular model, ref 41 in [25]
	5.1	Molecular models, ref 68 in [25]
$G_{23} = 2(1+\nu_{12})/E_{22}$	-	-
ν_{12}	0.011	Molecular model, ref 41 in [25]
	<0.005	Molecular model, ref 68 in [25]
	0.047	Estimated, ref 12 in [25]
ν_{23}	0.52	Molecular model, ref 68 in [25]
	0.48	Estimated, ref 12 in [25]

The stiffness of hemicellulose depends strongly on the moisture content. Cousins (reference 14 in [25]) measured the stiffness on hemicellulose extracted from wood fibres at different moisture contents, which proved to be isotropic. The relation is shown in Figure 2.16. The moisture content of hemicellulose is related to the surrounding humid air and has been measured by Cousins. The relation is shown in Figure 2.17. For instance, at equilibrium 20 % RH gives a moisture content of 8 % and 60 % RH a moisture content of 16 %.

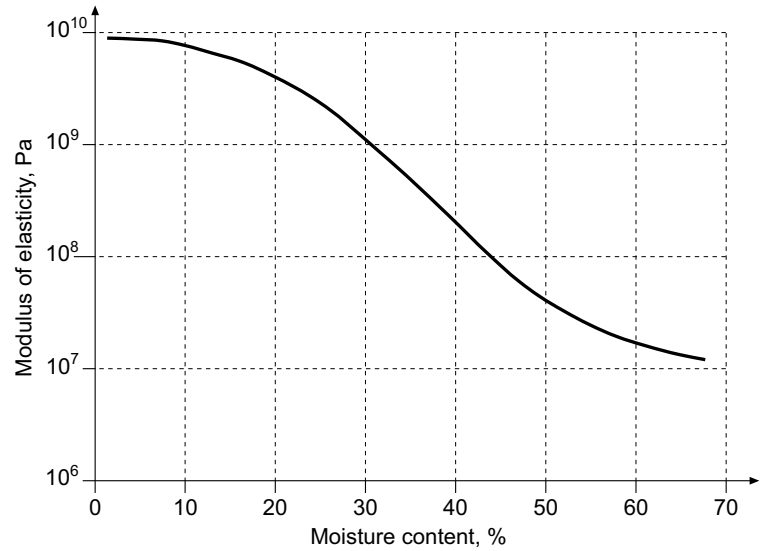

Figure 2.16 *Stiffness of extracted hemicellulose versus the moisture content* [25].

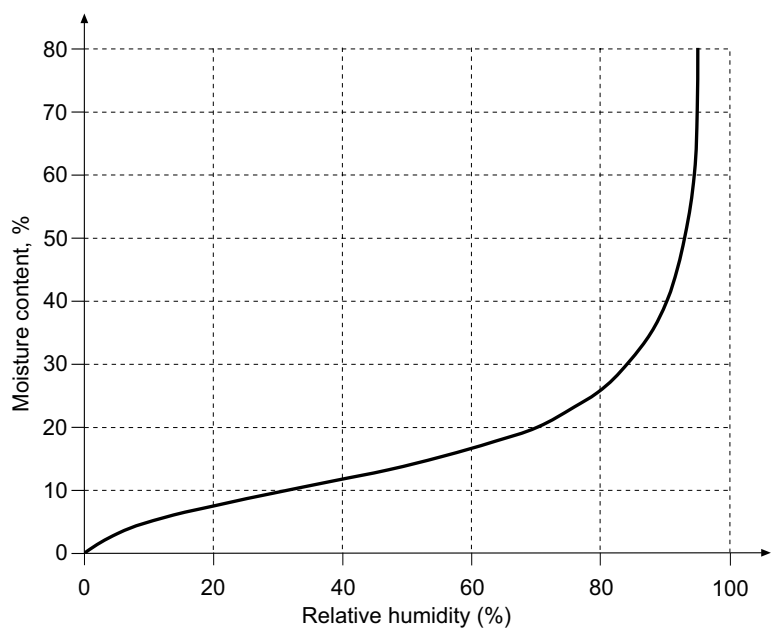

Figure 2.17 *Moisture content of extracted hemicellulose versus the relative humidity* [25].

In the fibre, the hemicellulose molecules tend to align with the fibril axis, which leads to an anisotropic material behaviour. Based on Cousins experiments, Cave (reference 12 in [25]) have suggested that hemicellulose (in the fibre) can be described as a transversely isotropic material:

$$\boldsymbol{D}_{\mathrm{H}}(\mathrm{w}) = \begin{bmatrix} 8 & 2 & 2 & 0 & 0 & 0 \\ 2 & 4 & 2 & 0 & 0 & 0 \\ 2 & 2 & 4 & 0 & 0 & 0 \\ 0 & 0 & 0 & 1 & 0 & 0 \\ 0 & 0 & 0 & 0 & 1 & 0 \\ 0 & 0 & 0 & 0 & 0 & 1 \end{bmatrix} c_{\mathrm{H}}(\mathrm{w}) \qquad 2.7$$

where $c_{\mathrm{H}}(\mathrm{w})$ is a moisture dependent function fitted to the experimental data shown in Figure 2.16. The values of the matrix are chosen to show the relation between different components of the matrix and are not to be taken as absolute physical properties. Following Figure 2.16 and Figure 2.17, a relative humidity of 60 % gives a moisture content of about 16 %, which gives a stiffness of the extracted isotropic hemicellulose of approximately 8 GPa. Since hemicellulose is considered as a transversely isotropic material in the fibre, the stiffness in the direction of the cellulose fibrils (11-direction) is higher and the transverse directions are lower. Estimates of stiffness coefficients at 60 % RH can be found in [25] and are summarised in Table 2.6. The curve presented in Figure 2.16 has to be scaled to these estimated stiffness coefficients. The scaled curve is the function $c_{\mathrm{H}}(\mathrm{w})$.

Table 2.6 *Stiffness coefficients of native cellulose* [25].

Coefficient	*Value*
E_{11}, GPa	14.0-18.0
E_{22}, GPa	3.0-4-0
G_{12}, GPa	1.0-2.0
ν_{12}	0.1
ν_{32}	0.40

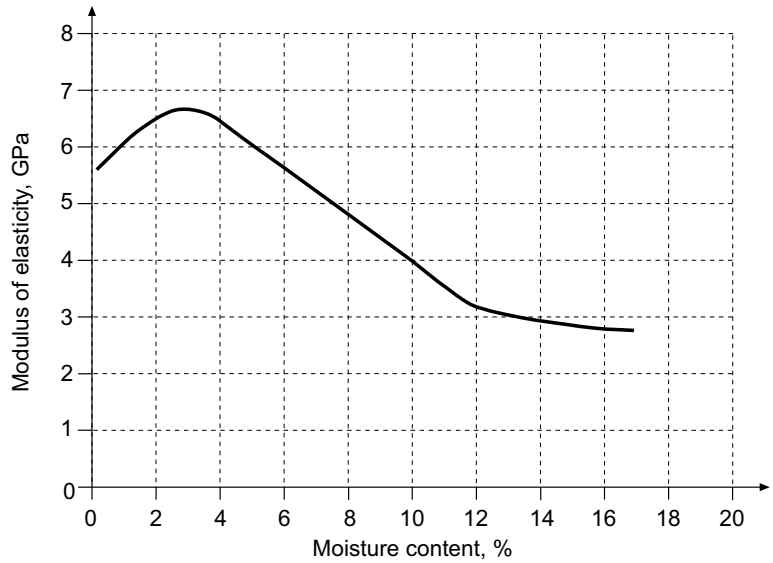

Figure 2.18 *Stiffness of lignin versus the moisture content* [25].

The stiffness of lignin also depends on the moisture content but to a lesser extent than hemicellulose. Lignin is amorphous and regarded as an isotropic material. Reference 12 in [25] have suggested the moisture dependent stiffness matrix $D_L(w)$ of lignin as

$$\boldsymbol{D}_L(w) = \begin{bmatrix} 4 & 2 & 2 & 0 & 0 & 0 \\ 2 & 4 & 2 & 0 & 0 & 0 \\ 2 & 2 & 4 & 0 & 0 & 0 \\ 0 & 0 & 0 & 1 & 0 & 0 \\ 0 & 0 & 0 & 0 & 1 & 0 \\ 0 & 0 & 0 & 0 & 0 & 1 \end{bmatrix} c_L(w) \qquad 2.8$$

where $c_L(w)$ is a moisture dependent function fitted to the experimental data of lignin shown in Figure 2.18 which is obtained in the same manner as for hemicellulose. As in the case of the stiffness matrix of hemicellulose the values in the stiffness matrix of lignin are not to be seen as absolute physical values.

As can be seen, the stiffness of the constituents of the elementary fibre is highly affected by the moisture content. Lacking experimental data for fibres, it is possible to determine their stiffness by micro mechanical modelling using the material data for the constituents. This is discussed in more detail in section 4.

The variation of strength of flax due to the moisture content has been examined in greater detail, than has the stiffness. In [15] it is reported that wet fibres have a 2-6% higher tensile strength than a dry fibre and in [26] it is reported a ~14% increase of strength. Reported values of increase of elongation at break are 25-30% and ~27 % respectively [15,26]. No values of strength of wet hemp fibres have been found in the literature. The tensile strength of elementary flax fibres has been measured at different levels of relative humidity [21]. The result is shown in Figure 2.19.

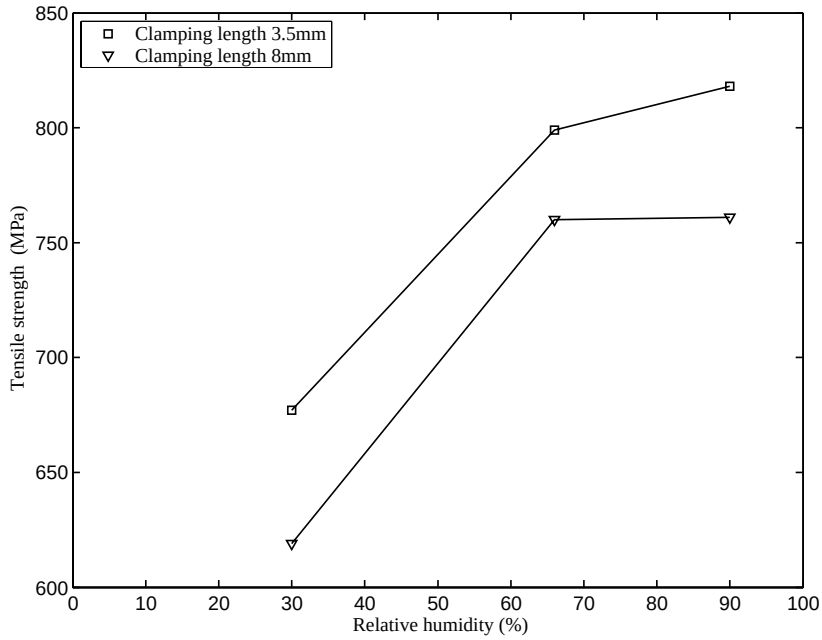

Figure 2.19 *Average tensile strength of flax fibres versus the relative humidity* [21].

2.3.3. Effects on durability

According to [27] flax fibres resists insect attacks and if the fibre is clean and dry, it has also a good resistance to attack by microorganisms. This suggests that the durability of a wet fibre is affected. However, a living proof that cellulose fibres used in composites is durable even when wet is the former East-German car brand Trabant. Trabant used a hybrid composite made of glass fibre and wood cellulose with a phenol resin in certain parts of the body. For daily use it is hard to find a more aggressive environment for a component than when it is used in exterior applications of a car. Since the constituents of wood and plant fibres seem to be similar, it is likely that flax and hemp fibres are rather resistant when wet as well, at least when within a phenol resin. The performance of flax and hemp might be similar to the performance of wood: it is durable when dry and when in water, but may rot if stored in air at a moisture content equal to or above the fibre saturation point.

2.3.4. Hygroexpansion

The fibre swells due to moisture. This is normally referred to as hygroexpansion or moisture induced expansion. Since no coefficients of hygroexpansion of flax and hemp have been found in the literature, the fibre constituents are described in this section. The description is obtained from [23], but applied to flax instead of wood.

Cellulose does not shrink or swell due to changes of the moisture content. Therefore, as in the case of stiffness, the microfibrils are assumed to be independent of moisture changes. The hemicellulose is assumed to be non expanding in the direction of the

microfibril and isotropic in the plane perpendicular to the direction of the microfibril [25]. The vectorial strain, $\Delta\boldsymbol{\varepsilon}_H^s$, due to hygroexpansion of hemicellulose can be approximated by:

$$\Delta\boldsymbol{\varepsilon}_H^s = \begin{bmatrix} 0 \\ 1/2 \\ 1/2 \\ 0 \\ 0 \\ 0 \end{bmatrix} \varepsilon_H^\circ(\Delta w_b) \qquad 2.9$$

The lignin is assumed to behave isotropically in hygroexpansion and its vectorial strain contribution, $\Delta\boldsymbol{\varepsilon}_L^s$, can be approximated by

$$\Delta\boldsymbol{\varepsilon}_L^s = \begin{bmatrix} 1/3 \\ 1/3 \\ 1/3 \\ 0 \\ 0 \\ 0 \end{bmatrix} \varepsilon_L^\circ(\Delta w_b) \qquad 2.10$$

The index *s* denotes hygroscopic expansion (swelling) and the indices *H* and *L* denotes hemicellulose and lignin respectively. The parameters ε_H° and ε_L° are functions of w_b and are related to the volumetric expansion of hemicellulose and lignin respectively. The variable w_b is the bound fraction of the absorbed water *w*. It is assumed that the parameters can be coupled to the volume of water absorbed by the hemicellulose and the lignin.

$$\varepsilon_H^\circ(\Delta w_b) = \Delta w_{bH}(w_b) \qquad 2.11$$

$$\varepsilon_L^\circ(\Delta w_b) = \Delta w_{bL}(w_b) \qquad 2.12$$

where Δw_{bH} and Δw_{bL} are the changes in bound water of hemicellulose and lignin respectively. Further, a relation between the total moisture content, *w*, and the bound water w_b is introduced;

$$w_b = b\ w \qquad 2.13$$

where *b* is a constant, which describes how much water is bound compared to the total amount of water.

It has been suggested that the bound water, w_b is divided between hemicellulose and lignin with the proportions 2.6:1, which yields that

$$\Delta w_{bH} = 2.6\Delta w_{bL} \tag{2.14}$$

The change of bound water can be written as

$$\Delta w_b = f_H \Delta w_{bH} + f_L \Delta w_{bL} \tag{2.15}$$

where f_H and f_L are the weight fractions of hemicellulose and lignin respectively. Now ε_H° and ε_L° can be written as

$$\varepsilon_H^\circ(\Delta w_b) = b\frac{2.6}{f_L + 2.6 f_H}\Delta w \tag{2.16}$$

$$\varepsilon_L^\circ(\Delta w_b) = b\frac{1}{f_L + 2.6 f_H}\Delta w \tag{2.17}$$

With the weight fractions of constituents of flax according to Table 2.2 adjusted to a dry fibre, the weight fractions of hemicellulose and lignin becomes f_H = 14.1% and f_L = 4.4%. Here the pectin has been assumed to behave as lignin. If all the absorbed water is assumed to be bound, i.e. b = 1, the strains due to hygroexpansion can be written as

$$\Delta\boldsymbol{\varepsilon}_H^s = \boldsymbol{\beta}_H(\Delta w) \tag{2.18}$$

$$\Delta\boldsymbol{\varepsilon}_L^s = \boldsymbol{\beta}_L(\Delta w) \tag{2.19}$$

where

$$\boldsymbol{\beta}_H = \begin{bmatrix} 0 \\ 3.166 \\ 3.166 \\ 0 \\ 0 \\ 0 \end{bmatrix} \tag{2.20}$$

and

$$\boldsymbol{\beta}_L = \begin{bmatrix} 0.812 \\ 0.812 \\ 0.812 \\ 0 \\ 0 \\ 0 \end{bmatrix} \tag{2.21}$$

Expression 2.20 and 2.21 can be used for determining the total hygroexpansion of the fibre. The methodology is discussed in section 4. The assumption that $b = 1$ has been used in [25], which gave a good correlation with experiments.

2.4. Miscellaneous mechanical properties

2.4.1. Creep

No information of the creep behaviour of flax and hemp fibres has been found in the literature. It is however likely that they behave as wood, since the constituents are believed to be the same. Wood creeps at constant moisture content, and change of the moisture content during loading increases the creep rate. If the load is high enough, wood experiences a creep-rupture. I.e. for a certain stress level the wood specimen fails after a certain time.

2.4.2. Fatigue

Fatigue of an elementary flax fibre has been examined by [10]. The test was carried out by applying a pulsating tensile force in the direction of the fibre. The force versus time is shown in Figure 2.20.
As mentioned in section 2.2, the fibre experiences a plastic deformation. The stiffness increases in every load-cycle until rupture occurs at approximately 200 cycles. The behaviour is shown in Figure 2.21.

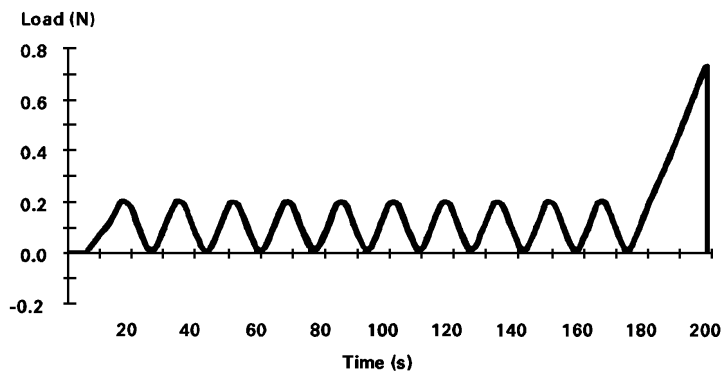

Figure 2.20 *Definition of fatigue tensile test* [10].

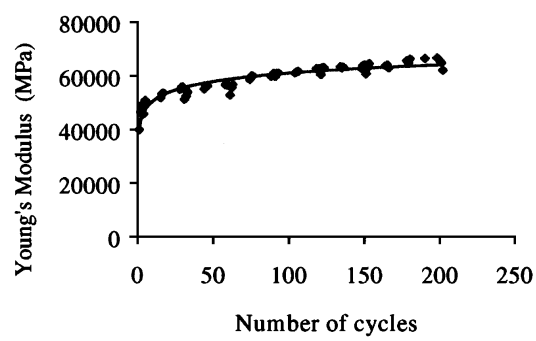

Figure 2.21 *Tensile fatigue test of single flax fibre. Evolution of the stiffness versus the number of cycles* [10].

2.4.3. Impact strength

The impact strength is related to the toughness of a material. In turn the toughness is related to the critical energy release rate G_c. G_c is a material property, which is a measure of how much energy per unit area that is needed to make a crack propagate. The energy balance, which must be fulfilled, for a crack to advance can be stated as:

$$\delta W \geq \delta U^{el} + G_c t \delta a \qquad 2.22$$

where δW is the energy due to external loads, δU^{el} is the change of elastic energy, t is the material thickness and δa is how much the crack advances.
The fracture toughness K_c is at plane stress related to G_c by

$$K_c = \sqrt{EG_c} \qquad 2.23$$

A crack is about to start to propagate in a stable or unstable manner when $K = K_c$, where K is the stress intensity factor of the crack.
No values of G_c or K_c have been found in the literature neither for flax nor for hemp.

3. Physical properties of matrix materials

The adhesive used for binding the fibres together in a composite is usually referred to as a matrix material. Many different types of matrix materials exist on the market, therefore only the most common materials will be covered in this text. Matrix materials can be divided into two groups, thermosetting and thermoplastic matrices. A thermosetting matrix is normally a mouldable resin, which after adding a curing agent, hardens to a network of the initial molecules. This process is irreversible. A thermoplastic matrix contains linear or branched molecule chains. At low temperatures weak van der Waal forces binds the molecules together creating a solid. At higher temperatures these forces decrease drastically which leads to that the material melts. When cooled the van der Waal forces reappear and the material solidifies. Hence, it is a reversible process [5]. Table 3.1 shows examples of thermosetting and thermoplastic matrices and some of their properties.

Table 3.1 *Properties of some thermosetting and thermoplastic matrices* [5].

Material	*Density (kg/m^3)*	*Tensile strength (MPa)*	*E-modulus (GPa)*
Thermo set			
Polyimide	1430-1890	100-110	3.1-4.9
Epoxy	1110-1400	49-85	2.6-4.5
Phenol Formaldehyde	1300-1500	17	4.1
Polyester	1100-1460	23-68	1.0-4.6
Thermoplastic			
Polyamide	1040-1140	70-84	1.5-3.3
Polyethylene	940-970	44	0.8
Polypropylene	900	31-42	1.1-2
Polycarbonate	1200	70	2.3
Polystyrene	1040-1090	50	3.3

The matrices shown in Table 3.1 are used for conventional composites such as glass fibre reinforced polyester or wood fibre particleboards with a phenol formaldehyde matrix and it seems that some of the matrices are possible to use for flax and hemp fibre composites as well. According to [28] the adhesion between the matrix and the fibre is not a problem when using a thermosetting resin since the functional groups on the surface of the fibres reacts with the resin, whereas it is a significant problem when using a thermoplastic matrix. A thermoplastic matrix, such as for instance polypropylene or polyethylene, has a bad compatibility with the lingocellulosic fibres. This is because the natural fibres are hydrophilic and the thermoplastic hydrophobic. Extensive research has been carried out in order to improve the compatibility between the fibre and the matrix. To mention one method, by adding the coupling agent maleic anhydride in polypropylene or polyethylene, the adhesion is increased.

In addition to the artificial matrices shown in Table 3.1, several biodegradable polymers usable as matrix materials are presented in [29,30].

4. Mechanical properties and modelling

4.1. General

In the process of designing a contemporary product it is of major importance to be able to predict the performance of the product. In this report, the performance of interest is limited to the mechanical properties of the composite material. During the last decade computer capacity has increased drastically which has lead to that complicated structures can be analysed accurately. It is fully possible to analyse a composite by modelling of the distinct phases on a microscale level [31]. This approach is however (still) too time consuming for large structures. Hence, it is more convenient to model the composite on a macroscale continuum level. An analogy is to model steel as a homogenous material instead of modelling the crystals and grains.

The method used when determining the macroscale continuum properties from the microscale properties, is referred to as homogenisation. The macroscale properties are obtained by analysing a representative volume element, RVE, of the composite on a microscale. Several different models of stiffness, strength, hygroexpansion etc are presented in the literature. Some of them are presented in this report.

Composite mechanics has developed during the latter part of the 20^{th} century. It seems that a lot of the theoretical and experimental work has been developed for artificial reinforcing materials in form of either continuous or short fibres or particles. Flax and hemp elementary fibres have a length/diameter ratio of more than 100. If this ratio is to be viewed as a continuous or a short fibre depends on the adhesion between the fibre and the matrix. If the fibre is damaged it might be more appropriate to consider the fibre as short.

As mentioned above a lot of research has been performed on composites based on artificial fibres. One of the advantages of artificial materials is their uniformity, which simplifies the modelling of stiffness and strength. For natural fibres with such a vast variation of both stiffness and strength a lot less research appears to have been performed.

The macroscopic properties of a composite, i.e. its density, stiffness, thermal and hygro expansion etc are determined by the equivalent properties of the fibre and matrix materials. A central parameter in micro mechanical modelling is the volume fraction of the fibres and the matrix. The volume fractions are V_f and V_m for the fibre and the matrix respectively. V_f and V_m are defined such that

$$V_f + V_m = 1 \qquad 4.1$$

This relation is valid if the composite is solid, i.e. it does not contain any pores.

4.2. Stiffness of the composite

4.2.1. The Voigt and Reuss approximation

By assuming that the strain in a RVE is homogeneous, the stiffness of a composite can be approximated by [32]:

$$\mathbf{D}_c = V_f \mathbf{D}_f + V_m \mathbf{D}_m \qquad 4.2$$

where $\mathbf{D}_c$, $\mathbf{D}_f$ and $\mathbf{D}_m$ are the stiffness matrices of the composite, fibre and the matrix respectively. V_f is the volume fraction of the fibres and V_m the volume fraction of the matrix.
Equation 4.2 is referred to as the Voigt approximation, the rule of mixture (ROM) or the parallel-coupling model. The approximation might be more familiar in its one-dimensional form [5]:

$$E_c = V_f E_f + V_m E_m \qquad 4.3$$

where E_c, E_f and E_m are the E-modulus of the composite, the fibre and the matrix respectively.

If the stress field is assumed to be homogeneous, the compliance matrix can be approximated according to [32]:

$$\mathbf{C}_c = V_f \mathbf{C}_f + V_m \mathbf{C}_m \qquad 4.4$$

and its one-dimensional form

$$\frac{1}{E_c} = \frac{V_f}{E_f} + \frac{V_m}{E_m} \qquad 4.5$$

which is referred to as the Reuss approximation or the series-coupling model.

It should be mentioned that both the Voigt and Reuss approximations are incorrect on the microscale level. Assuming a uniform strain field of the RVE leads to that the tractions at the boundaries of the phases cannot be in equilibrium. Similarly, if the stress field is assumed to be uniform, the matrix and the reinforcement material cannot remain bonded.

Although these approximations are incorrect on the microscale level, they are the most important equations for determining the stiffness of a composite. This is because they are the upper and lower bounds of the stiffness of a composite, independent of the geometry of the constituents. The Voigt model gives the upper bound of stiffness and the Reuss model the lower bound. This has been shown by [33].

4.2.2. The Halpin-Tsai equations

For composites with short unidirectional fibres, the Halpin-Tsai equations are often employed [5]. First two constants are determined according to equations 4.6 and 4.7.

$$C_L = \left[\frac{\frac{E_f}{E_m} - 1}{\frac{E_f}{E_m} + \frac{2L_f}{d_f}} \right] \tag{4.6}$$

where L_f is the length and d_f is the diameter of the fibres.

$$C_T = \left[\frac{\frac{E_f}{E_m} - 1}{\frac{E_f}{E_m} + 2} \right] \tag{4.7}$$

The stiffness of the composite in the direction of the fibres is then determined by:

$$E_L = E_m \left[\frac{1 + \frac{2L_f V_f C_L}{d_f}}{1 - C_L V_f} \right] \tag{4.8}$$

and in the transversal direction according to:

$$E_T = E_m \left[\frac{1 + 2V_f C_T}{1 - C_T V_f} \right] \tag{4.9}$$

4.2.3. Arbitrarily oriented fibres

A common way to use bast fibres is in curved or non-curved plates where the orientation of the fibres is distributed arbitrarily tangentially to the surface of the plate. By calculating the stiffness of a unidirectional fibre composite by means of the Voigt approximation and integrating all the infinitesimal contributors, the in-plane stiffness of the composite can be approximated as [31]:

$$\mathbf{D}_c = \int_0^{\pi} \mathbf{D}_u f(\varphi)\, d\varphi \tag{4.10}$$

where $f(\varphi)$ is the fibre orientation distribution in the plane with the angle φ measured from the x-axis and $\mathbf{D}_u$ is the stiffness matrix of the unidirectional fibre

composite transformed to the global coordinate system. The relation can also be extended to three dimensions for composites with spatial fibre orientation distribution.

$$\mathbf{D}_c = \int_0^{\pi} \mathbf{D}_u \psi(\varphi,\theta) \sin\theta \, d\varphi \, d\theta \qquad 4.11$$

where $\psi(\varphi,\theta)$ is the spatial fibre orientation distribution in a spherical coordinate system where the angle θ is measured between the fibre and the z-axis and φ is the angle between the projection of the fibres to the x-y plane and the x-axis.

4.2.4. Fibres with large variation of stiffness

Artificial materials such as glass and carbon fibres have uniform values of stiffness, which is not the case for natural fibres. This has the consequence that it might not be sufficient to use average values of stiffness of natural fibres. The large variation has to be dealt with in some manner. [34] has performed extensive measurements of the stiffness of flax fibres. The result reveals that the stiffness of the fibres decrease with increasing fibre diameter. Average values of stiffness vary from 78.7 GPa to 39.0 GPa at a diameter of 6.8 μm to 34.5 μm respectively. By classifying the diameter into classes and counting the number of fibres in each class a more accurate value of the stiffness in the direction of the fibres of a unidirectional composite can be obtained as [30]:

$$E_c = \sum_{i=1}^{n} \frac{n_i d_i^{\,2}}{\sum_{i=1}^{n} n_i d_i^{\,2}} E_i + V_m E_m \qquad 4.12$$

where n_i is the number of fibres in each class, d_i is the diameter in each class, E_i is the stiffness of the fibres in each class and n is the number of classes. Equation 4.12 is a development of the Voigt approximation in one dimension. It might be possible to generalise equation 4.12 to a continuous expression where the summations are replaced by integrals over a distribution function. Moreover, a generalisation to 2 and 3 dimensions might be possible.

4.2.5. Other models of stiffness

The sought after accurate predictions of stiffness has provided many different models. Interpolation between the Voigt and Reuss models [35,36], the self-consistent scheme [37] (particle composites) and the Hashin-Shtrikman bounds [38,39] are examples of such models. Several textbooks cover the mechanics of heterogeneous materials. For a thorough treatment, for instance [32,40,41], may be consulted.

4.2.6. Experimental values

In order to grasp the mechanical performance of flax or hemp fibre reinforced composites, for instance [42] may be referred to. In this article, both flax and hemp fibre-epoxy composites have been examined experimentally. The result of the tensile tests is presented in Table 4.1. As can be seen in the table, retted hemp fibres yield a

stiffer composite than unretted fibres. The reason according to [38] is that the resin can penetrate into the fibre tissue between the bundles where the retting has caused gaps to appear. In the composite containing unretted fibres the adhesion is poor between the fibre and the matrix. The exact mechanism leading to a lower stiffness is however not explained. One possible reason is that the strain increases, for a given stress, due to shearing of the matrix in between the fibres or maybe even slipping might occur. Slipping would however lead to a non-linear constitutive behaviour of the tensile performance of the composite.

Table 4.1 *Mechanical properties of flax and hemp fibre composites. M = mean, S = standard deviation, COV = coefficient of variation, n = number of specimens tested* [42].

Fibre and treatment			*E-modulus (GPa)*			*Strength (MPa)*		
	V_f	n	M	S	COV	M	S	COV
Unretted flax, mechanically decorticated	0.5	2	4.65	-	-	59.5	-	-
Unretted hemp, carefully extracted	0.5	3	4.5	0.3	6.7 %	62	1.15	1.9 %
7 days retted hemp, carefully extracted	0.5	4	12.65	2.27	17.9 %	145.5	8.1	5.6 %

4.3. Failure of the composite

The models of stiffness discussed above correlates quite well with experimental results. Models of failure and strength are much more difficult to achieve. According to [41], no accurate general models exist (1998) for predicting failure. It seems that this is the case also today. A general model should be able to predict failure at all levels of analysis, all load conditions and all types of composites [41].

The failure of a composite is often a consequence of accumulated damages/failures on the micro-level of the composite. It is hence, necessary to understand the failure mechanisms on the fibre and matrix level. The failure mechanisms on the micro level of the composite are fibre fracture, fibre buckling (kinking), fibre splitting, radial cracks, fibre pullout, debonding between the fibre and the matrix and matrix cracking. The description of failure mechanisms above is valid for unidirectional composites. Fibre fracture occurs when the strength of the fibre is attained either in tension or in compression. When the composite is subjected to compression it is more common that the composite fails due to local buckling of the fibres. Fibre fracture is often followed by fibre pullout accompanied by debonding of the fibres from the matrix. Fibre splitting and radial cracks in the fibre occur due to transversal stress and finally, matrix cracking occurs when the strength of the matrix is exceeded.

4.3.1. Axial tensile strength of composites with continuous fibres

The axial tensile strength of a unidirectional composite can be estimated by assuming that the composite contains continuous identical fibres aligned in a homogeneous manner. Equilibrium in the axial direction then yield the composite average stress [5,41]:

$$\sigma_c^{ult} = \sigma_f' V_f + \sigma_m' V_m \qquad 4.13$$

where σ_f' is the stress in the fibre and σ_m' is the stress in the matrix at composite failure.
Fracture of the composite occurs when either the fibre or the matrix fails. The strength of a composite failing due to fibre fracture is called the *fibre dominated composite failure stress*, which can be estimated by:

$$\sigma_c^{ult} = \sigma_f^{ult} V_f + \sigma_m' \left(1 - V_f\right) \qquad 4.14$$

where it has been assumed that the composite does not contain any pores, i.e. $V_f + V_m = 1$, and that the failure strain of the matrix is larger than the failure strain of the fibre. For the fibre to actually be reinforcing, the stress in the fibre portion at fracture must be larger than the stress in the matrix portion of the composite volume after fracture of all fibres. If the portion of fibres is too low, the composite will not fail after fibre fracture. Instead, the matrix will be able to carry the load. In such a case, the failure stress of the composite can be estimated by:

$$\sigma_c^{ult} = \sigma_m^{ult}\left(1 - V_f\right) \quad 4.15$$

Thus, it is evident that the volume fraction of fibres has to exceed a critical number in order to supply reinforcement. The critical fibre volume fraction is given by:

$$V_f^{crit} = \frac{\sigma_m^{ult} - \sigma_m'}{\sigma_f^{ult} - \sigma_m'} \quad 4.16$$

Equation 4.14-4.16 are valid when the limit failure strain of the matrix is greater than that of the fibres. When the opposite is prevailing, the fibre has to carry the entire load when the matrix fails. For low fibre fractions, the fibres will however not be able to carry the load. Thus the composite fails at matrix failure. In that case, the strength of the composite can be obtained by:

$$\sigma_c^{ult} = \sigma_f' V_f + \sigma_m^{ult}\left(1 - V_f\right) \quad 4.17$$

When the fibre fraction is high, the entire load is carried by the fibres after matrix failure. Hence, the strength of the composite can be estimated by:

$$\sigma_c^{ult} = \sigma_f^{ult} V_f \quad 4.18$$

If equation 4.17 or 4.18 should be used can be determined by setting the equations equal and solving for the fibre volume fraction.

4.3.2. Axial tensile strength of composites with non-continuous fibres

The strain field in axially loaded composites with continuous fibres is homogeneous. This is not the case in composites with non-continuous fibres. Short (or broken) fibres in the composite have the consequence that the strain field becomes inhomogeneous. If the fibre is short enough, the strain in the fibre is lower than in the matrix. For an increased fibre length the strain difference is smaller and finally the strain in the fibre and the matrix are equal. The length of the fibre at this point of equality is referred to as the critical fibre length, L_{crit}.

The critical length of a circular fibre can be estimated by assuming that the strain in the matrix is constant. Moreover, it is assumed that the strain in the fibre increases linearly from zero at the end surface of the fibre to the same level as in the matrix. This results in a critical fibre length according to [5]:

$$L_{crit} = \frac{\sigma_{\max} r_f}{\tau} \quad 4.19$$

where $\sigma_{\max}$ is the maximum stress in the fibre, r_f is the radius of the fibre, and τ is the maximal shear stress of the interface between the fibre and the matrix. Equation 4.19 shows that for a given fibre, a short critical length can be obtained by increasing

the adhesion between the matrix and the fibre. The average stress in the fibre can with the same assumptions be estimated by [5]:

$$\overline{\sigma}_f = \sigma_{\max}\left(1-\frac{L_{crit}}{2L_f}\right) \qquad 4.20$$

The short fibre ruptures at the location where the tensile stress is reached. The stress in the fibre just before rupture is then obtained by replacing $\sigma_{\max}$ with σ_f^{ult} in equation 4.20. With this in mind, the strength of a short fibre composite can be estimated by [5]:

$$\sigma_c^{ult} = \sigma_f^{ult} V_f\left(1-\frac{L_{crit}}{2L_f}\right)+\sigma'_m\left(1-V_f\right) \qquad 4.21$$

This relation shows that a full reinforcement can be obtained by using a high ratio between the fibre length and the critical fibre length, L_f/L_{crit}. Equation 4.21 is not valid for fibres with variation of strength as is the case with natural fibres.

4.3.3. Consideration to varying fibre strength

In composites containing fibres with large variation of strength, the fibres will fail successively. This leads to that the reinforcing effect will disappear on a length equal to the critical fibre length for each fractured fibre.

An important tool when dealing with variations of strength is Weibull statistics. Weibull [43] suggested that the probability of rupture, P_f, of a body in uniaxial homogenous tension can be described by:

$$P_f = 1-e^{-V\left(\frac{\sigma}{\sigma_0}\right)^m} \qquad 4.22$$

where V is the volume of the specimen, σ is the applied stress and σ_0 and m are two material parameters. The parameter m is related to the coefficient of variation in strength, e.g. $m = 2$ corresponds to COV ≈ 52 % and $m = 4$ corresponds to COV ≈ 28 %. The Weibull distribution has been modified by for instance [44] so that the volume, V, of the material can be referred to a reference volume, V_0.

$$P_f = 1-e^{-\frac{V}{V_0}\left(\frac{\sigma}{\sigma_0}\right)^m} \qquad 4.23$$

For fibres with identical cross sectional area the term V/V_0 may be replaced by the length ratio L/L_0. By taking the natural logarithm of the survival probability, $P_s = 1\text{-}P_f$, two times, the following is obtained:

$$\ln\ln\left(\frac{1}{P_s}\right) = \ln L - \ln L_0 + m\ln\sigma - m\ln\sigma_0 \qquad 4.24$$

The median strength of the fibres can be determined by calculating the stress where 50 % of the fibres have ruptured, i.e.

$$\ln\overline{\sigma}_f^{ult} = -\frac{1}{m}\ln L + k \qquad 4.25$$

where $k = \frac{1}{m}\ln\ln(2) + \frac{1}{m}\ln L_0 + \ln\sigma_0$.

The median strength then becomes:

$$\overline{\sigma}_f^{ult} = \frac{e^k}{L^{1/m}} \qquad 4.26$$

Proceeding by setting $\sigma_{\max} = \overline{\sigma}_f^{ult}$ in equation 4.19 and 4.20 yields:

$$\overline{\sigma}_f = \frac{e^k}{L_f^{1/m}}\left(1 - \frac{e^k r_f}{2L_f^{(1+1/m)}\tau}\right) \qquad 4.27$$

Inserting equation 4.27 into equation 4.14 gives the following estimate of the strength of a composite containing non-continuous fibres with large variation of strength:

$$\sigma_c^{ult} = \frac{e^k}{L_f^{1/m}}\left(1 - \frac{e^k r_f}{2L_f^{(1+1/m)}\tau}\right)V_f + \sigma'_m V_m \qquad 4.28$$

It should be pointed out that equation 4.28 does not take into account that the stress increases when fibres rupture successively: the Weibull model is a weakest-link model, meaning that the entire body is assumed to fail as soon as the weakest part fails.

In order to illustrate the importance of the fibre length, equation 4.27 is plotted in Figure 4.1 for different values of m and τ. The parameters used for the plot are; L_0 = 10 mm, σ_0 = 700 MPa, r_f = 10 μm.

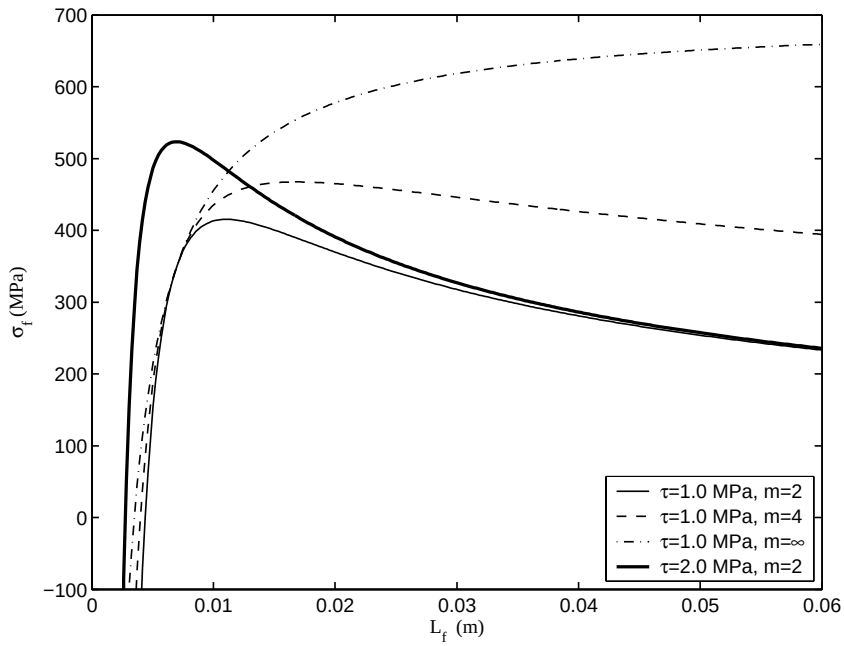

Figure 4.1 *Fibre strength according to equation 4.27.*

Figure 4.1 shows that a short fibre length gives a low reinforcement factor, which increases rapidly for an increased fibre length until the optimum length is reached. If the fibre length is increased more, the likelihood of damages on the fibre increase, which leads to that the strength of the fibre decreases. This is sometimes referred to as the Weibull or the size effect. Obviously, equation 4.27 reveals a drawback for very short fibres. When the fibre length decreases towards zero, $\overline{\sigma}_f$ increases towards negative infinity. This is, of course, not possible in reality.

In the equations above it is assumed that the cross sectional area of the fibres is constant. The diameter of flax and hemp fibres varies between approximately 10 and 40 μm and hence, the equations need to be modified for the variation of cross sectional area as well.

4.3.4. Axial compressive strength

Compressive failure of a unidirectional composite is somewhat different from a tensile failure. The failure mechanism is usually not only related to the compressive strength of the constituents, but rather to an instability phenomenon on the micro mechanical level. This phenomenon is often referred to as micro mechanical buckling which is influenced by for instance fibre size and shape, fibre waviness, strength of the interface between fibre and matrix and stiffness of the fibre and the matrix. In this section only three models of compressive strength will be treated.

Micro mechanical buckling basically occurs in the two different modes as shown in Figure 4.2. These are referred to as strain mode and shear strain mode. By applying

elementary beam theory for compressed beams on a lamella, where the lamella is assumed to consist of linear elastic fibres with a rectangular cross section embedded in a linear elastic medium (the matrix), the following estimates of the compressive strength are obtained [45].

The strain mode buckling strength:

$$\sigma_c^{comp} = \left[V_f + (1 - V_f)\frac{E_m}{E_f} \right] \sqrt{\frac{4V_f}{3(1 - V_f)} E_f E_m} \qquad 4.29$$

and the shear strain mode:

$$\sigma_c^{comp} = \frac{G_m}{1 - V_f} \qquad 4.30$$

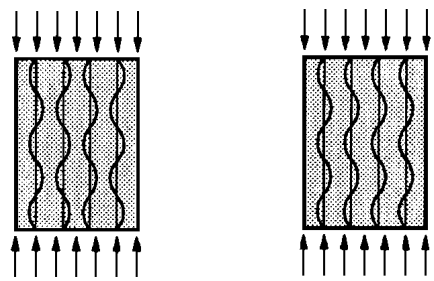

Figure 4.2 *Fibre deformations in a compressed lamella. Left figure shows the strain mode and the right figure the shear strain mode* [45].

Both equation 4.29 and 4.30 overestimates the compressive strength as can be seen in the example below. A model proposed by Hahn and Williams (1986) has shown good results when comparing with experimental data [41]. The model includes fibre imperfection (fibre curvature) and assumes an elastic-perfectly plastic composite with strong fibres and reads:

$$\sigma_c^{comp} = V_f \left(\frac{G_{12}\tau_y}{\tau_y + \frac{\pi f_0 G_{12}}{L}} \right) \qquad 4.31$$

where G_{12} is the shear modulus of the composite, τ_y is the shear yield stress and f_0 / L is a fibre curvature ratio.

As an example, a composite containing fibres with $E_f = 50\,\text{GPa}$ and $G_f = 19.23\,\text{GPa}$ and a matrix with $E_m = 3\,\text{GPa}$ and $G_f = 1.15\,\text{GPa}$ is analysed by equation 4.27-29. The shear yield stress is $\tau_y = 50\,\text{MPa}$, $f_0 / L = 0.005$ and G_{12} is estimated by:

$$\frac{1}{G_{12}} = \frac{V_f}{G_f} + \frac{\left(1 - V_f\right)}{G_m} \qquad 4.32$$

The result is presented in Figure 4.3 and clearly reveals that the strain and shear strain mode models overestimates the compressive strength. At a volume fraction of 50% the strain mode model gives a compressive strength of 7500 MPa, the shear strain mode model 2300 MPa and the Hahn and Williams model 650 MPa. The latter value is reasonable compared to the others.

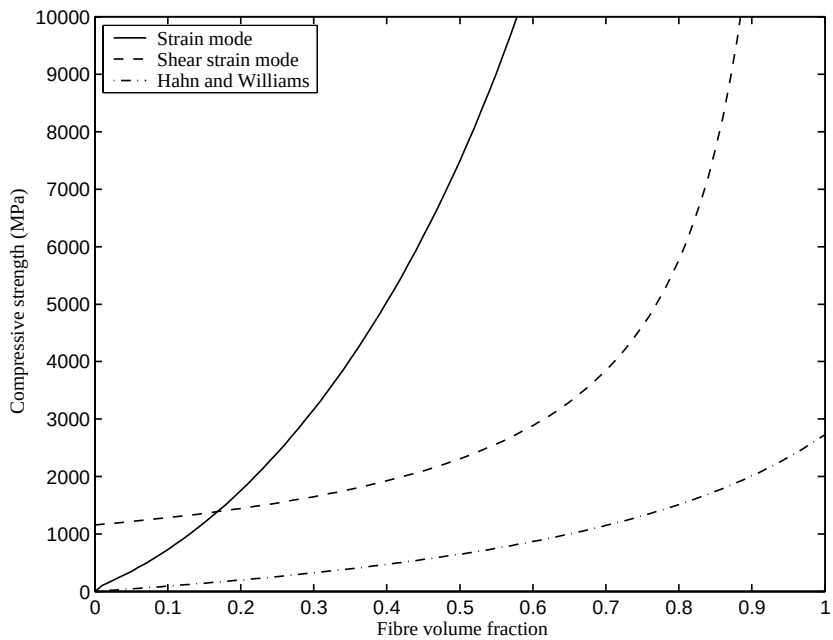

Figure 4.3 *Compressive strength versus the fibre volume fraction.*

4.3.5. Continuum failure theories

The information in this section is, if nothing else is stated, obtained from [41].

In the following section the unidirectional composite is assumed to be a continua i.e. the material is viewed as a homogenous continuum on the macro scale level. The material is assumed to be orthotropic with known strengths in the one-dimensional principal material directions. The principal material directions 1 and 2 are shown in Figure 4.4, the 3rd direction is perpendicular to the 1st and the 2nd.

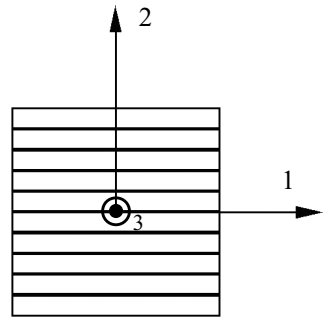

Figure 4.4 *Principal material directions.*

In the principal directions there is no sign dependence of the shear stress, whereas in another coordinate system the sign of the shear stress has a great influence on the stress in the principal coordinate system. This is illustrated in Figure 4.5.

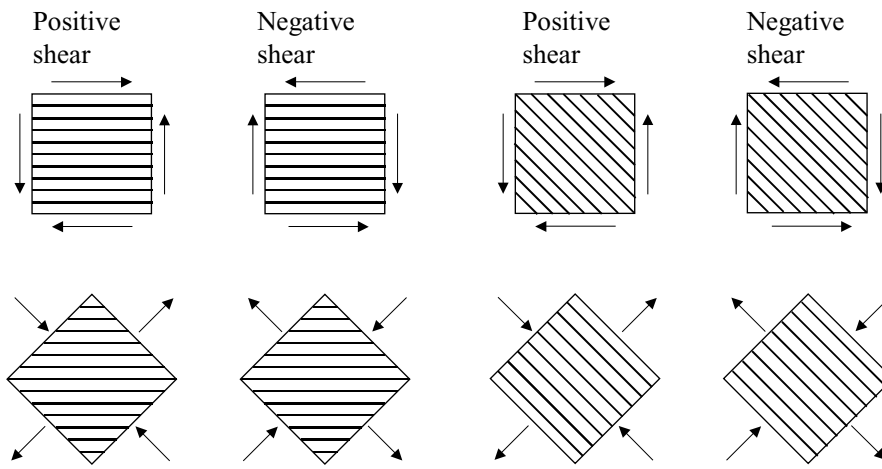

Figure 4.5 *Pure shear and its principal stresses in a unidirectional composite.*

Since the strengths in the different principal material directions are very different, positive and negative shear strength will vary vastly in the off axis directions.

Maximum stress theory

In the maximum stress theory, it is assumed that the composite fails when one component of stress reaches the maximum (or minimum) allowable value independent of the other stress components. The allowable stress level has to be determined in the principal material directions for each stress component. The failure criterion can then be stated as:

$$
\begin{aligned}
&\sigma_1^{C\max} < \sigma_1 < \sigma_1^{T\max} \\
&\sigma_2^{C\max} < \sigma_2 < \sigma_2^{T\max} \\
&\sigma_3^{C\max} < \sigma_3 < \sigma_3^{T\max} \\
&|\tau_{12}| < \tau_{12}^{\max} \\
&|\tau_{31}| < \tau_{31}^{\max} \\
&|\tau_{23}| < \tau_{23}^{\max}
\end{aligned}
\qquad 4.33
$$

where *T* indicates tension and *C* indicates compression.

For stress states others than the principal material directions, the maximum stress criterion can be transformed into another coordinate system. In order to illustrate this, the following example is useful. Consider a unidirectional composite with the off-axis loading σ_x as shown in Figure 4.6.

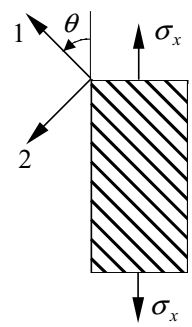

Figure 4.6 *Off-axis tensile strength.*

By assuming plane stress, the stress state can be transformed to:

$$
\begin{aligned}
&\sigma_1 = \sigma_x \cos^2\theta \\
&\sigma_2 = \sigma_x \sin^2\theta \\
&\tau_{12} = -\sigma_x \sin\theta\cos\theta
\end{aligned}
\qquad 4.34
$$

Inserting equation 4.34 in 4.33 yields:

$$
\begin{aligned}
&\frac{\sigma_1^{C\max}}{\cos^2\theta} < \sigma_x < \frac{\sigma_1^{T\max}}{\cos^2\theta} \\
&\frac{\sigma_2^{C\max}}{\sin^2\theta} < \sigma_x < \frac{\sigma_2^{T\max}}{\sin^2\theta} \\
&|\sigma_x| < \left|\frac{\tau_{12}^{\max}}{-\sin\theta\cos\theta}\right|
\end{aligned}
\qquad 4.35
$$

Equation 4.35 states that σ_x is safe if it lies within the limit values. For different angles θ, one of the three failure modes will give the lowest value, which is the current failure stress.

It should be mentioned that the maximum stress failure criterion is limited when trying to predict failure stress in multi-axial loading since there is no coupling between the stress components.

Tsai-Hill theory

The Tsai-Hill failure criterion is an application of Hill's anisotropic plasticity model to anisotropic failure. The failure surface is given by:

$$\begin{aligned}&(G+H)\sigma_1{}^2+(F+H)\sigma_2{}^2+(F+G)\sigma_3{}^2-2H\sigma_1\sigma_2-2G\sigma_1\sigma_3\\&-2F\sigma_2\sigma_3+2L\tau_{23}{}^2+2M\tau_{13}{}^2+2N\tau_{12}{}^2=1\end{aligned} \qquad 4.36$$

where *F, G, H, L, M* and *N* are parameters related to the strength of the material. These parameters can be expressed in the one-dimensional failure stresses by looking at the different possible one-dimensional stress states. As an example the stress state pure shear, $\tau_{12}\neq 0$ and all other stress components equal to zero yields:

$$2N=\frac{1}{\tau_{12}^{\max}} \qquad 4.37$$

Continuing in this manner for all possible one-dimensional stress states, gives all the material strength parameters expressed in the one-dimensional failure stress.

For the off-axis stress state, as shown in Figure 4.6, the failure criterion becomes:

$$\frac{\cos^4\theta}{\sigma_1^{\max 2}}+\left(\frac{1}{\tau_{12}^{\max 2}}-\frac{1}{\sigma_1^{\max 2}}\right)\sin^2\theta\cos^2\theta+\frac{\sin^4\theta}{\sigma_2^{\max 2}}=\frac{1}{\sigma_x^2} \qquad 4.38$$

Evidently, the Tsai-Hill failure criterion reveals a severe disadvantage. Since the equation is quadratic, no distinction between positive (tensile) and negative (compressive) strength is present. In general tensile and compressive strengths are not the same.

Tsai-Wu tensor polynomial failure criterion

In order to account for different tensile and compressive strengths, several tensor polynomial failure criteria have been suggested. They are invariant scalar functions of tensor quantities.

Here the Tsai-Wu tensor polynomial failure criterion is treated which reads [41]:

$$f(\tilde{\boldsymbol{\sigma}})=\tilde{\mathbf{F}}:\tilde{\boldsymbol{\sigma}}+\tilde{\boldsymbol{\sigma}}:\tilde{\tilde{\mathbf{F}}}:\tilde{\boldsymbol{\sigma}}\quad\text{or}\quad f(\sigma_{ij})=F_{ij}\sigma_{ij}+F_{ijkl}\sigma_{ij}\sigma_{kl} \qquad 4.39$$

or on reduced index notation

$$f(\sigma_i) = F_i\sigma_i + F_{ij}\sigma_i\sigma_j \qquad (i,j = 1,2,...,6) \tag{4.40}$$

where the components (F_i, F_{ij}) of the failure tensors are strength parameters.

Failure occurs when:

$$f(\sigma_i) \geq 1 \tag{4.41}$$

The Tsai-Wu criterion can be reduced to an orthotropic model by assuming that the failure tensors are symmetric and that the shear strengths are sign independent in the principal material directions. The orthotropic failure criterion becomes:

$$\begin{aligned} f(\sigma_i) = {} & F_1\sigma_1 + F_2\sigma_2 + F_3\sigma_3 + F_{11}\sigma_1^2 + F_{22}\sigma_2^2 + F_{33}\sigma_3^2 + F_{44}\sigma_4^2 + \\ & F_{55}\sigma_5^2 + F_{66}\sigma_6^2 + 2F_{12}\sigma_1\sigma_2 + 2F_{13}\sigma_1\sigma_3 + 2F_{23}\sigma_2\sigma_3 \end{aligned} \tag{4.42}$$

The components of the failure tensors can be expressed in the strengths in the principal material directions. This is carried out by working through the one-dimensional stress states. For instance, the axial stress state in tension and compression can be examined as follows.

For tensile failure at $\sigma_1 = \sigma_1^{T\max}$ the failure criterion can be reduced to:

$$F_1\sigma_1^{T\max} + F_{11}\sigma_1^{T\max\,2} = 1 \tag{4.43}$$

and for compressive failure at $\sigma_1 = \sigma_1^{C\max}$

$$F_1\sigma_1^{C\max} + F_{11}\sigma_1^{C\max\,2} = 1 \tag{4.44}$$

Solving equation 4.43 and 4.44 simultaneously gives:

$$F_1 = \frac{1}{\sigma_1^{T\max}} + \frac{1}{\sigma_1^{C\max}} \text{ and } F_{11} = \frac{-1}{\sigma_1^{T\max}\sigma_1^{C\max}} \tag{4.45}$$

For the off-axis stress state, as shown in Figure 4.6, the Tsai-Wu failure criterion becomes:

$$A\sigma_x^2 + B\sigma_x = 1 \tag{4.46}$$

where A and B are functions related to the load direction and the one-dimensional strength parameters. A and B are given by:

$$A = m^4\left(\frac{-1}{\sigma_1^{T\max}\sigma_1^{C\max}}\right) + n^4\left(\frac{-1}{\sigma_2^{T\max}\sigma_2^{C\max}}\right) + \frac{m^2n^2}{\tau_{12}^{\max 2}} \quad 4.47$$

$$B = m^2\left(\frac{1}{\sigma_1^{T\max}} + \frac{1}{\sigma_1^{C\max}}\right) + n^2\left(\frac{1}{\sigma_2^{T\max}} + \frac{1}{\sigma_2^{C\max}}\right) \quad 4.48$$

where $m = \cos\theta$ and $n = \sin\theta$.

4.3.6. Damage

In the models described in the previous section, failure has assumed to occur abruptly. In reality the fibre or the matrix fails successively forming micro cracks in the composite. Successive failures of the constituents lead to a non-linear material behaviour.

The interested reader can be referred to [41], where damage mechanics is thoroughly treated.

4.4. Modelling of hygroscopic and thermal expansion

Non-mechanical physical phenomena leading to deformations in a material are for instance hygroscopic and thermal expansion. These two effects are treated in this section. The models in this text are limited to an orthotropic level of anisotropy. The material behaviour is also assumed to be linear. The total strains in a composite subjected to elastic, hygroscopic and thermal deformation is commonly calculated by addition:

$$\boldsymbol{\varepsilon} = \boldsymbol{\varepsilon}^e + \boldsymbol{\varepsilon}^s + \boldsymbol{\varepsilon}^t \qquad 4.49$$

where $\boldsymbol{\varepsilon}^e$ are the elastic strains, $\boldsymbol{\varepsilon}^s$ are the hygroscopic strains and $\boldsymbol{\varepsilon}^t$ are the thermal strains.

Natural fibres as well as polymeric matrices absorb water, which leads to expansion of the composite. The hygroscopic strains are related to the moisture content in the composite, which is defined by [25]:

$$w = \frac{m_{H_2O}}{m_0} = \frac{m_w - m_0}{m_0} \qquad 4.50$$

where m_{H_2O} is the weight of the water, m_0 is the weight of the dry composite and m_w is the weight of the composite and the water. The linear orthotropic constitutive model for hygroscopic strains is expressed as a function of the moisture change and is given by:

$$\boldsymbol{\varepsilon}^s = \begin{bmatrix} \beta_1 \\ \beta_2 \\ \beta_3 \\ 0 \\ 0 \\ 0 \end{bmatrix} \Delta w = \boldsymbol{\beta}\, \Delta w \qquad 4.51$$

where β_i are the hygroscopic expansion coefficients in the principal material directions. For a transversely isotropic material two of the coefficients β_i are equal and for the isotropic case all β_i are equal.

Linear thermal expansion is treated mathematically exactly in the same manner but with the difference that the constitutive model is expressed as a function of temperature change instead of moisture change. The strains are modelled as:

$$\boldsymbol{\varepsilon}^t = \begin{bmatrix} \alpha_1 \\ \alpha_2 \\ \alpha_3 \\ 0 \\ 0 \\ 0 \end{bmatrix} \Delta T = \boldsymbol{\alpha}\, \Delta T \qquad 4.52$$

where α_i are the thermal expansion coefficients in the principal material directions. For a transversely isotropic material two of the coefficients α_i are equal and for the isotropic case all α_i are equal.

The constitutive equation for linear elasticity is given by:

$$\boldsymbol{\sigma} = \mathbf{D}\boldsymbol{\varepsilon}^e \qquad 4.53$$

where **D** is the stiffness matrix.

By using equation 4.49, the constitutive relation for elasticity, hygroscopic and thermal expansion becomes:

$$\boldsymbol{\sigma} = \mathbf{D}\boldsymbol{\varepsilon} - \mathbf{D}\boldsymbol{\varepsilon}^s - \mathbf{D}\boldsymbol{\varepsilon}^t \qquad 4.54$$

It should be mentioned that equation 4.54 is expressed in the principal material directions, but can easily be transformed into another coordinate system.

Having established the continuum constitutive relations for hygroscopic and thermal expansion it is necessary to be able to predict the coefficients from the behaviour of the constituents. According to [32], the effective coefficients of thermal (or hygroscopic) expansion of a two-phase composite with anisotropic elastic constituents and arbitrary geometry may be expressed as:

$$\boldsymbol{\alpha}_c^T = \boldsymbol{\alpha}_1^T + \left(\boldsymbol{\alpha}_2^T - \boldsymbol{\alpha}_1^T\right)\left(\mathbf{C}_2 - \mathbf{C}_1\right)^{-1}\left(\mathbf{C}_c - \mathbf{C}_1\right) \qquad 4.55$$

where $\boldsymbol{\alpha}_c$ is the thermal expansion of the composite and $\mathbf{C}_c$ is the compliance matrix of the composite. $\boldsymbol{\alpha}_1, \boldsymbol{\alpha}_2$ and $\mathbf{C}_1, \mathbf{C}_2$ are the thermal expansion coefficients and the compliance matrices for the two different phases respectively. The volume fractions of the different phases are included in equation 4.55 through the term $\mathbf{C}_c$, which is determined by some of the methods described above.

4.5. Homogenisation

Homogenisation is methods for obtaining the homogeneous macro scale continuum properties from the heterogeneous micro scale in a composite. The basic idea is that a small representative volume element (RVE) is analysed very accurately, yielding average properties of the RVE, which can be used for continuum modelling. Often, periodic boundary conditions are used for the RVE. This is because the RVE is chosen so that the adjacent RVE is similar [25,31,32,41].

A major advantage of homogenisation is that non-linear material behaviour of the constituents can be used. Several models of homogenisation are presented in the literature. Examples are; the method of cells (MOC), the generalised method of cells (GMC), the self-consistent method and the Mori-Tanaka method [41].
The most feasible way to predict advanced material behaviour appears to be the finite element method. With this method it is possible to homogenise composites containing constituents with complex geometries, non-linear materials and large deformation effects. Examples of non-linear materials are plasticity, non-linear elasticity and damage mechanics. Numerous studies have been performed on micro mechanical modelling using the finite element method. Examples are for instance [25,31,46,47].

4.6. Miscellaneous mechanical composite properties

4.6.1. Creep

No information of models of creep has been found in the literature for neither flax nor hemp composites. The creep behaviour is probably similar to wood or wood fibre composites. A simple creep model for a MDF is presented in [48].

A more elaborate model for creep behaviour of composites is presented in [49], where creep plasticity of polycrystals was homogenised using a second-order self-consistent scheme. A modification of this model might be possible to use for flax or hemp based composites.

In [50], two fibre bundle models are presented. They are based on microscopic mechanisms that lead to macroscopic creep behaviour. Also these models might be usable for flax and hemp fibre based composites.

4.6.2. Fatigue

According to [5], the typical fatigue fracture starts in the matrix where a stress concentration appears at each load change, which leads to a damage (matrix crack). This damage is often accumulated at micro cracks in the fibres, which leads to damage travel through the fibre. This is repeated until the damage in the composite leads to failure.

Not much work on fatigue properties appears to have been performed on flax and hemp fibre based composites. In [51] however, fibre properties and interface parameters affecting the fatigue properties have been examined.

One method, which might be possible to use for fatigue modelling is the homogenisation method in conjunction with the finite element method and damage mechanics.

4.6.3. Impact strength (toughness)

The impact strength of a composite is related to its fracture energy. The main mechanism leading to high fracture energy is often fibre pull-out in a crack running transverse the fibre direction. For a crack running parallel to the fibres, the main mechanism is fibre splitting or debonding [5].

Since fibre pull-out is an important factor for high fracture energy, the adhesion must be low in order to obtain a composite with high impact strength. This leads to that the strength of the composite subjected to a static load decreases. Hence, a low static strength often means that the impact strength is high [5]. When designing a composite it is thus often a compromise between strength and impact strength.

A possible method for modelling impact strength is (as for the case of fatigue) the homogenisation method in conjunction with the finite element method and damage

mechanics. By analysing a small part of the composite subjected to a static load, the elastic energy is small compared to the fracture energy and hence, the softening part of the fracture might be obtained. This method admits detailed studies of the mechanisms affecting the impact strength.

Several authors have examined the impact strength of natural fibre based composites, for instance [52,53] might be mentioned. It can be concluded that for instance a GMT (Glass fibre mat thermoplastic) has a superior impact strength compared to natural fibre based composites. It is thus evident that this issue needs further examination and development.

5. Discussion and conclusions

5.1. Additional aspects

Additional aspects concerning properties of natural fibre based composites are for instance degradation of the fibres in the composite. No such information has been found, but it can presumably be assumed that the composite behaves as the free fibre, which is described in section 2.3.3.

5.2. Concluding remarks

One important conclusion that can be drawn from this study is that a lot of research needs to be performed on flax and hemp fibre composite. The knowledge of the fibre on the micro and nano level is rather poor. Fundamental knowledge is crucial for development of the materials.

On the composite macro level, the stiffness predictions are rather well established, but more advanced material property predictions for properties such as strength, damage, creep and fracture needs further development. The most forthcoming method to model advanced material behaviour appears to be homogenisation using the finite element method.

The information in this text has been collected from various public sources. The knowledge in the private sector, especially in parts of the automotive industry, about manufacturing methods and properties of plant fibre composites is most probably more advanced than the knowledge given in the open literature, but unfortunately not available.

6. References

1 Forskning & Framsteg nr 1, 2003 pp23

2 B. Svennerstedt, *Plant fibres in sustainable constructions*, special report 243, JBT, SLU, 2003

3 M.F. Ashby & D.R.H. Jones, *Engineering materials 1*, Pergamon press, 1993

4 Tutorial for the course Composites (MFGT 247) 2001, California state university, Chico, webage: www.csuchico.edu/~jpgreene/m247/m247_ch05/

5 *Från fiber till komposit*, Division of production and materials engineering, Lund institute of technology, 1995.

6 *Bulk moulding Compound*, European Alliance for SMC

7 Hannele Sankari, *Towards bast fibre production in Finland: Stem and fibre yields and mechanical fibre properties of selected fibre hemp and linseed genotypes*, Academic dissertation university of Helsinki, Finland, 2000

8 H.L. Bos, J.A. van den Oever and O.C.J.J. Peters, *Tensile and compressive properties of flax fibres for natural fibre reinforced composites*, Journal of materials science 37 pp1683-1692, 2002

9 J. Militky, V. Bajzik and D. Kremenakova, *Selected properties of cottonized flax*, Textile Faculty, Technical University of Liberec, Czech Republic

10 C. Baley, *Analysis of the flax fibres tensile behaviour and analysis of the tensile stiffness increase*, Composites: part A, pp 939-948, 2002

11 Kent Persson, *Modelling of wood properties by a micromechanical approach*, Licentiate thesis, Structural mechanics Lund institute of technology, 1997

12 I. His, C. Andème-Onzighi, C. Morvan and A. Driouich, *Microscopic studies on mature flax fibres embedded in LR white: immunogold localization of cell wall matrix polysaccharides*, The Journal of Histochemistry & Cytochemistry, vol 49(12) pp 1525-1535, 2001

13 F. T. Madsen, I. Burgert, C. Felby, K. Jungnikl, A. B. Thomsen, *Effect of enzyme treatment and steam explosion on tensile strength and elongation of elementary hemp fiber.*

14 J. Gassan, A. Chate and A.K. Bledzki, *Calculation of elastic properties of natural fibres*, Journal of materials science 36 pp 3715-3720, 2001

15 A.K. Bledzki and J. Gassan, *Composites reinforced with cellulose based fibres*, Progress in polymer science 24, pp 221-274, 1998

16 Lars Wadsö, *Studies of Water Vapor Transport and Sorption in Wood*, Doctoral Dissertation Building materials, Lund university, 1993

17 C. Garcia-Jaldon, D. Dupeyre and M.R. Vignon, *Fibres from semi-retted hemp bundles by steam explosion treatment*, Biomass and bioenergy 3, pp 251-260, 1998

18 S.J Eichhorn, J. Sirichaisit, R.J. Young, *Deformation mechanisms in cellulose fibres, paper and wood*, Journal of materials science 36 pp 3129-3135, 2001

19 B. van Voorn, H.H.G. Smit, R.J. Snike, B. de Klerk, *Natural fibre reinforced sheet moulding compound*, Composites: part A 32 pp 1271-1279, 2001

20 Personal communication with Professor Rudolf Kessler, Institut für Angewandte Forschung, Fachhochschule Reutlingen, Germany, 2003

21 S. Stamboulis et.al., *Environmental durability of flax fibres and their composites based on polypropylene matrix*, Applied composite materials 7: 273-294, 2000

22 D. Nilsson, B. Svennerstedt, C. Wretfors, *Adsorption equilibrium moisture contents of flax straw, hemp stalks and reed canary grass*, Biosystems engineering (2005) 91 (1) 35-43.
23 B.V. Ramarao, *Moisture sorption and transport processes in paper materials*, Adsorption and its applications in industry and environmental protection, Studies in surface science and catalysis, Vol 120, 1998
24 G.I. Efremov, *Quasistationary method of describing the kinetics of treatment process for fibre materials*, Fibre Chemistry, Vol 34, No 5, 2002
25 Kent Persson, *Micromechanical modelling of wood and fibre properties*, Doctoral thesis, Structural mechanics Lund institute of technology, 2000
26 E.E. Smirnova et. al. *Change in the properties of textile materials containing polyester and cellulose fibres caused by moisture*, Fibre chemistry, vol 34, no 3, 2002
27 D. Starkie, *Chapter 3 in Materials and technology, Wood, paper, textiles plastics, photographic materials*, Longman Group Ltd, 1973
28 T. Lindström and L. Wågberg, *An overview of some possibilities to modify fibre surfaces for tailoring composite interfaces*, Sustainable natural and polymeric composites – Science and technology, 23 rd Risö international symposium on materials science, Denmark, 2002
29 K. Van de Velde, P. Kiekens, *Biopolymers: overview of several properties and consequences on their applications*, Polymer Testing 21 (2002) 433-442.
30 B. Svennerstedt, *Recycled and renewable resources for construction, insulation and automotive composites*, Proceedings of NTC 2005
31 Kristian Stålne, *Modelling of stiffness and hygroexpansion of wood fibre composites*, Licentiate thesis, Structural mechanics Lund institute of technology, 2001
32 J. Aboudi, *Mechanics of composite materials*, Elsevier, Amsterdam, The Netherlands, 1991
33 R. Hill, *Elastic behaviour of a crystalline aggregate.* Proceedings of the physical society, Section A, 349-354, 1952
34 B. Lamy and C. Baley, *Stiffness prediction of flax fibres-epoxy composite materials*, Journal of materials science letters 19, 979-980, 2000
35 A. Hillerborg, *Kompendium I Byggnadsmateriallära FK*, Division of building materials, Lund university, Sweden (1986)
36 K. Stålne, P. J. Gustafsson, *A 3D model for analysis of stiffness and hygroexpansion properties of fibre composite materials*, Journal of engineering mechanics.
37 R. Hill, *A self consistent mechanics of composite materials,* Journal of the mechanics and physics of solids, 13, 213-222, 1965
38 Z. Hashin, S. Shtrikman, *A variational approach to the theory of the elastic behaviour of multiphased materials*, J. Mech Phys. Solids, 11, 127-140, 1963
39 Z. Hashin, *On elastic behaviour of fibre reinforced materials of arbitrary transverse phase geometry*, Journal of the mechanics and physics of solids, 13, 119-134, 1965
40 S. Nemat-Nasser, M. Hori, *Micromechanics: overall properties of heterogeneous materials*, North-Holland series in applied mathematics and mechanics, 1993
41 C. T. Herakovich, *Mechanics of fibrous composites*, John Wiley & sons, 1998

42 D.G. Hepworth, D.M. Bruce, J.F.V. Vincent, G. Jeronimidis, *The manufacture and mechanical testing of thermosetting natural fibre composites*, Journal of materials science 35 (2000) 293-298
43 W. Weibull, A statistical theory of the strength of materials. Proceedings no 151, Ingenjörsvetenskapsakademien, Sweden, 1939
44 M.F. Ashby & D.R.H. Jones, *Engineering materials 2*, Pergamon press, 1993
45 J. Hult, H. Bjarnehed, *Styvhet och styrka*, Studentlitteratur, 1993
46 O. Kristensson, *Micromechanical modelling using computational homogenisation,* Doctoral thesis, Division of mechanics Lund institute of technology, 2005
47 S. Heyden, *Network modelling for the evaluation of mechanical properties of cellulose fibre fluff*, Doctoral thesis, Structural mechanics Lund institute of technology, 2000
48 A. Planche, P. Morlier, *Strength, stiffness and creep of medium density fibreboards*, Proceedings of the international conference on Wood and wood fiber composites, Germany 2000.
49 M. Bornert, P. Ponte Castañeda, *Second-order estimates of the self-consistent type for viscoplastic polycrystals*, Proceedings: mathematical, physical and engineering sciences, vol. 454, no 1979 (Nov. 8 1998), 3035-3045
50 F. Kun et.al., *Scaling laws of creep rupture of fibre bundles*, ArXiv:cond-mat/0209308v1 13 Sep 2002
51 J. Gassan, *A study of fibre and interface parameters affecting the fatigue behaviour of natural fibre composites*, Composites: part A 33 (2002) 369-374
52 A. C. N. Singelton et.al., *On the mechanical properties, deformation and fracture of a natural fibre/recycled polymer composite*, Composites: part B 34 (2003) 519-526
53 K. Oksman, *Mechanical properties of natural fibre mat reinforced thermoplastic*, Applied composite materials 7:403-414, 2000

7. Acknowledgments

The financial support from Formas that made this study possible is gratefully acknowledged.

I also wish to thank my supervisor Professor Per Johan Gustafsson for his invaluable comments on this report.

8. Appendix

The linear relation between strain and stress in three dimensions of a transversely isotropic material can be described on matrix format as:

$$\begin{bmatrix} \varepsilon_{11} \\ \varepsilon_{22} \\ \varepsilon_{22} \\ \gamma_{12} \\ \gamma_{13} \\ \gamma_{23} \end{bmatrix} = \begin{bmatrix} \frac{1}{E_{11}} & -\frac{\nu_{12}}{E_{22}} & -\frac{\nu_{12}}{E_{22}} & 0 & 0 & 0 \\ -\frac{\nu_{12}}{E_{22}} & \frac{1}{E_{22}} & -\frac{\nu_{23}}{E_{11}} & 0 & 0 & 0 \\ -\frac{\nu_{12}}{E_{22}} & -\frac{\nu_{23}}{E_{11}} & \frac{1}{E_{22}} & 0 & 0 & 0 \\ 0 & 0 & 0 & \frac{1}{G_{12}} & 0 & 0 \\ 0 & 0 & 0 & 0 & \frac{1}{G_{12}} & 0 \\ 0 & 0 & 0 & 0 & 0 & \frac{1}{G_{23}} \end{bmatrix} \begin{bmatrix} \sigma_{11} \\ \sigma_{22} \\ \sigma_{33} \\ \tau_{12} \\ \tau_{13} \\ \tau_{23} \end{bmatrix}$$

or as

$\boldsymbol{\varepsilon} = \mathbf{C}\boldsymbol{\sigma}$

with the inverse relation

$\boldsymbol{\sigma} = \mathbf{D}\boldsymbol{\varepsilon}$ where $\mathbf{D} = \mathbf{C}^{-1}$

Paper 2

Influence of dislocations and plasticity on the tensile behaviour of flax and hemp fibres

TORULF NILSSON and PER JOHAN GUSTAFSSON

Influence of dislocations and plasticity on the tensile behaviour of flax and hemp fibres

By Torulf Nilsson[1] and Per Johan Gustafsson

Division of Structural Mechanics, Lund University, P.O. Box 118, SE-221 00 Lund, Sweden

Abstract

This paper presents finite element analyses of the tensile behaviour of elementary fibres of flax and hemp, focusing on the non-linear tensile behaviour of the fibres and the relationship between the stiffness and the diameter of the fibre. The non-linear tensile behaviour is modelled by introducing dislocations in the helical structure of the cellulose fibrils and assuming that the hemicellulose has an elastoplastic constitutive relation. The relationship between the elastic stiffness and the diameter of the fibres is analysed similarly, using an elastic constitutive behaviour of the hemicellulose. The results agree with experimental results found in the literature.

Keywords: Fibres (A), Mechanical properties (B), Finite element analysis (C)

[1] Corresponding author. Tel +46 46 222 14 26; fax +46 46 222 44 20, torulf.nilsson@byggmek.lth.se

1. Introduction

Flax and hemp are annual plants that yield bast fibres with good mechanical properties. These bast fibres are composed of elongated cells (elementary fibres) glued together in bundles by pectins. The bundles of elementary fibres are often referred to as technical fibres. The mechanical behaviour of the elementary fibres is related to the cell wall structure and the mechanical properties of the constituents. The subject of this study is the tensile properties of the elementary fibres, specifically how the helical microstructure, the dislocations and the plastic performance of the hemicellulose affect the non-linear stress vs. strain performance of the fibres and the relation between fibre diameter and elastic stiffness.

The cell wall is divided into a primary cell wall and a secondary cell wall. The primary cell wall, with a thickness of ~0.2 μm, makes up only a very small portion of the cell wall ([1],[2]). The primary cell wall is chemically composed of pectin, lignin and randomly oriented cellulose. The secondary cell wall is mainly composed of lignin, hemicellulose and highly crystalline cellulose disposed in a helical structure. The microfibril angle is about 10° with respect to the fibre axis [1]. According to [3] the density of the constituents are in the same order of magnitude. By assuming that they have the same density no distinction between weight or volume fraction is needed. Only small or no errors are introduced by this assumption. The volume fractions of the various constituents in the elementary fibres have been reported to be as follows: for flax –cellulose 64.1%, hemicellulose 12.0% and lignin 2.0% [4]; for hemp –cellulose 68.1%, hemicellulose 15.1% and lignin 10.6% [5]. The content of lignin is low in the early stages of growth and high at the end. This lignification may explain why the volume fraction numbers found in the literature are somewhat scattered.

A thorough literature review relating to the stiffness of the constituents is given in [6]. The stiffness of the cellulose is independent of the moisture content and is in the range of 135–165 GPa [6], although a lower value of 130 GPa has also been reported [7]. The stiffness of the hemicellulose and lignin constituents is dependent on the moisture content. The stiffness of isolated hemicellulose ranges from 8 GPa at low moisture content to about 0.01 GPa at a moisture content of 70%. Lignin is less dependent on the moisture content, the range being from 6.5 GPa at 4% moisture to 3 GPa at 20% moisture content and higher.

Extensive experimental tests of the tensile properties of elementary flax fibres were carried out by Baley [8]. The test results revealed two important phenomena: the stiffness varies with the diameter of the fibre, and the constitutive relation between stress and strain is non-linear with a characteristic S-shape to the stress vs. strain curve. In this paper, the hypothesis is that the dislocations in cellulose and shear strain plastic yield of the hemicellulose between the chains of cellulose explain Baley's experimental observations. A dislocation is a microstructural misalignment from the otherwise perfectly helical cellulose chains. In this paper, larger structural misalignments such as kink bands are treated, but also waviness of the cellulose chains might be considered as dislocations. In a paper by Northolt et al [9], the tensile and compressive performances of polymeric materials are examined by means of experimental and theoretical methods. In the theoretical method, the waviness of the

polymer chains is introduced in the model, which leads to a non-linear material behaviour. This method is similar to the work in this paper. Representative dislocations, i.e. microstructural misalignments, in an elementary fibre can be seen in Figure 1 [10].

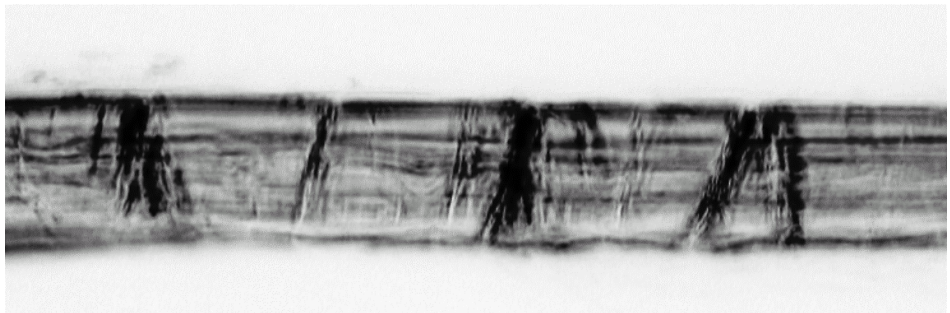

Figure 1 *Dislocations in hemp [10]*

The hypothesis regarding the significant influence of the dislocations is given initial support by the magnitude of the experimentally recorded elastic stiffness of the fibres. If we assume a microfibril angle of 10° in the secondary cell wall and a cellulose content of 65%, both reasonable assumptions, the stiffness of the fibre would, according to simple calculations, be about 85 GPa. However, the experimental results reported by Baley indicate a much lower average stiffness, about 55 GPa.
In this paper the tensile behaviour is modelled using FE analysis, taking into account relevant geometric and material non-linear actions within the microstructure of the fibre.

2. Method

The FE model of the elementary fibre is somewhat idealised. The fibre is assumed to be circular rather than polygonal as observed under a microscope. This assumption substantially simplifies the geometric modelling. Further, only the secondary layer is modelled. The primary cell wall layer has a thickness of only about 0.2 μm whereas the secondary cell wall has a thickness of several μm.

The secondary cell wall layer is composed mainly of cellulose, hemicellulose and lignin. Since cellulose is the main constituent and is far stiffer than the other constituents, it is assumed that it does not matter much whether the surrounding matrix is hemicellulose or lignin. It appears that the relative proportion of hemicellulose is higher than that of lignin, which leads to the assumption that it is sufficient to model only the hemicellulose and the cellulose.

2.1. Geometry of the FE models

The FE models employed in this study are made up of truss elements with the mechanical properties of cellulose embedded in 3D continuum elements with the properties of hemicellulose. Abaqus, the commercial software used to perform the analysis, refers to these as embedded elements [11].

The elementary fibre is modelled as a thick walled tube, with the size of the lumen set to 5% of the cross-sectional area of the elementary fibre. The cellulose is modelled as a helix with several layers. The pitch (axial distance for one revolution), $2\pi p$, of the helix is assumed to be constant along the radius, r. The parameter, p, is used for the mathematical description of the geometry of the helical structure. The resultant variations of the microfibril angle, α, are in accordance with the formula $\alpha = \text{atan}(r/p)$, i.e. the microfibril angel increase with increasing radius. According to several sources in the literature, the microfibril angle is about 10° at the outer surface of the S-layer [1,4,5]. The parameter, p, for this angle has been determined at a radius of 12 μm, i.e. $p = 12/\tan(10°) \approx 68.1$ μm. The coordinates of the nodes in the model of the cellulose are determined by the mathematical formulation of a helix in parameterised form:

$$\begin{cases} x = r\cos\theta \\ y = r\sin\theta \\ z = p\theta \end{cases} \tag{1}$$

where the z-axis is measured in the axial direction of the fibre.

The volume fraction of cellulose is set to 65% and that of the hemicellulose to 35%. An FE model of an ideal elementary fibre without dislocations is shown in Figure 2.

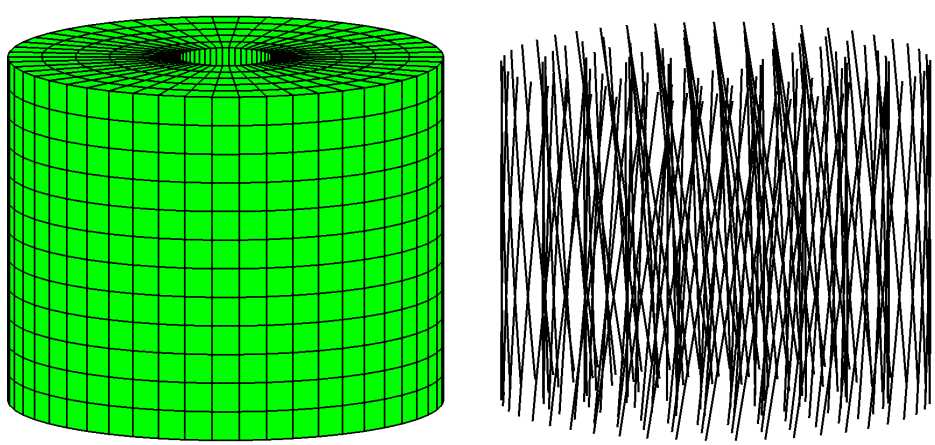

Figure 2 *FE model without dislocations, hemicellulose to the left and embedded cellulose to the right.*

The hypothesis considered in this paper is that dislocations are of major importance for the tensile behaviour of the elementary fibre. The type of dislocation studied

corresponds to rotation of a part of the perfect helical cellulose structure around the z-axis. This rotational misalignment gives a kinked shape to the microfibrils, as illustrated in Figure 3. The dislocation in the FE model is achieved by a rotational movement of the relevant nodes around the z-axis.

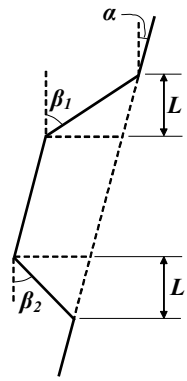

Figure 3 *Geometric model of the dislocation*

An analysis performed in the appendix shows that the dislocation angles β_1 and β_2 vary according to

$$\beta_{1,2}(r) = 90° - \arctan\left(\left(r\left(\frac{\sin(\beta_1(R_y) - \alpha(R_y))}{R_y \cos\alpha(R_y)\cos\beta_1(R_y)} \pm \frac{1}{p}\right)\right)^{-1}\right) \tag{2}$$

where $\alpha\left(R_y\right)$ and $\beta_1\left(R_y\right)$ are the microfibril angle and the dislocation angle at $r = R_y$ on the outside of the fibre and at the kink, respectively. Here it is assumed that $\alpha\left(R_y\right) = 10°$ and $\beta_1\left(R_y\right) = 45°$ at $R_y = 12\mu\text{m}$. The dislocation angle β_1 is an example of a reasonable choice. The angle β_2 can be determined by equation 2.

The magnitude of the dislocation (dislocation ratio) of a fibre is defined by the ratio of the total length of the dislocations, $2nL$, to the total length of the fibre, L_f,:

$$D = \frac{2nL}{L_f} \tag{3}$$

where $2n$ is the number of β_1-dislocations plus the number of β_2-dislocations.

The dislocation ratio is adjusted so that the initial stiffness of a fibre with a radius of 12 μm is approximately 55 GPa, i.e. it is calibrated to a mean value of the results obtained by Baley. This results in the dislocation ratio employed in this study being approximately 13%. A part of the FE model of a representative part of an elementary fibre with dislocations is shown in Figure 4.

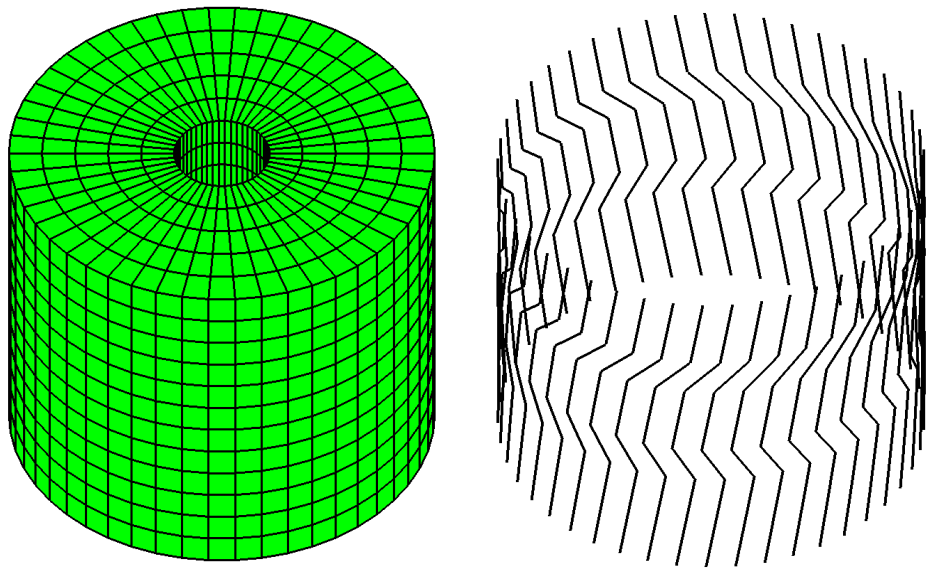

Figure 4 *Part of an FE model with dislocations, hemicellulose to the left and the embedded cellulose with dislocations to the right. Note that only the outermost truss elements are shown.*

2.2. Elastic model

During isolation of hemicellulose, the molecular arrangement changes, making the material behaviour isotropic. In the plant, the hemicellulose molecules tend to align with the cellulose chains. On the basis of Cousins' [12] measurement of the stiffness of hemicellulose, Cave [13] has suggested a transversely isotropic material model of hemicellulose in wood. The stiffness matrix is given by

$$\boldsymbol{D}_{\mathrm{H}}(\mathrm{w}) = \begin{bmatrix} 8 & 2 & 2 & 0 & 0 & 0 \\ 2 & 4 & 2 & 0 & 0 & 0 \\ 2 & 2 & 4 & 0 & 0 & 0 \\ 0 & 0 & 0 & 1 & 0 & 0 \\ 0 & 0 & 0 & 0 & 1 & 0 \\ 0 & 0 & 0 & 0 & 0 & 1 \end{bmatrix} c_{\mathrm{H}}(\mathrm{w})\ \mathrm{GPa} \tag{4}$$

Where $c_{\mathrm{H}}(\mathrm{w})$ is a moisture dependent function fitted to the experimental data reported by Cousins.

In this study, the main mechanism of the tensile behaviour is, however, not assumed to be related primarily to the anisotropy of the hemicellulose, but instead to the shear strain performance. Thus an isotropic material model of the hemicellulose is used. At a relative humidity of 60%, which corresponds to a moisture content of approximately 16 %, the stiffness of isolated hemicellulose is about 4.5 GPa. In the plant, the stiffness along the cellulose fibrils is higher and the cross-directional stiffness lower.

The stiffness along the cellulose fibrils employed in this study is set to 16 GPa, which has been used in [6] with good results. This is also the E-modulus used in the isotropic elastic material. Poisson's ratio is set to 0.3. Since the embedded element does not 'fill out' the continuum elements, the E-modulus of the hemicellulose is reduced by multiplying it by its volume fraction, i.e.: E_{HC}=16(1-0.65) = 5.6 GPa.

The E-modulus of the cellulose is set to 130 GPa [7] and Poisson's ratio to 0.3.

2.3. Plasticity models

In analysing the S-shaped stress vs. strain behaviour of fibres, the main mechanisms are assumed to be plastic shearing of the hemicellulose between the chains of cellulose and large deformation geometric effects corresponding to the decrease in the kink angles β_1 and β_2 during tensile loading. This assumption of elasto-plastic hemicellulose is supported by Baley's [8] experiments, where an elementary fibre was loaded and unloaded in a progressively increasing manner. The results indicate that the elementary fibres experience plastic deformation. In this study, two different von Mises plasticity models are used. The associated tensile behaviour is shown in Figure 5.

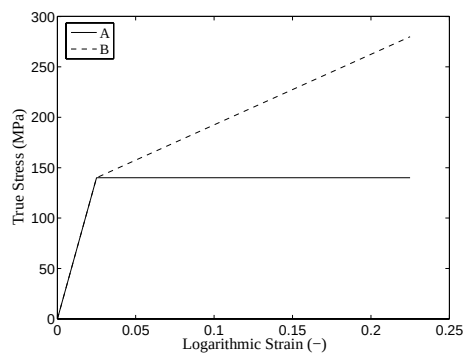

Figure 5 *Plasticity models*

The software Abaqus uses true stress and logarithmic strain when describing plasticity. True stress is defined as the current force divided by the current area. Logarithmic strain in one dimension is defined by [14]

$$\varepsilon = \int_{l_0}^{l} \frac{dl}{l} = \ln\left(\frac{l}{l_0}\right) = \ln(1+\varepsilon_n) \tag{5}$$

where l is the current length, l_0 is the initial length and $\varepsilon_n = (l - l_0)/l_0$ is the nominal strain. The initial yield stress of hemicellulose is adjusted to 140 MPa so that the fibre's departure from Hookean behaviour starts at the same strain level as in the tensile test in Baley's experiments.

2.4. Boundary conditions

The boundary conditions of the models are applied at both ends of the fibre. At one end, displacement is prevented in the axial and rotational degrees of freedom. At the other end, only the rotation is prevented and a prescribed axial deformation is applied. The displacement in the radial direction is not prescribed.

2.5. Analyses

Three different types of analyses were performed. The relation between stiffness and diameter of the fibre was analysed using linear elasticity and small deformation theory. The non-linear tensile behaviour was analysed using the two plasticity models in Figure 5 together with large deformation theory. The three kinds of models are summarized in Table 1. The non-linear analysis was only performed for the diameter 24 μm.

Table 1 *Description of the different analyses*

Model 1	*Model 2*	*Model 3*
Elastic cellulose E_C = 130 GPa	Elastic cellulose E_C = 130 GPa	Elastic cellulose E_C = 130 GPa
Elastic hemicellulose E_{HC} = 5.6 GPa	Elasto-plastic hemicellulose model A in Figure 5	Elasto-plastic hemicellulose model B in Figure 5
Small deformation theory	Large deformation theory	Large deformation theory

3. Results

The global average or nominal stress versus strain performance of the fibre is obtained from the reaction forces in the axial direction in the fixed end and the displacements of the other end. The nominal stress in the elementary fibre is calculated by dividing the total reaction force by the initial cross-sectional area, not including the area of the lumen. The nominal strain is calculated by dividing the applied elongation by the initial length of the fibre. In model 1, the stiffness of the fibre is calculated using Hooke's law, and in models 2 and 3 the stress is plotted versus the strain.

The results of Baley's experimental S-shaped tensile test were given in a force-displacement diagram, showing the clamping length, but not the cross-sectional area of the fibre. The area of the experimental fibre was therefore adjusted so that the initial stiffness of the experimental result correlates with the theoretical stiffness. The results from the analyses are shown in Figure 6 and 7.

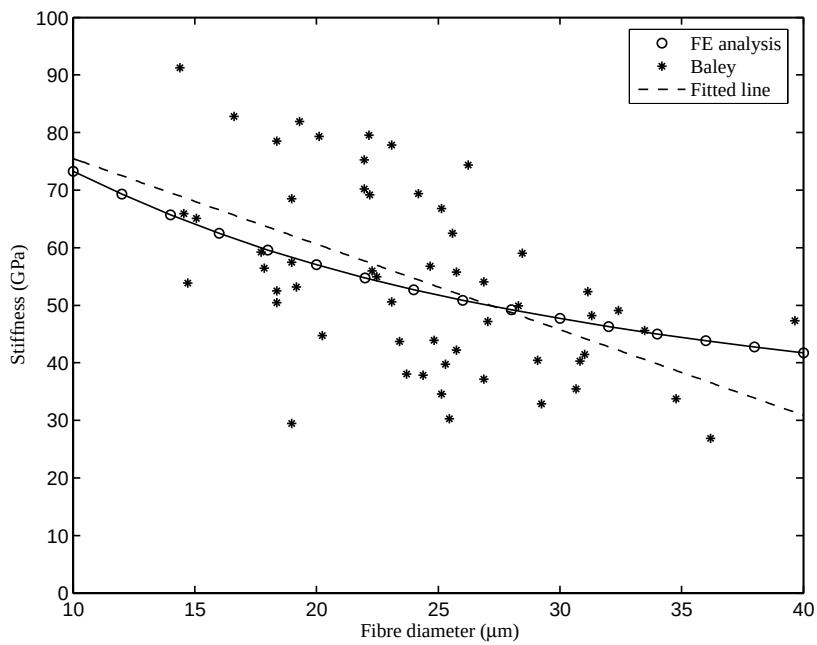

Figure 6 *Stiffness versus fibre diameter. Results from the FE analyses compared with the Baley experiments*

Figure 6 shows the relation between fibre stiffness and fibre diameter. Baley's experimental results are represented by a dashed straight line fitted by least square estimation to the experimental values, while the results of the FE analyses are indicated by circles. Although the FE solution does not correlate perfectly with the experimental result, the tendency is clear: the stiffness of the fibre decreases with increasing diameter.

The results of the non-linear analyses are shown in Figure 7 and reveal the typical S-shape. This curve is produced by local rotations of the fibre as a consequence of plastic shearing of the hemicellulose. The rotation straightens the dislocated cellulose fibrils, which in turn increases the stiffness of the fibre.

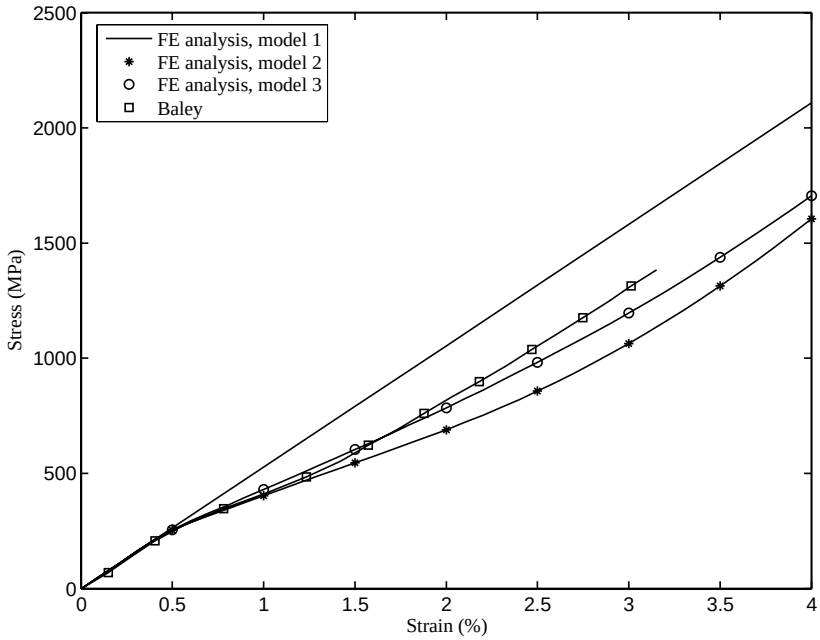

Figure 7 *Tensile behaviour of the elementary fibre*

4. Concluding remarks

The hypothesis that dislocations affect the tensile behaviour seems reasonable. The FE models do, however, introduce several uncertainties. While the exact geometry of the modelled dislocations probably does not correlate perfectly with those in nature, the main mechanisms seem to have been captured. Other uncertainties relate to the material models, especially that of hemicellulose. The plasticity models employed are normally used for metals, whereas hemicellulose is a polymer. If more correct constitutive measurements were available as regards the behaviour of hemicellulose, the results might have been different. But no such results are available. Alternative material models of the hemicellulose should include non-linear elasticity and linear elastic damage.

The typical non-linear tensile behaviour of elementary fibres is not observed in the technical fibres. The technical fibres manifest linear elastic tensile behaviour, probably because the pectin interface between the elementary fibres prevents local rotations.

It is not known how the dislocations are created. It is possible that compressive stress in the elementary fibre during growth causes local buckling of the cellulose fibrils. The helical arrangement of the microfibrils in flax and hemp is spun in different directions. However, this does not influence the results.

In conclusion, it has been found that the elastic stiffness of a fibre is greatly affected by dislocations and that the S-shaped stress vs. strain performance can be explained by non-linear geometric effects and yielding of the hemicellulose in the dislocation areas. It has further been found that the decrease in elastic stiffness with increase in the fibre diameter can be explained by the increase in dislocation angle according to equation 2. The variation of the dislocation angle by the radius and the true geometry of the dislocations remain to be verified experimentally with the aid of a microscope. Other future work should include a thorough parametric study of dislocation angles, dislocation ratio and microfibril angle in order to validate the hypothesis.

A1 Appendix: Determination of the microfibril and dislocation angles.

A part of a microfibril with a dislocation is shown in Figure A.1. The dislocation in the model is created by a rotational movement of the relevant nodes around the z-axis. The arc length of the rotational movement is given by:

$$s(r) = \gamma\, r \qquad \text{A.1}$$

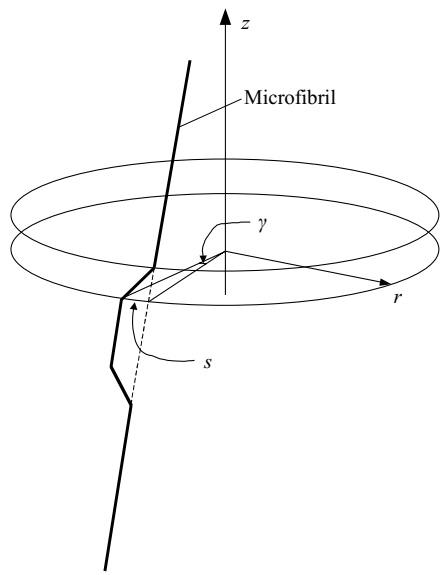

Figure A.1 *Dislocated microfibril in the fibre.*

If the outer surface of the layer where the microfibril is present is unfolded, the geometry is mapped to the plane as shown in Figure A.2. The microfibril angle is defined as:

$$\tan\alpha = \frac{2\pi r}{2\pi p} = \frac{r}{p} \qquad \text{A.2}$$

The law of sines for the geometry in Figure A.2 (right) gives:

$$\frac{L}{\cos\alpha^{ref}\,\sin(90^\circ - \beta_1^{ref})} = \frac{s}{\sin(\beta_1^{ref} - \alpha^{ref})}$$

and with the expression; $\sin(90^\circ - \beta_1^{ref}) = \cos\beta_1^{ref}$, the arc length can be expressed as:

$$s = \frac{L\sin(\beta_1^{ref} - \alpha^{ref})}{\cos\alpha^{ref}\cos\beta_1^{ref}} \qquad \text{A.3}$$

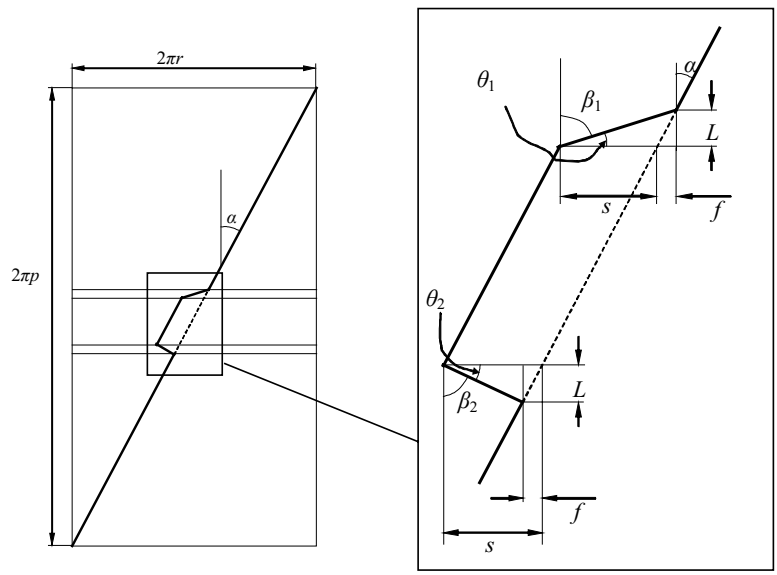

Figure A.2 *Mapped geometry of the dislocated microfibril in the fibre.*

The angles $\alpha^{ref} = \alpha(R_y)$ and $\beta_1^{ref} = \beta_1(R_y)$ are reference angles chosen at the reference radius at the surface of the fibre. By utilising equation A.1 the rotation angle around the z-axis of the dislocation becomes:

$$\gamma = \frac{L\sin(\beta_1(R_y) - \alpha(R_y))}{R_y\cos\alpha(R_y)\cos\beta_1(R_y)} \qquad \text{A.4}$$

Since γ is constant, the arc length as a function of the radius can be determined according to:

$$s(r) = \frac{L\sin(\beta_1(R_y) - \alpha(R_y))}{R_y\cos\alpha(R_y)\cos\beta_1(R_y)}r \qquad \text{A.5}$$

The distance f in Figure A.2 is calculated according to:

$$f(r) = L\tan\alpha = L\frac{r}{p} \qquad \text{A.6}$$

The relationship for the angles θ_1 and θ_2 are then obtained by :

$$\tan\theta_1 = \frac{L}{s(r)+f(r)} = \left(r\left(\frac{\sin(\beta_1(R_y)-\alpha(R_y))}{R_y \cos\alpha(R_y)\cos\beta_1(R_y)} + \frac{1}{p} \right) \right)^{-1} \quad \text{A.7}$$

$$\tan\theta_2 = \frac{L}{s(r)-f(r)} = \left(r\left(\frac{\sin(\beta_1(R_y)-\alpha(R_y))}{R_y \cos\alpha(R_y)\cos\beta_1(R_y)} - \frac{1}{p} \right) \right)^{-1} \quad \text{A.8}$$

The dislocation angles β_1 and β_2 are finally obtained as:

$$\beta_{1,2}(r) = 90° - \arctan\left(\left(r\left(\frac{\sin(\beta_1(R_y)-\alpha(R_y))}{R_y \cos\alpha(R_y)\cos\beta_1(R_y)} \pm \frac{1}{p} \right) \right)^{-1} \right) \quad \text{A.9}$$

References

1. Bos HL, van den Oever JA, Peters OCJJ. *Tensile and compressive properties of flax fibres for natural fibre reinforced composites.* J Mat Sci 2002; 37:1683–1692.
2. Thiery IP. J. Microsc. 1967; 6**:** 987.
3. Fengel D. *The ultrastructure of cellulose from wood. Part 1: Wood as the basic material for the isolation of cellulose.* Wood Sci Tech. 1969; 3: 203-217.
4. Bledzki AK and Gassan J. *Composites reinforced with cellulose based fibres.* Prog in Polymer Sci 1998; 24: 221–274.
5. Militky J, Bajzik V, Kremenakova, D. *Selected properties of cottonized flax.* Textile Faculty, Technical University of Liberec, Czech Republic
6. Persson K. *Micromechanical modelling of wood and fibre properties.* Doctoral thesis, Structural Mechanics, Lund Institute of Technology, 2000.
7. Berglund L. Biofibre Materials Centre, Royal Institute of Technology, Sweden.
8. Baley C. *Analysis of the flax fibres tensile behaviour and analysis of the tensile stiffness increase.* Composites: Part A 2002: 939–948.
9. Northolt MG, Baltussen JJM. *The tensile and compressive deformation of polymer and carbon fibers.* J app Pol Sci 2002; 88:508-538.
10. Thygesen LG, Hoffmeyer P. *Quantification of dislocations in hemp fibres.* Technical University of Denmark. Part of the project: 'High performance hemp fibres and improved fibre network for composites' 2003.
11. Hibbit, Karlsson & Sorensen, Inc. Abaqus User's Manual Version 6.4, 2003.
12. Cousins WJ. *Young's modulus of hemicellulose as related to moisture content*, Wood Sci Tech. 1978; 19: 161-167.
13. Cave ID. *Modelling moisture-related mechanical properties of wood. Part I: Properties of the wood constituents.* Wood Sci Tech 1978; 12: 75–86.
14. Ashby FA, Jones DRH. *Engineering materials 1; An introduction to their Properties and Applications.* Int Ser Mat Sci Tech 1993

Paper 3

Micromechanical modelling and testing of strength of natural fibres

TORULF NILSSON and PER JOHAN GUSTAFSSON

Micromechanical modelling and testing of strength of natural fibres

By Torulf Nilsson[1] and Per Johan Gustafsson

Division of Structural Mechanics, Lund University, P.O. Box 118, SE-221 00 Lund, Sweden

Abstract

This paper presents a finite element model of bundles of natural fibres. The model takes into account defects, which are described by Weibull theory, and the shear interface properties adhering the elementary fibres. The complete constitutive behaviour including softening of the fibre is obtained. Tensile tests of flax and hemp technical fibres are performed for glued and non-glued fibres in order to examine the effect of shear interface properties. The computational result gives a good correlation with tensile tests and an extensive study of the influence of different material parameters is performed.

Keywords: Fibres (A), Mechanical properties (B), Finite element analysis (C)

[1] Corresponding author. Tel +46 46 222 14 26; fax +46 46 222 44 20, torulf.nilsson@byggmek.lth.se

1. INTRODUCTION 2

2. METHOD 3

2.1. Experimental 3
2.1.1. Fibre material 3
2.1.2. Scanning electron microscopy 3
2.1.3. Tensile test 3

2.2. Material model 6
2.2.1. Structure 6
2.2.2. Elementary fibres 7
2.2.3. Shear transfer 8

2.3. FE-analysis 11
2.3.1. FE-model 11
2.3.2. Spring properties 11
2.3.3. Boundary conditions 13
2.3.4. Solution strategy 14
2.3.5. Analyses types 15

3. RESULT 16

3.1. Experiment 16
3.1.1. SEM-result 16
3.1.2. Tensile test 16

3.2. FE-analysis 19
3.2.1. General 19
3.2.2. Convergence results 20
3.2.3. Adjustment of parameters to fit experimental results 21
3.2.4. Parameter study 23

4. DISCUSSION 27

4.1. Tensile test 27

4.2. Computational result 27

4.3. Future work 27

5. REFERENCES 29

1. Introduction

The main subject of the present study is the mechanical properties of technical flax and hemp fibres. Knowledge of the strength and stiffness of the bundle of elementary fibres that make up a technical fibre is necessary in the course of developing material models for fibre composite material design. It is crucial to understand the underlying mechanisms leading to the mechanical behaviour of the composite. The study is also an attempt to link fibre quality quantification to mechanical properties of fibres when being in a composite. The quality quantification of the fibres has been described by Wretfors [1].

The empirical observation that gave the incitement and idea for this study was presented by Kessler [2], who had experienced that retted fibres have a low tensile strength whereas their composites have high strength and the opposite for non-retted fibres.

It is common knowledge that the adhesive of the fibre to matrix shear interface in composites affects their tensile strength to a great extent. Since technical fibres are composites themselves, the same mechanism is believed to be the reason to the behaviour observed by Kessler. This hypothesis has been introduced by Bos [3] but it appears that models explaining and predicting this behaviour are missing.

More specifically, the tensile properties of flax and hemp technical fibres are examined by means of experimental tests and micromechanical modelling. The focus is on fracture and fibre strength, but also stiffness is treated. Glued and non-glued flax and hemp technical fibres of different length are tensile tested in order to examine the influence of the shear interface. A model describing the influence of damage and shear interface properties is presented.

2. Method

2.1. Experimental

2.1.1. Fibre material

The flax and hemp fibres examined in this paper were grown in the south of Sweden during 2003 on the research farm of SLU, Alnarp. The flax variety was Belise and the hemp variety was Futura 75. The flax stems were field retted for a month (October) and the hemp stems were water retted in 55˚C for 10 days. The flax fibres were decorticated by the traditional method, breaking, scutching and hackling. The hemp fibres were extracted by ripping them of the stem by hand and thereafter hackled.

2.1.2. Scanning electron microscopy

In order to get an indication of frequency and location of dislocations and other defects in the fibres, samples of flax were examined in a scanning electron microscope (SEM). Bundles of fibres, i.e. technical fibres, were examined in the SEM and the number of dislocations per length in the elementary fibre was counted. Only flax fibres were studied. For hemp has similar but more elaborate tests been performed by Thygesen & Hoffmeyer [4].

2.1.3. Tensile test

Tensile tests of individual technical fibres were carried out for four different types of technical fibres; flax, glued flax, hemp and glued hemp. For each type were tests made with 3 test lengths: 3, 9 and 27 mm. The number of nominally equal tests was 8-17 for each of the 12 test groups.
The specimens were prepared in the following manner: The fibres were randomly selected from a pile. Then the length and the weight of the fibres were measured. By assuming that the cross sectional area of a fibre is constant along its length and using a density of 1500 kg/m^3, the area was determined. This method is rather blunt, but still believed to give a reasonable estimation of the size of the cross sectional area.
The glued fibres were soaked in a low viscosity epoxy (type NM Laminering 650) and then they were hung vertically to cure between two clothes pegs. After curing, the fibres were weighed again in order to obtain the amount of added glue.
Attachment of fibres to the tensile loading machine was arranged by gluing the end parts of the fibres between washers, Figure 2.1. The glue was of the make X60. Each type of fibre was clamped with the three lengths; 3, 9 and 27 mm. The total length was for all fibres greater than 27 mm and the fibres clamped with different lengths were nominally equal. The fibres with clamps were placed in the testing device MTS 810 as shown in Figure 2.1.
Load and elongation were recorded during the tests. The stroke rate was 0.1mm/min and the time to failure in the order of 30-60 seconds. The tests were made at temperature 22 ˚C and RH 50%.

Since the clamping system, i.e. washers, glue and hook, is deformable, the recorded deformation is not only due to the elongation of the fibre. The stiffness of the fibres is therefore underestimated if evaluated from the load and the recorded total deformation. In an attempt to account for the additional deformation, a method of least squares is used.
The fibre and the clamping system can be represented by springs in series. The stiffness of two linear springs in series is given by:

$$\frac{1}{k_{tot}} = \frac{1}{k_f} + \frac{1}{k_c} \qquad 2.1$$

where k_{tot} is the measured stiffness, k_f is the actual fibre stiffness and k_c is the stiffness of the clamping. Further, by assuming that fibres of different lengths have the same *E*-modulus and cross sectional area and that the stiffness of the clamping system is the same in each nominally equal test, the following equation system is obtained:

$$\begin{bmatrix} 1 & L_3/A \\ 1 & L_9/A \\ 1 & L_{27}/A \end{bmatrix} \begin{bmatrix} 1/k_c \\ 1/E_f \end{bmatrix} = \begin{bmatrix} L_3/A\,E_3 \\ L_9/A\,E_9 \\ L_{27}/A\,E_{27} \end{bmatrix} \qquad 2.2$$

where E_f, is the actual stiffness of the fibre material and E_3, E_9 and E_{27} the apparent stiffness as evaluated from the total deformation recorded during the tests of fibre lengths 3, 9 and 27 mm, respectively. On matrix format, the system of equations can be written as:

$$\mathbf{A}\mathbf{x} = \mathbf{b} \qquad 2.3$$

This system of equations has the least-square solution [5]:

$$\mathbf{x} = \left(\mathbf{A}^T\mathbf{A}\right)^{-1}\mathbf{A}^T\mathbf{b} \qquad 2.4$$

where the matrix **x** contains the estimated stiffness of the clamping and the E-modulus of the fibre, i.e.

$$\mathbf{x} = \begin{bmatrix} 1/k_c & 1/E_{tot} \end{bmatrix}^T \qquad 2.5$$

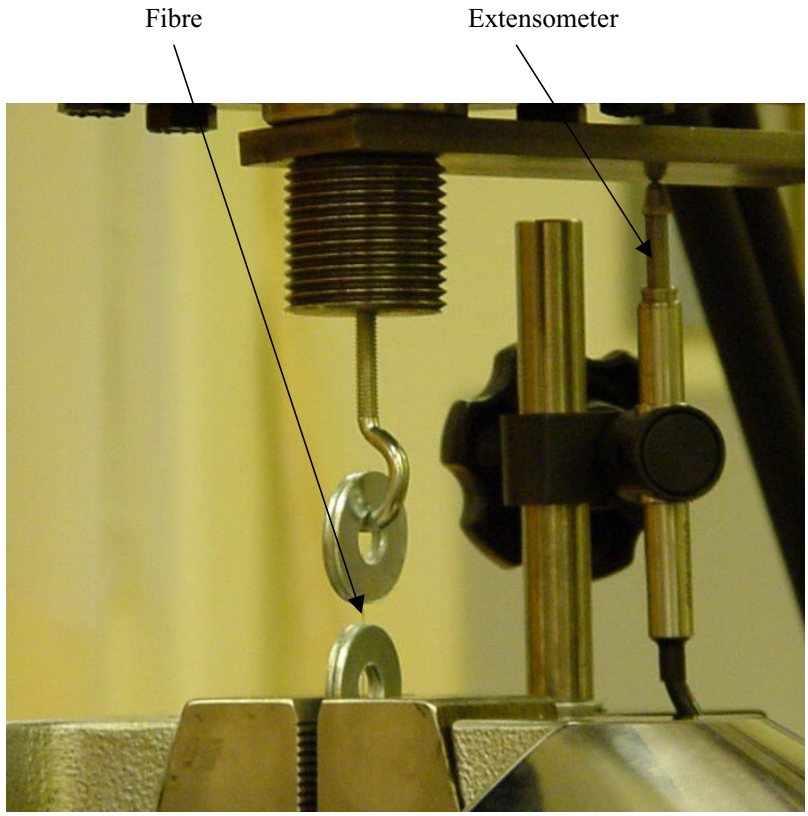

Figure 2.1 *Setup for tensile test*.

2.2. Material model

2.2.1. Structure

When micrographs of flax and hemp fibres in the stem are studied (His et. al. [6]) it can be observed that most of the elementary fibres are hexagonal and arranged in a hexagonal pattern, much like a honeycomb. Since the fibres are of varying size, some fibres however deviate from this pattern. In order to simplify the modelling, the fibres are assumed circular and the diameters of the fibres are assumed to be equal. This leads to a perfect hexagonal structure of a technical fibre as shown in Figure 2.2 and 2.3. The diameter of the elementary fibres was assumed to be 20 μm.

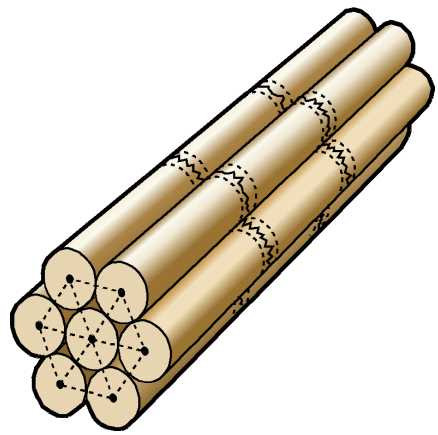

Figure 2.2 *Model of a piece of a technical fibre.*

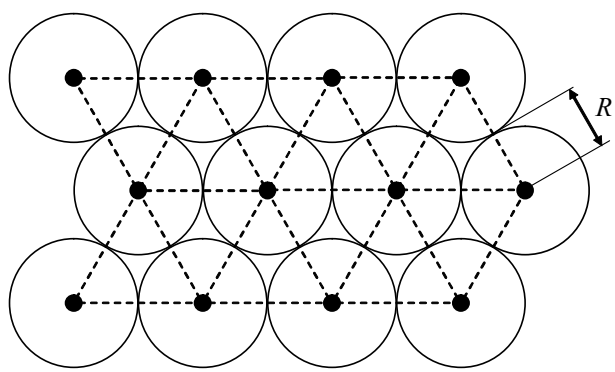

Figure 2.3 *Cross section model of a technical fibre.*

A side view of a part of the technical fibre model is shown in Figure 2.4. The elementary fibres are bonded to each other by a layer denoted shear interface. Defects of random magnitude and location are present in the elementary fibres. The fibres are divided into material length units denoted l_m. The elementary fibre material properties are homogenous within each length l_m. The strength and stiffness properties of the

fibre length units l_m and the shear interface are modelled as described below. The defects present in the fibres are assumed to be distributed over one fibre diameter. The damaged area, in this paper referred to as one material length unit, l_m, is marked with dotted lines in the figure.

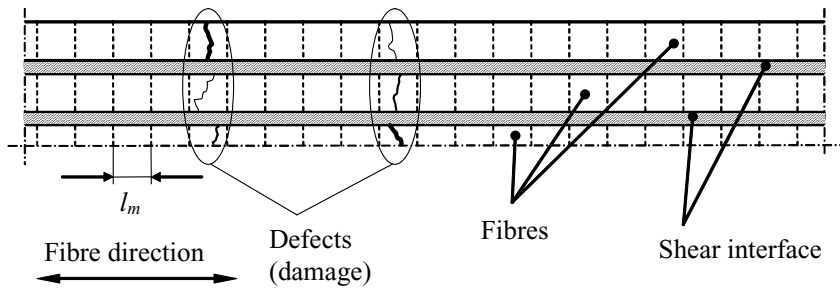

Figure 2.4 *Model of technical fibre.*

2.2.2. Elementary fibres

Stiffness

The stiffness values of flax and hemp fibres in uniaxial tension reported in the literature are very scattered. Examples of stiffness values of flax fibres are E = 27.6 GPa and E = 80 GPa reported by Bledzki et al. [7] and van Voorn et al. [8], respectively. Likewise, the stiffness of hemp fibres range between E = 19.1 GPa and E = 70 GPa reported by Eichhorn et al. [9] and Kandachar [10], respectively. An example of a reasonable choice is E = 55 GPa, which is the value used in the present analyses.

Strength

The uniaxial tensile strength of the elementary unit fibre lengths, l_m, that has a defect is described by means of Weibull [11] theory. The probability of failure, P_f, of a volume of a material exposed to a homogenous tensile stress, σ, is given by:

$$P_f = 1 - e^{-\frac{V}{V_0}\left(\frac{\sigma}{\sigma_0}\right)^m} \qquad 2.6$$

where V_0 is a reference volume and σ_0 and m are material parameters indicating the magnitude and scatter in strength respectively. In the present model is the strength of those of the elementary fibre lengths, l_m, that are damaged defined according to

$$P_f = 1 - e^{-\left(\frac{\sigma}{\sigma_0}\right)^m} \qquad 2.7$$

Occurrence and localisation of damage is at random. However, if the technical fibre is damaged at some location, then all of the elementary fibres at that location are

assumed to be more or less damaged. This assumption is supported by the results of the SEM-observations and also by argument of damage localisation when a technical fibre is bent when decorticated. The occurrence and localisation of damage is in the model made by taking random numbers between 0 and 1 for each technical fibre length l_m. If the random number is less than the damage ratio, D_r, the cell is assumed damaged. The damage ratio is defined as the number of defects per number of lengths l_m:

$$D_r = l_m D \qquad 2.8$$

where D is the number of defects per unit length. The SEM-pictures gave D = 8.1 defects/mm which is used for the analyses. The length of the cells, l_m, was set to the fibre diameter $2R$, i.e. 20 μm, giving D_r = 0.16.
For each damaged cell, a new random number between 0 and 1 is used in Equation 2.7 to obtain the strength, σ_f. Undamaged cells are assumed to have unlimited strength.
The constitutive behaviour of elementary fibres is somewhat uncertain after the peak stress, but is assumed very brittle. The principle of the constitutive behaviour adopted in the analyses is shown in Figure 2.5 (marked with B).

2.2.3. Shear transfer

The strength and stiffness properties of the shear interface between the elementary fibres reflects the properties of the actual interface surface, i.e. the bounding agent (normally pectin) and also the longitudinal shear properties of the walls of the elementary fibres. In the present model is the interface assigned a linear elastic brittle shear stress versus shear slip performance according to curve B in Figure 2.5. The true performance is probably non-linear, e.g. according to curve A. This means that different shear stiffness values are relevant dependent on the magnitude of load and the purpose of the analysis. For analysis of stiffness at low load is the elastic shear properties of the fibre wall relevant and for analysis of the strength of the technical fibre is correct modelling of the shear fracture energy relevant. In the case of strength analysis should accordingly the shear stiffness be chosen so that the areas under curves A and B are equal. In the below is first the elastic stiffness discussed and then the fracture energy relevant stiffness discussed.

Stiffness

It appears that no value of shear modulus of the cell wall has been reported in the literature. However, linear elastic coefficients of the main constituents of wood fibres (cellulose, hemicellulose and lignin) are given in a doctoral thesis by Persson [12]. Since the constituents of flax and hemp are the same as in wood; it is assumed that the mechanical properties also are the same.
Cellulose and hemicellulose are both considered as transversely isotropic materials with the stiffer axis along the cellulose molecule chain. The stiffness of cellulose has a low dependence on moisture changes, whereas the stiffness of hemicellulose is highly dependent on the moisture content. Lignin is considered as an isotropic material with a moderate dependence on the moisture content. Shear stiffness coefficients of the constituents valid at 60 % relative humidity are for longitudinal shear compiled in Table 2.1.

Table 2.1 *Shear stiffness coefficients according to Persson [12]*

	Cellulose	Hemicellulose	Lignin
G (GPa)	3.0-6.0	1.0-2.0	0.8-1.3

In order to estimate the shear modulus of the cell wall, micro mechanical modelling is a feasible method. Several micro mechanical models can be found in the literature. For instance Herakovich [13] may be consulted. Since there are many uncertainties concerning the stiffness values and the proportion of the constituents, the chosen model is of minor importance. Here the Reuss model in one dimension is chosen for its simplicity. This model constitutes the lower bound of stiffness. The equation reads:

$$\frac{1}{G} = \frac{V_1}{G_1} + \frac{1 - V_1}{G_2} \qquad 2.9$$

where G is the overall shear modulus of the composite, G_1 and G_2 are the shear modulus of the two different phases and V_1 is the volume fraction of phase 1.
According to Nilsson [14], the content of cellulose in flax fibres reported in the literature ranges between 64 and 78 %, hemicellulose approximately 12 % and lignin between 2 and 8.5 %. It is, hence, difficult to obtain an accurate value of the shear modulus of the cell wall. It is however possible to determine the range of possible values according to equation 2.9. This is carried out by choosing the limiting values, the maximum is obtained by assuming that only cellulose and hemicellulose are present and using their maximum values, i.e. $V_1 = 0.78$, $G_1 = 6$ GPa and $G_2 = 2$ GPa and the minimum is obtained by assuming that only cellulose and lignin are present and using their minimum values, i.e. $V_1 = 0.64$, $G_1 = 3$ GPa and $G_2 = 0.8$ GPa. With these values the shear modulus of the cell wall becomes: $G = 1.5$-4.2 GPa. Since Equation 2.9 determines the lower bound, a value of $G = 3$ GPa seems reasonable for modelling of the shear stiffness.

Strength and energy equivalent stiffness

The shear strength of the interface is denoted τ_f and is in the present numerical calculations assigned various deterministic values ranging from 10 MPa to 60 MPa, representing a probable range of magnitude for the shear strength of the polymers that constitutes the shear interaction layer.
Increasing tensile loading and the subsequent failure of a technical fibre involves tensile failures of the elementary fibres. The load transfer between the elementary fibres is then similar to the performance of a glued lap joint, see Figure 2.6. The load carrying capacity of such a joint is according to Gustafsson [15] strongly affected not only by shear strength, τ_f, but by the fracture energy, G_f, of the shear layer, defined as the area under the shear stress, τ, versus shear displacement, δ, curve:

$$G_f = \int_0^\infty \tau \, \mathrm{d}\delta \qquad 2.10$$

If τ_f and G_f are correctly represented, then the actual shape of the τ-δ curve does commonly not affect the load capacity very much (Gustafsson [15]). If modelling the

shear performance as a linear performance, i.e. curve B in Figure 2.5, when the fracture energy equivalent shear stiffness is by the condition of equal energy found to be:

$$G_f = \frac{R\tau_f^{\,2}}{G} \qquad 2.11$$

where G by definition is τ/γ (γ indicating shear strain) and by the kinematics $\delta = 2R\gamma$, see Figure 2.6. The present numerical analyses focus on the strength rather than the stiffness of technical fibers. Equation 2.11 is therefore applied. Results obtained for values of G_f in the range of 100 J/m^2 to 800 J/m^2 are presented.

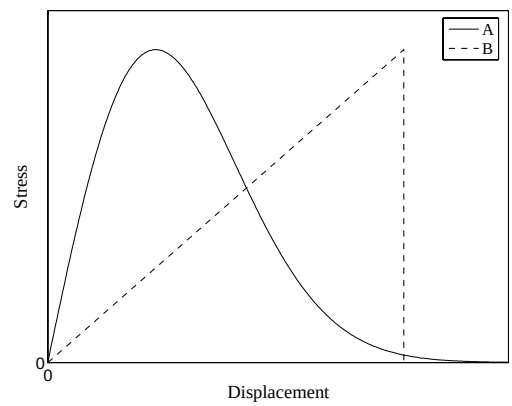

Figure 2.5 *Two different shapes of stress-displacement curves.*

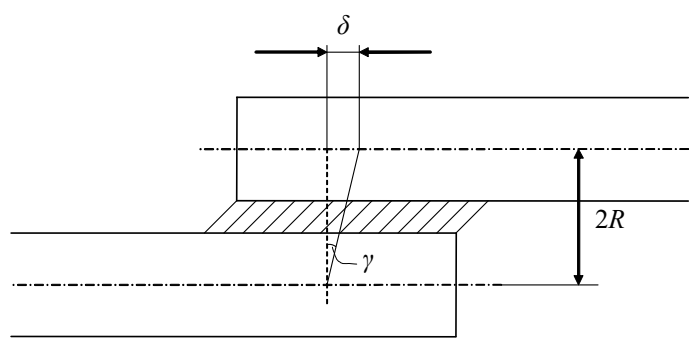

Figure 2.6 *Deformation principle of two adhered fibres.*

2.3. FE-analysis

2.3.1. FE-model

The FE-model of the technical fibre is described by spring elements. The cross sectional structure follows the geometry of the dashed lines in Figure 2.3. The side view of the FE-model is shown in Figure 2.7. The spring element representing the elementary fibre is indicated by 1 and the shear spring element by 2. The shear spring elements transfer shear forces between adjacent fibres.

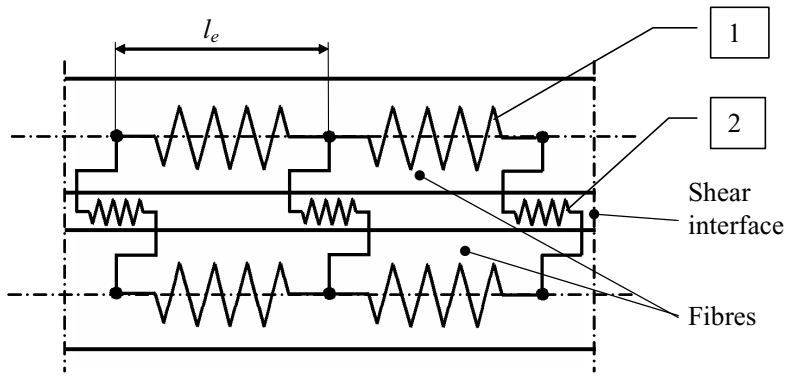

Figure 2.7 *Side view of a small part of the FE-model of the technical fibre.*

By assembling the system of springs, the finite element equation system becomes:

$$\mathbf{K}\mathbf{u} = \mathbf{f} \qquad 2.12$$

Where **K** is the global stiffness matrix containing the individual stiffness of the spring and shear spring elements, **u** is the nodal displacement matrix and **f** is the external nodal force matrix. The boundary conditions needed to solve the system of equations are described in section 2.3.3.

2.3.2. Spring properties

The stiffness of the springs that represent the elementary fibres is given by:

$$k_f = \frac{EA}{l_e} \qquad 2.13$$

where E is Young's modulus, A is the cross sectional area of the elementary fibre and l_e is the spring element length. The ultimate force in the fibre is calculated by $F_f^{ult} = \sigma_f A$. If the finite elements, l_e, are chosen to a length shorter than l_m then more than one defect may be present in the element. In such a case the smallest strength value is selected.

In the case of strength analyses of a technical fibre is the shear modulus G of shear spring elements determined according to Equation 2.11. The shear modulus then has to be related to the shear spring stiffness. An estimate can be obtained by analysing a homogenous cylinder (fibre) constrained at the outer surface and subjected to a homogenous body force, b_V (N/m^3). The strain energy in the cylinder is then set equal to the strain energy in the spring element. Equilibrium in the axial direction of the homogenous cylinder is given by:

$$\tau 2\pi rh - b_V \pi r^2 h = 0 \quad \Rightarrow \quad \tau(r) = \frac{b_V r}{2} \tag{2.14}$$

Where τ is the shear stress and r is the radius. The strain energy of the cylinder is given by:

$$W = \int \frac{\tau\gamma}{2} \mathrm{d}V \tag{2.15}$$

With equation 2.14 and the shear strain, $\gamma = \tau/G$, the strain energy is obtained as;

$$W = \frac{{b_V}^2 \pi h}{4G} \int_0^R r^3 \mathrm{d}r = \frac{{b_V}^2 \pi h R^4}{16G} \tag{2.16}$$

Where G is the shear modulus and R and h are the outer radius and the length of the cylinder respectively.
The strain energy of the spring element is determined in a similar manner. The body force is replaced by a line load, b_l (N/m) and the constitutive behaviour is $b_l h = k_s \delta$, where k_s is the shear spring stiffness and δ is the deformation of the spring. The strain energy of the spring can then be determined to:

$$W_l = \frac{k_s \delta^2}{2} = \frac{{b_l}^2 h^2}{2k_s} \tag{2.17}$$

By setting the total load equal, i.e. $b_l h = b_V \pi R^2 h$, the body force can be related to the line force and the energy stored in the spring becomes:

$$W_l = \frac{{b_V}^2 \pi R^4 h^2}{2k_s} \tag{2.18}$$

Finally, by setting the strain energy of the cylinder and the spring equal, the spring stiffness is obtained as:

$$k_s = 8G\pi h \tag{2.19}$$

Peculiarly, the spring stiffness obtained by this model is independent of the radius.
In order to obtain the stiffness of the shear spring element, h is set equal to l_e.

The maximum shear force of the shear spring elements is estimated by dividing the shear strength by the transferring area. This area is defined by the element length of the elementary fibres and one sixth of the circumference of the fibre, i.e.

$$F_s^{ult} = \tau_f \frac{l_e 2\pi R}{6} = \tau_f \frac{l_e \pi R}{3} \qquad 2.20$$

2.3.3. Boundary conditions

The boundary conditions, i.e. the assumed condition at the two ends of the modelled piece of a technical fibre, affect the stress distribution and accordingly the calculated strength and stiffness. In the present analyses are cyclic boundary conditions applied in order to simulate the stress distribution in a very long fibre. The modelled piece of fibre is considered as one of many identical pieces of an infinite fibre. This leads to continuity requirements, meaning that the pieces have to have matching boundary displacements (Heyden [16]). Considering the simple example in Figure 2.8 the continuity requirement is fulfilled if u_6-u_4 = c and u_3-u_1 = c, where c is the applied elongation of the structure.

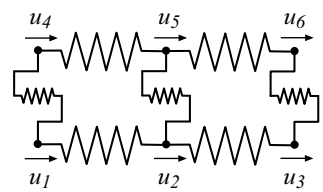

Figure 2.8 *Simple spring model to show principle of cyclic boundary conditions.*

Introduction of boundary condition implies reduction of the number of degrees of freedom from 6 to 4 according to:

$$\begin{bmatrix} u_1 \\ u_2 \\ u_3 \\ u_4 \\ u_5 \\ u_6 \end{bmatrix} = \begin{bmatrix} 1 & 0 & 0 & 0 \\ 0 & 1 & 0 & 0 \\ 1 & 0 & 0 & 0 \\ 0 & 0 & 1 & 0 \\ 0 & 0 & 0 & 1 \\ 0 & 0 & 1 & 0 \end{bmatrix} \begin{bmatrix} u_1 \\ u_2 \\ u_4 \\ u_5 \end{bmatrix} + \begin{bmatrix} 0 \\ 0 \\ c \\ 0 \\ 0 \\ c \end{bmatrix} \qquad 2.21$$

Generally, this type of boundary condition can be written on matrix format as:

$$\mathbf{u} = \mathbf{B}\mathbf{u}^{red} + \mathbf{c} \qquad 2.22$$

Insertion of 2.22 in 2.12 gives:

$$\mathbf{K}\mathbf{B}\mathbf{u}^{red} + \mathbf{K}\mathbf{c} = \mathbf{f} \qquad 2.23$$

A symmetric stiffness matrix is obtained by multiplying all terms with $\mathbf{B}^T$ i.e:

$$\mathbf{B}^T\mathbf{K}\mathbf{B}\mathbf{u}_{red} = \mathbf{B}^T\mathbf{f} - \mathbf{B}^T\mathbf{K}\mathbf{c} \quad 2.24$$

where the reduced global stiffness matrix is defined as:

$$\mathbf{K}_{red} = \mathbf{B}^T\mathbf{K}\mathbf{B} \quad 2.25$$

And the reduced force matrix is given by:

$$\mathbf{f}_{red} = \mathbf{B}^T\mathbf{f} - \mathbf{B}^T\mathbf{K}\mathbf{c} \quad 2.26$$

2.3.4. Solution strategy

The analyses are performed in Matlab with use of the CALFEM toolbox. The procedure is as follows. First, the geometry is determined, and then the elements are assigned their strength according to the method described in Section 2.2.2. The structural analysis is then carried out in a step-wise manner where each computational step corresponds to rupture of a fibre element or a shear element. The applied deformation, c, is for each step set to $0.1L_f$, where L_f is the total length of the fibre and the system of equations is then solved by:

$$\mathbf{u}_{red} = \mathbf{K}_{red}^{-1}\mathbf{f}_{red} \quad 2.27$$

The nodal displacements **u** are obtained by Equation 2.22. Then the element forces, F_i^{an}, and reaction force, F^r, are extracted. In order to determine which element to fracture, the fraction between the element forces obtained in the analysis step, F_i^{an}, and the assigned strengths $F_{f,i}^{ult}$ is calculated according to (i indicates element number):

$$\lambda_i = \frac{F_i^{an}}{F_{f,i}^{ult}} \quad 2.28$$

The fractured element is then found by:

$$\lambda_f = \max\left(\left|\lambda_i\right|\right) \quad 2.29$$

If the fractured element represents a fibre, the stiffness of the fractured spring element is multiplied with 0.0001 and if the fracture occurs in a shear spring element the stiffness is set to zero. The difference is due to requirement of numerical stability of the analysis. Then the next step in the analysis is performed with the new values. The result from the analysis is the global force-displacement curve, due to the applied deformation, c. The actual global reaction force and displacement are obtained by $\delta^g = cL_f / \lambda_f$ and $F^g = F^r / \lambda_f$ which are registered in each analysis step. This operation is possible since the analysis is linear. The global stress in the technical

fibre is calculated by dividing F^g with the total cross sectional area. The global strain is obtained by $\varepsilon^g = \delta^g / L_f$.

2.3.5. Analyses types

Three types of analyses are performed. These are element convergence, adjustment of parameters to fit experiments and parameter study. The element convergence is performed in order to get an indication of how coarse the mesh can be without affecting the accuracy of the analysis. The adjustment of parameters is carried out by performing a large number of analyses for the parameters believed to affect the result. The parameters are; fracture energy G_f = 100, 200, 400 and 800 J/m^2, the shear strength, τ_f = 10, 20, 40 and 60 MPa, the Weibull material parameters σ_0 = 6000, 7000, 8000 and 9000 MPa and m = 2.0, 2.5, 3.0 and 3.5. All combinations for two lengths, 3 and 9 mm, of the technical fibre were analysed with 10 different seeds to the random generator (nominally equal fibres). This gave a total of 5120 analyses. The analyses were performed at the LUNARC cluster at Lund University.
Combining the result from the two lengths and comparing them with result from the tensile test gives an indication of the magnitude of the parameters.

The parameter study was made by means of numerical results obtained during the parameter fitting analyses in order to show their influence on the fibre strength. Additionally, analyses are performed to show the influence of number of elementary fibres per technical fibre. Furthermore, the influence of the number of defects per mm, D, and the material length units, l_m, are studied.

3. Result

3.1. Experiment

3.1.1. SEM-result

The SEM study gave pictures of the kind shown in Figure 3.1. The pictures were used to estimate the number of defects per unit length. The counted type of defects is indicated by ellipses in the figure. The defects were counted for several fibre pieces along a total length of 3575 μm. The count resulted in 29 defects.
Another important result is that the elementary fibres seem to have the same thickness along a long part of the fibre. However, since only the surface of the fibre can be seen, it cannot for certain be concluded that the cross sectional area is constant.

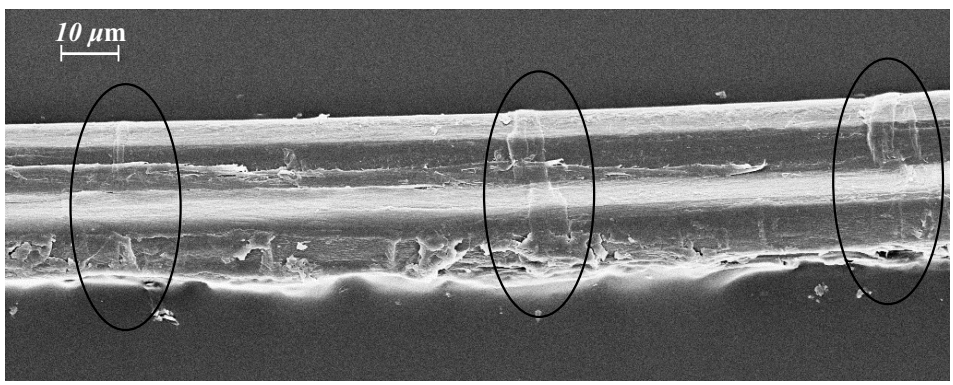

Figure 3.1 *SEM-picture of flax fibres.*

3.1.2. Tensile test

The results from the tensile tests are presented in this section. The cross sectional area of the technical fibres was estimated to range between 3145 μm^2 and 8527 μm^2 for flax and between 11532 μm^2 and 94600 μm^2 for hemp. With a mean diameter of the elementary fibre of 20 μm and a lumen size of 5 % of its cross sectional area the mean number of elementary fibre per technical fibre is 18 for flax and 112 for hemp. The larger number for hemp is because the technical hemp fibres are coarser. This large number of elementary fibres of hemp leads to that FE-analyses of hemp are to time consuming for the present study. The analyses are however possible to carry out.
Figure 3.2 shows an example of three different stress-strain curves obtained in the tests. The curves show that the recorded stiffness is higher for longer fibres, which is a consequence of less influence of the deformation in the clamping system. Therefore is the stiffness result only shown for the fibres of 27 mm length and also the stiffness values estimated by the least-squares method (LS), i.e. Equation 2.4. The result of the tests is compiled in Table 3.1. The least-square result is somewhat uncertain since the clamping stiffness was at random. The glue between the washers was not applied in exactly the same manner for the different tests. Residue of the glue in varying amount was in contact with the hook, which gave different stiffness in each test.

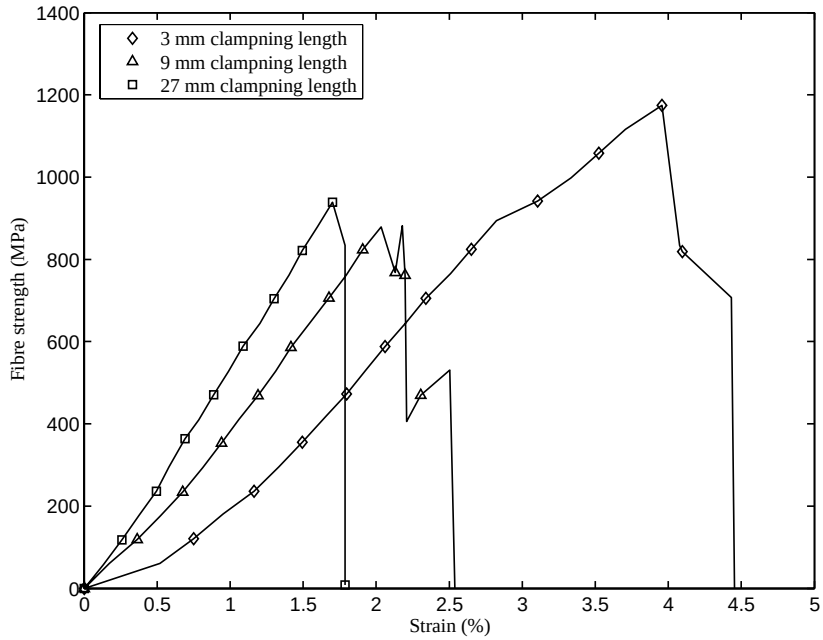

Figure 3.2 *Representative tensile behaviour of flax fibres.*

Table 3.1 *Result from tensile test, E = E-modulus, S = strength, cov = coefficient of variation, n = number of tested fibres*

	E (GPa) LS	E (GPa) L=27 mm	S (MPa) L=3 mm	S (MPa) L=9 mm	S (MPa) L=27 mm
Retted hemp	50.4 cov=29%	40.3 cov=24%	731.9 cov=31% n = 8	653.8 cov=36% n = 11	434.7 cov=33% n = 11
Retted glued hemp	65.1 cov=44%	50.1 cov=30%	819.7 cov=31% n = 10	735.1 cov=27% n = 11	599.4 cov=36% n = 14
Retted flax	67.1 cov=22%	63.4 cov=19%	931.6 cov=41% n = 9	623.6 cov=31% n = 17	500.4 cov=52% n = 16
Retted glued flax	75.8 cov=45%	60.6 cov=32.5%	999.9 cov=31% n = 8	726.5 cov=49% n = 14	555.7 cov=48% n = 14

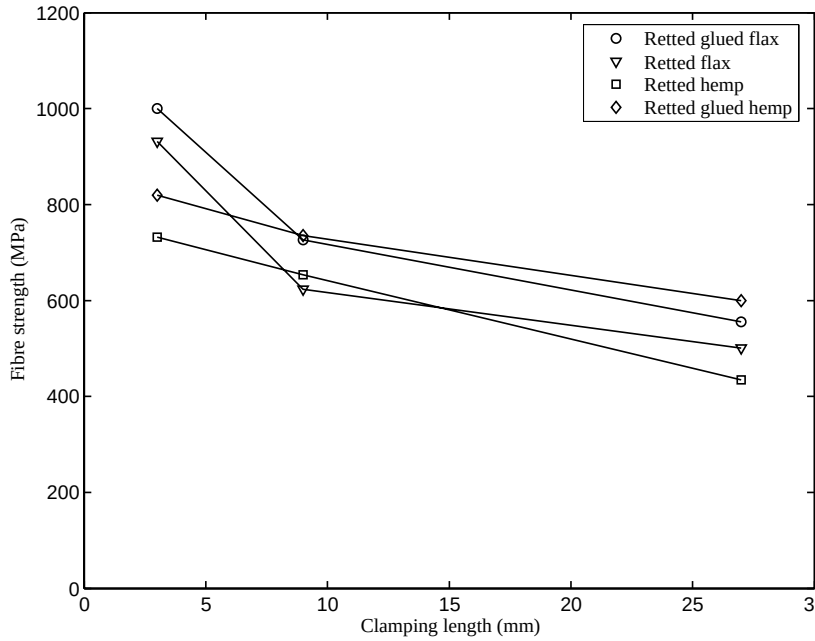

Figure 3.3 *Measured tensile strength versus clamping length.*

3.2. FE-analysis

3.2.1. General

The results from the analyses are in global force-displacement curves. The stress-strain curve is easily obtained by dividing by the total cross sectional area and fibre length respectively. An example of such a curve is shown in Figure 3.4. The sharp large summits are due to rupture of elementary fibres (examples are marked with arrows in the figure). The smaller summits are due to rupture of the shear interface. The strength of the fibre is by definition the maximum stress in the global stress-strain curve, indicated by a circle in the figure. The strength of the fibre in Figure 3.4 is dependent on the 3-4 weakest elementary fibres. This number of ruptures is different in different analyses but the weakest fibres are limiting in all the analyses. As depicted in Figure 3.4, the stress-strain relation experiences snap-back. This behaviour is very difficult to record experimentally since it would require an extremely sensitive and fast control system. The loading in the present experimental tensile tests is deformation controlled and hence only monotonically increasing deformation can be registered. In order to compare the computational and experimental results, the computational result is made monotonically increasing in strain. The corresponding curve is represented by the dotted line in the figure. The figure shows that the monotonic curve gives a fracture that in a global sense is stable. Stable fracture was only captured a few times for the weaker fibres during the test. One reason to this is that the elastic energy stored in the clamping system, is released dynamically on the softening part of the stress-strain curve. This leads to that the fibre snaps faster in the tests than in the computational analyses.

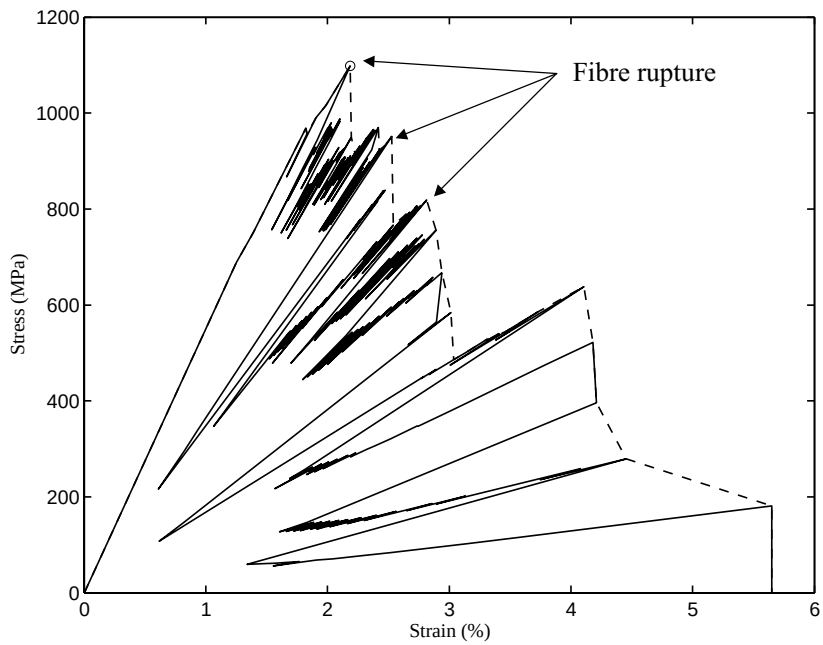

Figure 3.4 *Global stress-strain curve from one of the analyses of technical fibres.*

3.2.2. Convergence results

The deviation in strength from the analysis with the finest mesh is calculated for different mesh size. The result from the convergence study is shown in Figure 3.5. It appears that the strength is almost insensitive to element size. This has a great impact on the required analysis time. For an element size equivalent to 5 elements/mm the, deviation from the finest mesh is less than approximately 4 %. For further analysis this mesh size is used. The number of elementary fibres modelled per technical fibre is 3 times 6, i.e. 18 elementary fibres. That is the mean number found in the tensile tests. The parameters used for the analyses was τ_f = 20 MPa, σ_0 = 9000 MPa, m = 2 and D_r = 0.16.

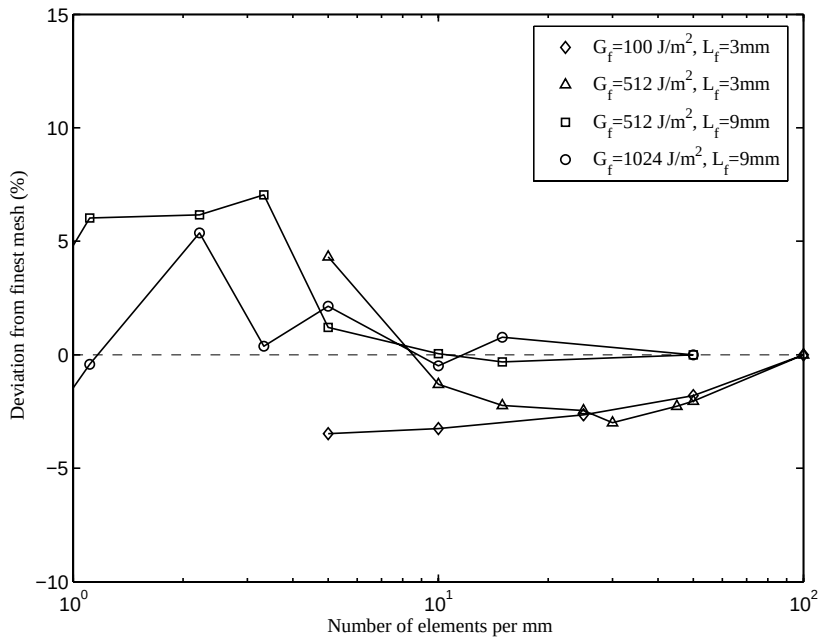

Figure 3.5 *Result from convergence study.*

3.2.3. Adjustment of parameters to fit experimental results

The 5120 analyses were performed for 512 technical fibres with the same number of parallel elementary fibres, 18, and the same damage ratio, D_r = 0.16, as in the convergence analysis. The technical fibre with a length of 3 mm was given an element mesh with 15 element lengths, l_e, along the fibre and the 9 mm ditto an element mesh with 45 element lengths. The strength values of the fibres were calculated as the mean obtained for 10 nominally equal fibres. The technical fibres with a length of 27 mm would require a large number of elements and computational increments. An estimate of the strength of fibres with length 27 mm is however obtained by dividing the nominally equal fibres of length 9 mm into groups of 3. The mean value of the minimum of each group is taken as the strength of technical fibres with the length 27 mm. In order to simplify comparison, the fraction between computational and tested result is determined. The fractions are named f_3, f_9 and f_{27}. The results closest to the tested results and their parameters are presented in Table 3.2 and 3.3. The parameters investigated are presented in section 2.3.4.

Table 3.2 *Result comparison of flax*

G_f (J/m^2)	τ_f (MPa)	m (-)	σ_0 (MPa)	f_3	f_9	f_{27} (estimated)
100	10	2.0	9000	1.0	1.0	1.1
100	10	2.5	6000	1.0	1.0	1.2
100	20	2.0	8000	1.0	1.0	1.2
200	10	2.0	8000	0.9	1.0	1.2
200	10	2.0	9000	1.0	1.1	1.3

Table 3.3 *Result comparison of glued flax*

G_f (J/m^2)	τ_f (MPa)	m (-)	σ_0 (MPa)	f_3	f_9	f_{27} (estimated)
100	20	2.5	6000	1.0	1.0	1.2
200	10	2.5	6000	1.0	0.9	1.2
200	20	2.0	9000	1.0	1.1	1.3
400	10	2.0	9000	1.0	1.0	1.2
800	10	2.0	8000	1.0	1.0	1.2
300	15	2.0	9000	1.0	1.1	1.3

If it is assumed that the glue does not affect the elementary fibres, its Weibull parameters are the same for non-glued and glued fibres. The number of possible parameters is thereby further reduced. From the tables it can be seen that the closest fit to test values with the same Weibull parameters, m = 2.0 and σ_0 = 9000, is for non-glued fibres G_f = 100 J/m^2, τ_f = 10 MPa, in the below referred to Analysis 1, and for glued fibres G_f = 400 J/m^2, τ_f = 10 MPa, in the below referred to Analysis 2.
These values show that the shear fracture energy is higher for the glued fibres, which also is expected. It is however expected that also the shear strength should be higher

for glued fibres. In order to check the result also for fibres of 27 mm length, 10 nominally equal fibres each, with the parameters obtained in the fitting procedure, was performed. The number of element lengths was 135. The result is illustrated in Figure 3.6 and compiled in Table 3.4.

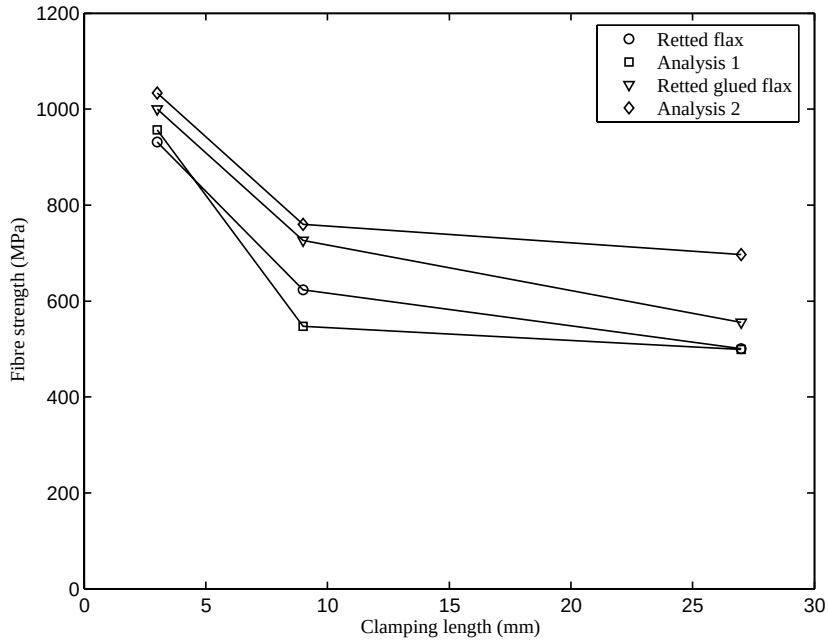

Figure 3.6 *Tested and fitted analysis results.*

Table 3.4 *Result comparison of computational and tested result.*

	Mean strength ± std (MPa)		
	$L = 3$	$L = 9$	$L = 27$
Retted flax	931.6±382	623.6±193	500.4±260
Analysis 1	957.2±223	596.4±48	499.0±59
Retted glued flax	999.9±310	726.5±356	555.7±267
Analysis 2	1033±196	759.9±64	697.2±60

The computational and tested results agree rather well but an even better fit should be possible to obtain by investigating the strength for the parameters divided in closer intervals. The standard deviation presented in Table 3.4 is for short fibres (3 mm) of the same order of magnitude in computational and tested result. For longer fibres (9 & 27 mm) the standard deviation of the computational result is much lower than the tested fibres. The reason is probably that shear properties are taken as deterministic values. If a variation of the modelled properties of the shear interface had been used, the standard deviation of the computational result would probably have been larger.

3.2.4. Parameter study

Material property parameters

The result from the analyses used for the fitting procedure is used in order to show the influence of the different parameters. The strength of the fibre is plotted versus its length for the parameters G_f, τ_f, m and σ_0. The strength values of fibres with the length 27 mm are estimated in the same manner as described previously. These values are therefore not as accurate as the strength values for fibres of the length 3 and 9 mm but still believed to show the influence of the strength. The damage ratio used was D_r = 0.16.

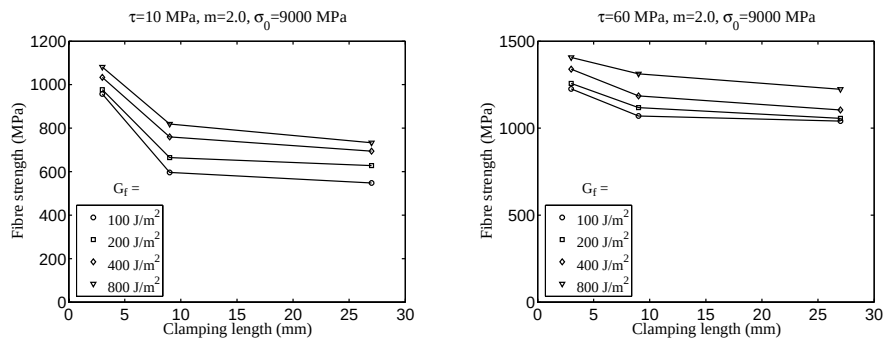

Figure 3.7 *Influence of shear interface fracture energy on the fibre strength.*

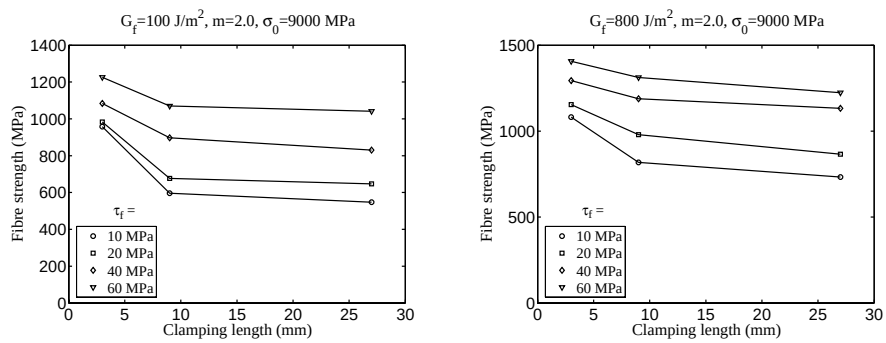

Figure 3.8 *Influence of shear interface strength on the fibre strength.*

As depicted in Figure 3.7 and 3.8, an increase in both the fracture energy and the strength of the shear interface increases the strength of the technical fibre. The explanation to this is that when an elementary fibre is broken, the shear interface distributes the force to the adjacent fibres. This behaviour is more evident for longer fibres because the shear force can act on a longer distance. For shorter fibres the shear force transfer consequently has less influence on the strength. If the analyses would have been performed for very short fibres, the strength difference would have been very small.

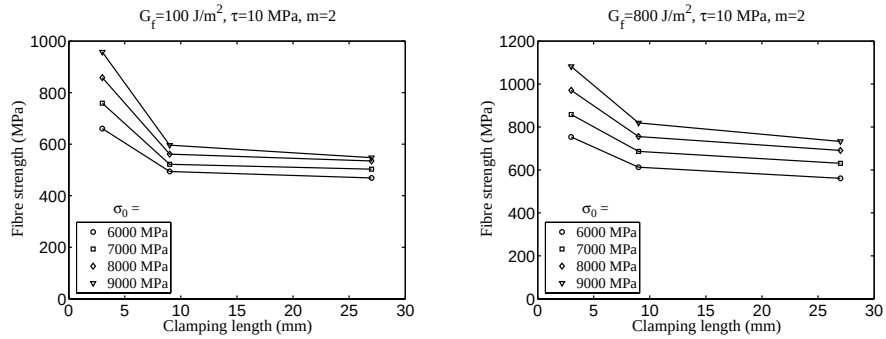

Figure 3.9 *Influence of the Weibull parameter σ_0 on fibre strength.*

The Weibull parameter σ_0 influence the strength of short technical fibres to a greater extent than long fibres. σ_0 represents the stress where approximately 63 % of the fibres have ruptured. Since the probability of damage is larger for longer fibres and the weaker part of the elementary fibres are limiting, more weak elementary fibres are present and thereby is the influence smaller for longer technical fibres. The behaviour is the same for different shear interface fracture energy, but less for higher values of G_f. The reason is that shear forces are transferred to adjacent elementary fibres, where the strength of the elementary fibre might be higher.

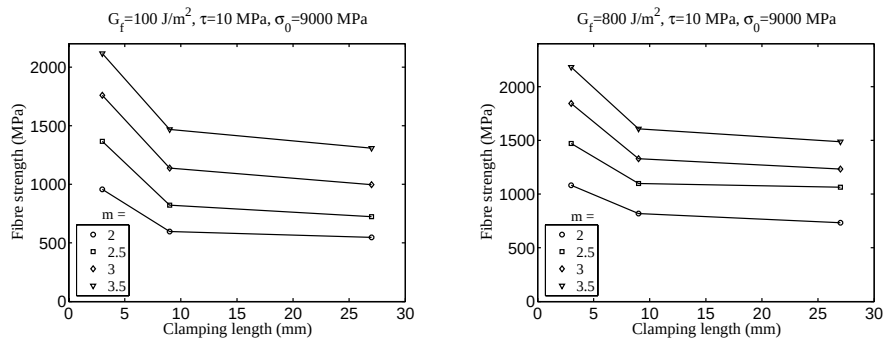

Figure 3.10 *Influence of the Weibull parameter m on fibre strength.*

The Weibull parameter *m* has a great influence on the strength of technical fibres. The reason is that the interval of strength of the elementary fibre decrease for an increasing *m*. The probability of weak fibres is decreased and the strength of the technical fibre increases. As depicted in Figure 3.10, an increase of the shear interface fracture energy gives an increasing strength of the technical fibre, but the length effect is not evident.

Geometrical parameters

The parameters studied in the below are number of elementary fibres per technical fibre, the number of defects per mm, D, and the material length units, l_m. All the analyses are performed for the material parameters G_f = 100 J/m2, τ_f = 10 MPa, m = 2 and σ_0 = 9000 MPa and the length of the technical fibre was 3 mm. Unless otherwise stated it was further assumed that the number of elementary fibres was 18, D = 8.1 defects/mm, l_m = 10 μm and l_e = 0.2 mm.

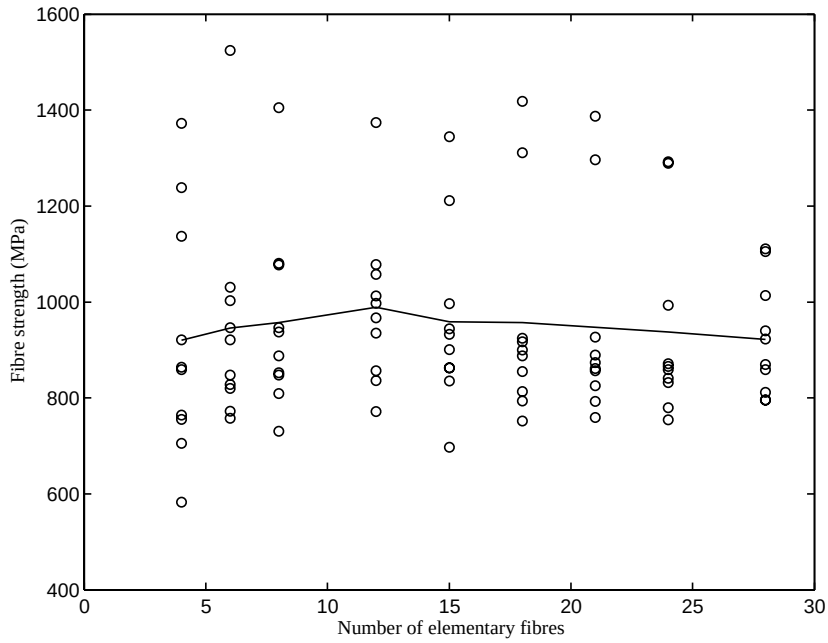

Figure 3.11 *Fibre strength versus number of elementary fibres per technical fibre.*

The result from the study of the number of elementary fibres per technical fibre is shown in Figure 3.11. The circles represent the strength obtained in each individual analysis and the line the mean strength. It appears that the influence of the number of elementary fibres is very small. A tendency can however be discerned; the strength of the technical fibre increases if the number of elementary fibres is increased up to 12. If the number of elementary fibre is increased further, the strength of the technical fibres decreases. It is expected that the strength decrease for a larger volume of material as described by the Weibull theory. It is however uncertain what causes the increase of strength for fewer fibres. One reason might be that if one elementary fibre is weak in a technical fibre with few elementary fibres, the failure of the whole technical fibre will occur at this elementary fibre's stress level. If more elementary fibres are present, the limiting fibre might be the second or third elementary fibre which would give a stronger technical fibre.

The result from the analyses where the number of defects per mm, D, has been varied is compiled in Table 3.5. The strength value indicated is the average ± standard deviation. It is obvious that an increased number of defects gives a decrease of the strength of the technical fibre since the probability of weaker fibres is increased.

Table 3.5 *Influence of number of defects on fibre strength.*

D (defects/mm)	4.0	8.1	16
Strength (MPa)	1298±164	957±223	628±67

Finally, the influence of the material length units, l_m, is studied. The result from the analyses is shown in Table 3.6. The result shows that the influence is small. The number of nominally equal fibres was 10. If more analyses had been performed, a more statistically accurate result would have been obtained, most probably showing an even smaller influence of l_m on the mean strength values. The reason can be explained by the following example which is valid if D_r is small. D_r is small for small l_m. Assume that l_m is doubled. Then is also D_r doubled. Since the random number is compared with D_r, the probability of having a defect is the same for the doubled l_m as for 2 non-doubled l_m.

Table 3.6 *Influence of material length l_m on fibre strength.*

l_m (μm)	10	20	40
Strength (MPa)	912±197	957±223	916±171

4. Discussion

4.1. Tensile test

The results obtained in the tensile test seem reasonable. Other authors [3] have obtained similar results with respect to the absolute values of strength and stiffness and with respect to the influence of length results in the same order of magnitude. It is obvious, that the scatter of recorded strength and stiffness is great which makes it difficult to make certain conclusions regarding results obtained for different treatment of the fibres. However the mean values for both strength and stiffness were found to be increased by gluing both for the flax and the hemp.

4.2. Computational result

The presented computational model shows that the constitutive behaviour and strength of technical fibres can be predicted. It has also been shown that the shear interface properties affect the strength of the technical fibre. Also the Weibull parameters are important for the strength of the technical fibre. The Weibull parameters are linked to the number of defects present in the elementary fibres. Hence, the parameters of the fibres possible to affect by man, in order to change the strength of a technical fibre (or a composite) are strength and fracture energy of the shear interface and the number of defects. In an industrial process, the inducing of defects is however difficult to avoid, which implies that the only factor possible to affect is the shear interface.
The explanation to the empirical observation by Kessler [2], i.e. that retted fibres have a low tensile strength whereas their composites have high strength and the opposite for non-retted fibres, can be explained by the computational result. Since the retting decrease the strength of the shear interface, the strength of the technical fibre decreases and the opposite for non-retted fibres. When technical fibres are used in the composite, the retted fibres allow resin to penetrate into the technical fibre (between the elementary fibres). Since it is likely that the shear properties of the resin are superior to the pectin in the middle lamella, retted fibres will give a stronger composite. It can then be concluded that if a strong composite is to be obtained, the technical fibre should not be used at all. In stead, the elementary fibre should be completely separated from each other, so that resin has contact with the whole elementary fibre. Further, it is important that the resin adheres to the elementary fibres. This implies that the elementary fibre has to be free from residue from the stem. In practice, it might still be more feasible to use technical fibres since the separation process might induce damage to the elementary fibres. It is hence a question of optimising the degree of separation versus inducing of damage.

4.3. Future work

The scatter of both stiffness and strength when testing the technical fibres is vast and it can be questioned whether the strength and stiffness properties of an un-glued fibre is relevant for estimation of the properties of a fibre in the composite. It is therefore proposed that a standard composite is developed for evaluation of the stiffness and the strength of natural fibres. This composite should be unidirectional and the resin and

manufacturing method should be standardised. Testing of such a composite is much easier to perform and the scatter will most likely decrease, since a large number of fibres are loaded simultaneously. Studies of the influence of variables like harvesting time, retting degree and retting method would probably be facilitated.
It is believed that the proposed computational model can be developed for modelling of unidirectional composites by increasing the number of elementary fibres and changing the random model for how defects are distributed. In a composite, the fibres can come from different locations in the stem or different plants. This implies that the defects are located completely at random.
Furthermore, it would be interesting to examine how a non-linear shear stress interface performance according to curve A in Figure 2.5 would affect the properties of a technical fibre and composite.

5. References

1. Wretfors C, *Cultivation, processing and quality analysis of fibres from flax and industrial hemp – an overview with emphasis on fibre quality*, Report 139, JBT, SLU, 2005
2. Personal communication with Professor Rudolf Kessler, Institut für Angewandte Forschung, Fachhochschule Reutlingen, Germany, 2003
3. Bos H, *The potential of flax fibres as reinforcement for composite materials*, Doctoral thesis, Technische Universiteit Eindhoven, the Netherlands, 2004
4. Thygesen L G, Hoffmeyer P, *Image analysis for the quantification of dislocations in hemp fibres*, Industrial Crops and Products 21 (2005) 173–184
5. Råde L, Westergren B, *Mathematics handbook for science and engineering*, Third edition, studentlitteratur, 1995
6. His I et al, *Microscopic Studies on Mature Flax Fibers Embedded in LR White: Immunogold Localization of Cell Wall Matrix Polysaccharides.* The Journal of Histochemistry & Cytochemistry 2001; Vol 49(12): 1525–1535
7. Bledzki A K and Gassan J, *Composites reinforced with cellulose based fibres*, Progress in polymer science 24, pp 221-274, 1998
8. van Voorn B, Smit H H G, Snike R J, de Klerk B, *Natural fibre reinforced sheet moulding compound*, Composites: part A 32 pp 1271-1279, 2001
9. Eichhorn S J, Sirichaisit J, Young R J, *Deformation mechanisms in cellulose fibres, paper and wood*, Journal of materials science 36 pp 3129-3135, 2001
10. Kandachar P, *Opportunities for product development for industrial applications in polymers reinforced with natural fibres*, Proceedings of the 23rd Risö International symposium on materials science, Risö national laboratory, Denmark 2002
11. Ashby M F& Jones D R H., *Engineering materials 2*, Pergamon press, 1993
12. Persson K, *Micromechanical modelling of wood and fibre properties*, Doctoral thesis, Structural mechanics Lund institute of technology, 2000
13. Herakovich C T, *Mechanics of fibrous composites*, John Wiley & sons, 1998
14. Nilsson T, *Flax and hemp fibres and their composites –A literature study of structure and mechanical properties*, Division of structural mechanics, Lund University, 2005
15. Gustafsson P J, *Analysis of generalized Volkersen-joints in terms of non-linear fracture mechanics*, Mechanical behaviour of adhesive joints, pp. 323-338, 1987
16. Heyden S, *Network modelling for the evaluation of mechanical properties of cellulose fibre fluff*, Doctoral thesis, Structural mechanics Lund institute of technology, 2000

Appendix

Analytical calculation of stiffness of fibres with dislocations

TORULF NILSSON and PER JOHAN GUSTAFSSON

Analytical calculation of stiffness of fibres with dislocations

In addition to finite element analyses of the elementary fibre as reported in Paper 2, this short report presents an analytical expression for how the stiffness varies with the fibre diameter. The calculations are performed on a lamella where the micro fibrils are oriented as shown in Figure A.2 (b) in Paper 2. The lamella is assumed to be a thin layer of the elementary fibre at the radius *r*. The stiffness in the direction of the fibre of the non-dislocated part is called E_α, the stiffness of the β_1-dislocation E_{β_1} and the stiffness of the β_2-dislocation E_{β_2}. By assuming a constant force in the fibre, the overall stiffness of the dislocated lamella is obtained as:

$$\frac{1}{E} = \frac{1-D}{E_\alpha} + \frac{D}{2E_{\beta_1}} + \frac{D}{2E_{\beta_2}} \qquad 1$$

where *D* is the dislocation ratio as defined in Paper 2.

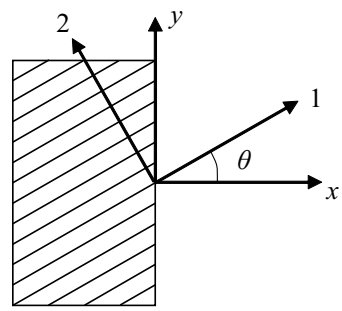

Figure 1 *Lamella showing material and global directions.*

The lamella shown in Figure 1 represents the cell wall of the elementary fibre. The x-axis is the direction of the fibre and the 1-axis is the direction of the non-dislocated or dislocated micro fibril. The material model is assumed orthotropic. The compliance matrix in the 1-2 coordinate system is given by:

$$\mathbf{C}_{1-2} = \begin{bmatrix} \frac{1}{E_1} & -\frac{\nu_{21}}{E_2} & 0 \\ -\frac{\nu_{12}}{E_1} & \frac{1}{E_2} & 0 \\ 0 & 0 & \frac{1}{G_{12}} \end{bmatrix} \qquad 2$$

The compliance matrix is transformed to the x-y system by the relation:

$$\mathbf{C}_{x-y} = \mathbf{T}^T \mathbf{C}_{1-2} \mathbf{T} \qquad 3$$

The transformation matrix, **T**, is defined by:

$$\mathbf{T} = \begin{bmatrix} c^2 & s^2 & 2sc \\ s^2 & c^2 & -2sc \\ -sc & sc & c^2 - s^2 \end{bmatrix} \quad 4$$

where $c = \cos\theta$ and $s = \sin\theta$.

The linear elastic relation can then be written as:

$$\boldsymbol{\varepsilon} = \mathbf{C}_{x-y}\boldsymbol{\sigma} \quad 5$$

or

$$\begin{bmatrix} \varepsilon_{xx} \\ \varepsilon_{yy} \\ \gamma_{xy} \end{bmatrix} = \begin{bmatrix} C_{11} & C_{12} & C_{13} \\ C_{21} & C_{22} & C_{23} \\ C_{31} & C_{32} & C_{33} \end{bmatrix} \begin{bmatrix} \sigma_{xx} \\ \sigma_{yy} \\ \tau_{xy} \end{bmatrix} \quad 6$$

Where the components are functions of θ according to equation 3. The functions are not written out explicitly since the expressions are very long.

Two boundary conditions are examined; $\sigma_{yy} = 0$ and $\tau_{xy} = 0$, and $\sigma_{yy} = 0$ and $\chi_{xy} = 0$. The first condition corresponds to free rotation of the thin walled tube made up of the thin layer of the fibre under consideration. The second condition corresponds to prevented rotation.
For the first condition is Equation 6 reduced to:

$$\varepsilon_{xx} = C_{11}\sigma_{xx} \quad 7$$

For the second condition is Equation 6 reduced to:

$$\varepsilon_{xx} = \left(C_{11} - \frac{C_{13}C_{31}}{C_{33}} \right) \sigma_{xx} \quad 8$$

The *E*-modulus is calculated by the inverse of the compliances in Equation 7 and 8. The stiffness values E_α, E_{β_1} and E_{β_2} are calculated by setting θ to $-\alpha$, $-\beta_1$ and β_2, respectively. These angles are functions of the fibre radius, and thus is also the overall stiffness a function of the radius. The expressions of the angles are:

$$\alpha = \arctan\left(\frac{r}{p} \right) \quad 9$$

$$\beta_{1,2}(r) = 90° - \arctan\left(\left(r\left(\frac{\sin(\beta_1(R_y) - \alpha(R_y))}{R_y \cos\alpha(R_y)\cos\beta_1(R_y)} \pm \frac{1}{p}\right)\right)^{-1}\right) \quad 10$$

These expressions are derived in Paper 2.

For the case $\sigma_{yy} = 0$ and $\tau_{xy} = 0$, the E modulus as a function of the radius becomes:

$$E(r) = 1\Big/\left((1-D)(C_{11})_{-\alpha} + \frac{D}{2}(C_{11})_{-\beta_1} + \frac{D}{2}(C_{11})_{\beta_2}\right) \quad 11$$

For the other case, $\sigma_{yy} = 0$ and $\gamma_{xy} = 0$, the E-modulus is obtained as:

$$E(r) = 1\Big/\left((1-D)\left(C_{11} - \frac{C_{13}C_{31}}{C_{33}}\right)_{-\alpha} + \frac{D}{2}\left(C_{11} - \frac{C_{13}C_{31}}{C_{33}}\right)_{-\beta_1} + \frac{D}{2}\left(C_{11} - \frac{C_{13}C_{31}}{C_{33}}\right)_{\beta_2}\right) \quad 12$$

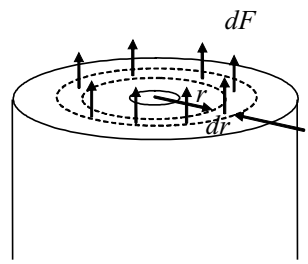

Figure 2 *Cross section of fibre for equilibrium calculation.*

By assuming that the strain in the fibre is constant, it is possible to determine the total force in the fibre by equilibrium calculations in the direction of the fibre as shown in Figure 2.

$$F = 2\pi\varepsilon \int_{R_i}^{R_o} r E(r) dr \quad 13$$

The average stress is obtained by division of the cross sectional area, i.e.,

$$\overline{\sigma} = \frac{2}{R_o^2 - R_i^2} \int_{R_i}^{R_o} r E(r) dr\, \varepsilon \quad 14$$

where the average global stiffness is obtained as:

$$\overline{E} = \frac{2}{R_o^2 - R_i^2} \int_{R_i}^{R_o} r E(r) dr \qquad 15$$

The functions *E(r)* (Equation 11 and 12) are evaluated in Maple and thereafter is the integral in Equation 15 calculated numerically in Matlab. The parameters used are adjusted to be similar to those used for the finite element analyses in Paper 2. The stiffness properties are $E_1 = E_C V_C + E_{HC}(1 - V_C) = 130 \cdot 0.65 + 5.6 \cdot 0.35 \approx 86.5$ GPa, $E_2 = E_{\mathrm{HC}} = 5.6$ GPa, $\nu_{12} = 0.3$ and $G_{12} = E_2 / (2(1 + \nu_{12})) \approx 2.15$ GPa. The reference parameters of the geometry of the fibre and the dislocations are $R_y = 12$ μm, $\alpha(12) = 10^\circ$, $\beta_1(12) = 45^\circ$ and $p = 12/\tan(10^\circ)$. The size of the lumen is set to 5 % of the cross sectional area which gives $R_i = \sqrt{0.05} R_o$. The dislocation ratio is set to $D = 0.13$.
Calculations are performed for diameters between 10 and 40 μm for the two different models. A plot of the result is shown in Figure 3, where also the experimental and finite element results are plotted for comparison. Additionally, the influence of the dislocation ratio, *D*, is investigated. The result is shown in Figure 4 and 5.

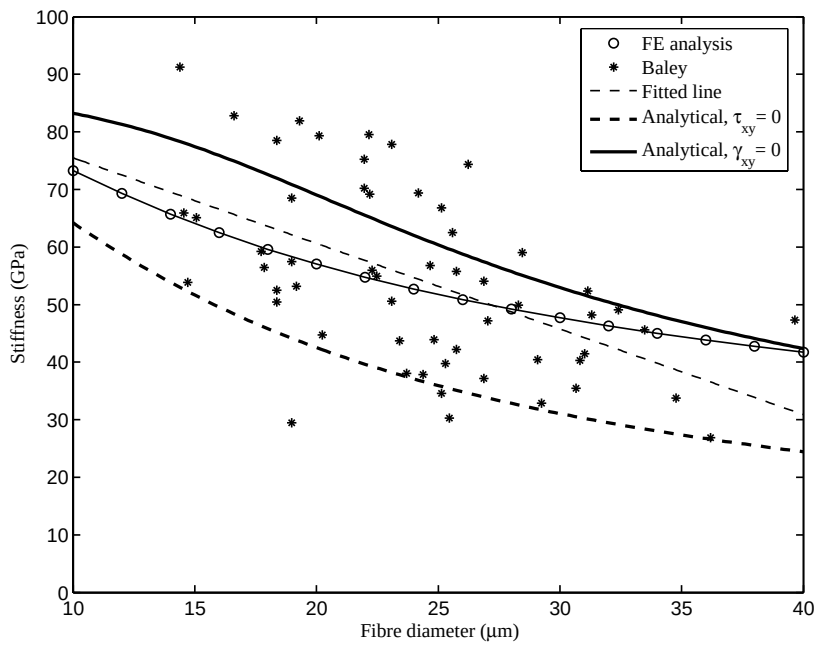

Figure 3 *Stiffness versus the fibre diameter.*

The result shows that the boundary conditions $\sigma_{yy} = 0$ and $\tau_{xy} = 0$ underestimates the stiffness whereas the boundary conditions $\sigma_{yy} = 0$ and $\gamma_{xy} = 0$ overestimates the stiffness of the fibre compared to the result obtained in the finite element analyses. For larger diameters the boundary conditions $\sigma_{yy} = 0$ and $\gamma_{xy} = 0$, appears to give a stiffness closer to the result from the finite element analyses. The reason might be that neither τ_{xy} nor γ_{xy} are zero. In a composite it seems reasonable to use $\gamma_{xy} = 0$, since rotations are prevented by the adhesive between the fibres.

The result obtained for varying dislocation ratio (Figure 4 and 5) shows that the dislocation ratio has a large impact on the stiffness of the fibres.

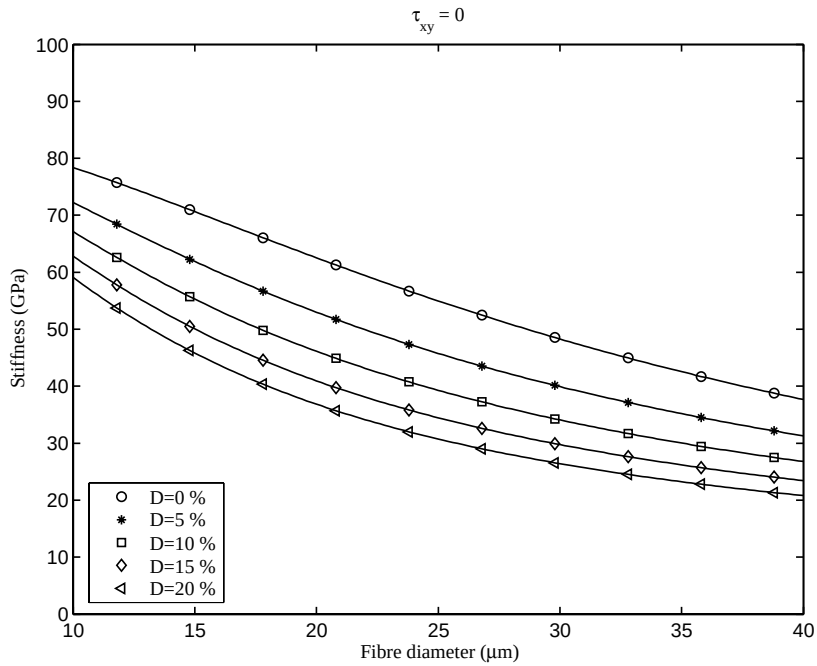

Figure 4 *Influence of dislocation ratio on fibre stiffness for* $\tau_{xy} = 0$.

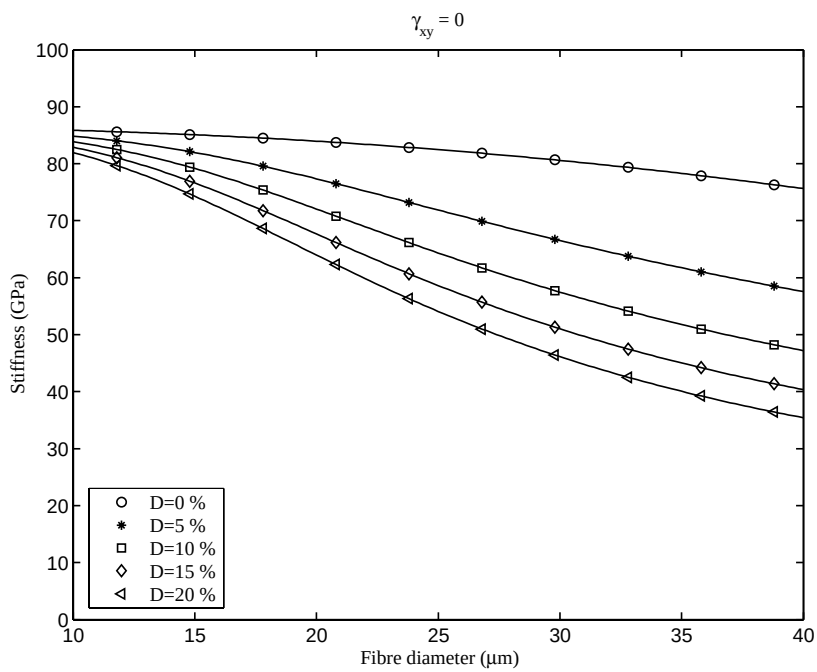

Figure 5 *Influence of dislocation ratio on fibre stiffness for* $\gamma_{xy} = 0$.

References

1 T. Nilsson and P. J. Gustafsson (2005), *Influence of dislocations and plasticity on the tensile behaviour of flax and hemp fibres*, submitted for publication in Composites Part A: Applied Science and Manufacturing

2 J. Hult, H. Bjarnehed, *Styvhet och styrka*, Studentlitteratur, 1993